



UNIVERSITY OF  
BIRMINGHAM

CHARACTERISATION OF *FUSOBACTERIUM NUCLEATUM* BIOFILMS  
AND CYCLIC DI-NUCLEOTIDE PRODUCTION

by

MÁRIA MUCHOVÁ

A thesis submitted to  
The University of Birmingham  
for the degree of  
MSc by Research in Dentistry

Institute of Clinical Sciences  
School of Dentistry  
College of Medical & Dental Sciences  
University of Birmingham  
April 2020

UNIVERSITY OF  
BIRMINGHAM

**University of Birmingham Research Archive**

**e-theses repository**

This unpublished thesis/dissertation is copyright of the author and/or third parties. The intellectual property rights of the author or third parties in respect of this work are as defined by The Copyright Designs and Patents Act 1988 or as modified by any successor legislation.

Any use made of information contained in this thesis/dissertation must be in accordance with that legislation and must be properly acknowledged. Further distribution or reproduction in any format is prohibited without the permission of the copyright holder.

## **Abstract**

*Fusobacterium nucleatum* is an anaerobic oral species, a key player in the formation of periodontal disease-associated dental plaque, also known as dental biofilm. Oral commensals and pathogens residing in the dental biofilm communicate using multiple systems and molecules, one type being the secondary messengers called cyclic di-nucleotides (CDNs). These small molecules control processes such as motility, secretion and adhesion, which are important for biofilm assembly and maturation. The importance of CDNs in biofilm formation and virulence has been studied in true periodontal pathogens, such as *Porphyromonas gingivalis*. Yet, the role of CDNs in the biofilm formation of *F. nucleatum*, which is also a causative agent in systemic diseases, remains elusive.

This thesis analysed the formation of mono-species biofilms of *F. nucleatum* subspecies and significant differences among the subspecies were revealed. The interaction of two *F. nucleatum* ssp. *nucleatum* strains was studied in a periodontitis-related multi-species biofilm model. The genes involved in the synthesis and hydrolysis of CDNs were found to be downregulated overtime in planktonic cultures. Additionally, the intracellular CDN concentration in bacteria grown on agar plates was found to differ significantly between subspecies. Low levels of CDNs were detected in mono-species biofilms.

Our findings established a base for further research into CDNs, their role in virulence and their potential as therapeutic targets.

## **Acknowledgements**

I would like to wholeheartedly thank Dr Sarah Kuehne, my main supervisor, who supported me immensely during this project, especially during the time when none of the experiments worked. Thank you so much for all your patience with my constant questions and for everything you taught me about my beloved *Fusobacterium nucleatum*. I am ever grateful for all the opportunities you gave me during my project.

I would also like to thank the gentlemen on my supervisory team, Prof Michael Milward and Prof Paul Cooper for their ideas on how to improve my experiments and for motivating me to learn and be a better microbiologist.

One huge thank you goes to Raphael Merand, who helped massively with the process of RNA extraction optimisation and also provided a lot of moral support when the experiments did not work.

I would not be able to finish my project successfully without the help of the technical staff, especially Gay Smith, who was always nice and friendly, even when I broke something, Dr Helen Wright, who turned the complicated language of qRT-PCR into a human language, and Jianguo Liu, who was always there to tame the SEM. I am also grateful to Khawla Doudin and Michelle Holder who trained me at the beginning of the project.

Additionally, I thank the Research Core Unit Metabolomics in Hannover, Germany, who kindly performed the quantification of intracellular CDNs.

# Table of Contents

CHAPTER 1: INTRODUCTION .....	1
1.1. <i>Fusobacterium nucleatum</i> .....	2
1.1.1. <i>F. nucleatum</i> and human diseases.....	2
1.2.    Dental biofilm.....	6
1.2.1.    Role of <i>F. nucleatum</i> in the dental biofilm .....	8
1.2.2.    Pathogenic dental biofilm assembly, structure and virulence of the residents .....	9
1.3.    Communication in the dental biofilm .....	12
1.3.1.    Quorum sensing (QS) in dental biofilms .....	13
1.3.2.    Stringent response and alarmones .....	14
1.3.3.    Cyclic di-nucleotides (CDNs).....	15
1.4.    Aims and objectives .....	16
1.4.1.    Objectives .....	17
CHAPTER 2: MATERIALS AND METHODS.....	19
2.1.    Growth of bacteria .....	20
2.2.    Growth curves of <i>Fusobacterium nucleatum</i> subspecies .....	21
2.2.1.    Miles and Misra method.....	21
2.2.2.    Automated spectrophotometric method.....	22
2.3.    Growth of <i>Fusobacterium nucleatum</i> subspecies in the presence of oxygen .....	22
2.4.    Conventional polymerase chain reaction (PCR).....	23
2.5.    Confirmation of <i>Fusobacterium nucleatum</i> subspecies .....	24
2.6.    Mono-species biofilm setup.....	25
2.7.    Multi-species biofilm setup.....	26
2.8.    Preparation of biofilms and scanning electron microscopy (SEM) .....	28
2.9.    Preparation of planktonic bacteria for scanning electron microscopy.....	29
2.9.1.    Bacteria visualised on Nunc™ Thermanox™ coverslips.....	29
2.9.2.    Bacteria visualised on Isopore™ membranes.....	29
2.10.    Extraction and quantification of cyclic di-nucleotides from bacteria grown on agar plates	30
2.11.    Extraction and quantification of cyclic di-nucleotides from single-species biofilms .....	31
2.12.    Bicinchoninic acid (BCA) protein assay .....	31
2.13.    Biomass quantification using crystal violet stain.....	32
2.14.    RNA extraction .....	32
2.14.1.    Quick-RNA™ Fungal/Bacterial Miniprep Kit (Zymo Research, R2014).....	33
2.14.2.    Monarch® Total RNA Miniprep Kit (T2010, New England Biolabs).....	33

2.14.3.	<i>RNeasy® Mini kit (Qiagen, 74104)</i> .....	34
2.14.4.	<i>Phenol/chlorophorm – RNeasy Mini kit hybrid</i> .....	35
2.14.5.	<i>RNA isolation from Brucella species adapted to Fusobacterium nucleatum</i> .....	36
2.15.	<i>Complementary DNA (cDNA) synthesis</i> .....	37
2.16.	<i>Reverse transcription – quantitative polymerase chain reaction (RT-qPCR)</i> .....	38
2.17.	<i>Statistical analysis</i> .....	40
CHAPTER 3: RESULTS .....		41
3.1.	<i>Characterisation of Fusobacterium nucleatum subspecies</i> .....	42
3.1.1.	<i>Colony and cell morphology</i> .....	42
3.1.2.	<i>Bacterial growth in anaerobic conditions</i> .....	49
3.1.3.	<i>Growth of Fusobacterium nucleatum subspecies in the presence of oxygen</i> .....	52
3.1.4.	<i>Confirmation of Fusobacterium nucleatum subspecies using 16S rRNA sequencing</i> ...	55
3.1.5.	<i>Chapter conclusions</i> .....	58
3.2.	<i>Characterisation of mono-species Fusobacterium nucleatum biofilms and multi-species periodontitis-related biofilms</i> .....	59
3.2.1.	<i>Evaluation of biomass production in mono-species biofilms</i> .....	59
3.2.2.	<i>Mono-species biofilm architecture and structure analysed by SEM</i> .....	67
3.2.3.	<i>Evaluation of biomass production in multi-species biofilms</i> .....	75
3.2.4.	<i>Multi-species biofilm architecture and structure analysed by SEM</i> .....	77
3.2.5.	<i>Chapter conclusions</i> .....	80
3.3.	<i>Optimisation of RNA extraction from Fusobacterium nucleatum subspecies</i> .....	81
3.3.1.	<i>Optimisation of RNA extraction – Extraction n. 1</i> .....	81
3.3.2.	<i>Optimisation of RNA extraction – Extraction n. 2</i> .....	83
3.3.3.	<i>Optimisation of RNA extraction – Extraction n. 3</i> .....	84
3.3.4.	<i>Optimisation of RNA extraction – Extraction n. 4</i> .....	85
3.3.5.	<i>Optimisation of RNA extraction – Extraction n. 5</i> .....	87
3.3.6.	<i>Optimisation of RNA extraction – Extraction n. 6</i> .....	91
3.3.7.	<i>Optimisation of RNA extraction – Extraction n. 7</i> .....	92
3.3.8.	<i>Optimisation of RNA extraction – Extraction n. 8</i> .....	94
3.3.9.	<i>RNA extraction from all Fusobacterium nucleatum subspecies</i> .....	97
3.3.10.	<i>Chapter conclusions</i> .....	101
3.4.	<i>Analysis of differential expression of genes involved in synthesis and hydrolysis of cyclic di-nucleotides (CDNs) and quantification of CDNs</i> .....	102
3.4.1.	<i>Primer validation - specificity</i> .....	102
3.4.2.	<i>Primer validation – efficiency</i> .....	104
3.4.3.	<i>Optimisation of qRT-PCR – assay n. 1</i> .....	105

3.4.4.	<i>Optimisation of qRT-PCR – assay n. 2</i> .....	107
3.4.5.	<i>Optimisation of qRT-PCR – assay n. 3</i> .....	109
3.4.6.	<i>Quantification of CDNs</i> .....	114
3.4.7.	<i>Chapter conclusions</i> .....	119
CHAPTER 4:	DISCUSSION.....	120
4.1.	<i>Characterisation of Fusobacterium nucleatum subspecies</i> .....	121
4.2.	<i>Characterisation of mono-species Fusobacterium nucleatum biofilms and multi-species periodontitis-related biofilms</i> .....	123
4.2.1.	<i>Single-species biofilms</i> .....	123
4.2.2.	<i>Multi-species biofilms</i> .....	126
4.3.	<i>Optimisation of RNA extraction from Fusobacterium nucleatum subspecies</i> .....	127
4.4.	<i>Analysis of differential expression of genes involved in synthesis and hydrolysis of cyclic di-nucleotides (CDNs) and quantification of CDNs</i> .....	128
4.4.1.	<i>Differential expression of genes analysed by qRT-PCR</i> .....	128
4.4.2.	<i>Quantification of CDNs</i> .....	130
4.5.	<i>Concluding remarks</i> .....	131
References	.....	133
APPENDICES	.....	141
Appendix 1	.....	142
Appendix 2	.....	147
Appendix 3	.....	150
Appendix 4	.....	154
Appendix 5	.....	156
Appendix 6	.....	157
Appendix 7	.....	159
Appendix 8	.....	160

## List of figures

<b>Figure number</b>	<b>Figure title</b>	<b>Page</b>
1.1.	Progression from healthy state through gingivitis to periodontitis	3
1.2.	Schematic representation of the subgingival biofilm	10
2.1.	Setup of mono-species <i>F. nucleatum</i> biofilm	26
2.2.	Setup of multi-species biofilms	28
3.1.	Colony morphology of <i>F. nucleatum</i> subspecies	43
3.1.	Colony morphology of <i>F. nucleatum</i> subspecies (continued)	44
3.2.	Gram staining of <i>F. nucleatum</i> subspecies	45
3.3.	Comparison of bacterial cell length of <i>F. nucleatum</i> subspecies	46
3.4.	Scanning electron micrographs of <i>F. nucleatum</i> subspecies	47
3.4.	Scanning electron micrographs of <i>F. nucleatum</i> subspecies (continued)	48
3.5.	Growth profiles of <i>F. nucleatum</i> subspecies grown in anaerobic conditions	50
3.6.	Growth profile of <i>F. nucleatum</i> ssp. <i>nucleatum</i> 25586 grown in anaerobic conditions	52
3.7.	Growth profiles of <i>F. nucleatum</i> subspecies grown in oxic conditions	53
3.8.	Agarose gel showing amplified 16S rRNA gene fragments	56
3.9.	The amount of biofilm formed by individual subspecies	61
3.9.	The amount of biofilm formed by individual subspecies (continued)	62
3.10.	The amount of biofilm formed by all subspecies at specific time points	64
3.11.	<i>F. nucleatum</i> subspecies biofilms stained with Crystal violet	66
3.12.	Mono-species FNA biofilms	69
3.12.	Mono-species FNF biofilms	70
3.12.	Mono-species FNN23 biofilms	71
3.12.	Mono-species FNN25 biofilms	72
3.12.	Mono-species FNP biofilms	73
3.12.	Mono-species FNV biofilms	74
3.13.	The amount of biomass quantified in the multi-species biofilms	76
3.14.	Pattern of biofilm formation in multi-species biofilms	77
3.15.	Micrograph of the multi-species biofilm containing FNP	78
3.16.	Micrograph of the multi-species biofilm containing FNN23	79
3.17.	RNA extraction n.1 from FNN25	82
3.18.	RNA extraction n.2 from FNN25	83
3.19.	RNA extraction n.3 from FNN25	85
3.20.	RNA extraction n.4 from FNN25	86
3.21.	RNA extraction n.5 from FNN25 and <i>E. coli</i>	88
3.22.	Optimisation of PCR conditions for pde2 primers	89
3.22.	Optimisation of PCR conditions for pde2 primers (continued)	90
3.23.	RNA extraction n.6 from FNN25	92
3.24.	RNA extraction n.7 from FNN25	93
3.25.	RNA extraction n.8 from FNN23	96
3.26.	RNA extracted from FNA, FNN25, FNP and FNV	99
3.27.	RNA extracted from FNN25 re-treated with Ambion DNase I	100
3.28.	Validation of primers used in this study	103

3.29.	Differential expression of target genes in FNN23 and FNN25 – assay n.1	106
3.30.	Differential expression of target genes in FNN23 and FNN25 – assay n.2	108
3.31.	Confirmation of sample purity and quality	111
3.32.	Differential expression of target genes in FNN23 and FNN25 – assay n.3	112
3.33.	Relative expression of target genes in FNN23 and FNN25	113
3.33.	Relative expression of target genes in FNN23 and FNN25 (continued)	114
3.34.	Quantification of intracellular c-di-AMP from liquid <i>F. nucleatum</i> subspecies cultures	115
3.35.	Quantification of intracellular c-di-AMP from <i>F. nucleatum</i> subspecies grown on agar plates	116
3.36.	The concentration of c-di-AMP from <i>F. nucleatum</i> subspecies grown on agar plates related to the amount of protein	117
3.37.	The concentration of c-di-AMP in single-species biofilms related to the amount of protein	118

## List of tables

<b>Table number</b>	<b>Table title</b>	<b>Page</b>
2.1.	List of bacterial species used in this study	21
2.2.	Cycling conditions for conventional PCR as used for all primers in this study	23
2.3.	List of primers used in this study	39
2.4.	Cycling conditions for RT-qPCR	40
3.1.	Percentages of identity of 16S rRNA genes from <i>F. nucleatum</i> subspecies	57
3.2.	List of DNase digestion methods	94
3.3.	Final RNA concentration after corresponding DNase treatment(s)	95
3.4.	RNA concentration of the remaining <i>F. nucleatum</i> subspecies	98
3.5.	Efficiency values of primers used in this study	104
3.6.	Concentration of RNA used in the qRT-PCR assay n.2	107
3.7.	Concentration of cDNA used in the qRT-PCR assay n.2	109
3.8.	Concentration of cDNA used in the qRT-PCR assay n.3	110

## Abbreviations

AA	<i>Aggregatibacter actinomycetemcomitans</i>
AI-2	Autoinducer-2
AS	Artificial Saliva
ATCC	American Type Culture Collection
ATP	Adenosine triphosphate
BCA	Bicinchoninic Acid
c-di-AMP	Cyclic dimeric adenosine monophosphate
c-di-GMP	Cyclic dimeric guanosine monophosphate
CDN(s)	Cyclic di-nucleotide(s)
CFU	Colony Forming Units
C <sub>p</sub>	Crossing point
CRC	Colorectal Cancer
CV	Crystal Violet
DGC	Diguanylate Cyclase
DisA	DNA Integrity Scanning Protein A
ECM	Extracellular Matrix
EP	Exponential Phase
EPS	Extracellular Polymeric Substance
FNA	<i>Fusobacterium nucleatum</i> ssp. <i>animalis</i>
FNF	<i>Fusobacterium nucleatum</i> ssp. <i>fusiforme</i>
FNN23	<i>Fusobacterium nucleatum</i> ssp. <i>nucleatum</i> ATCC 23726
FNN25	<i>Fusobacterium nucleatum</i> ssp. <i>nucleatum</i> ATCC 25586
FNP	<i>Fusobacterium nucleatum</i> ssp. <i>polymorphum</i>
FNV	<i>Fusobacterium nucleatum</i> ssp. <i>vincentii</i>
GCF	Gingival Crevicular Fluid
gDNA	Genomic DNA
GDP	Guanosine diphosphate
GTP	Guanosine triphosphate
HMDS	Hexamethyldisilazane
IBD	Inflammatory Bowel Disease
IL	Interleukin
LC-MS/MS	Liquid Chromatography-Tandem Mass Spectrometry
LLOQ	Lower Limit of Quantification
NTC	No Template Control
OD	Optical Density
PBS	Phosphate Buffered Saline
PCR	Polymerase Chain Reaction
PDE	Phosphodiesterase
PG	<i>Porphyromonas gingivalis</i>
ppGpp	Guanosine 5'-diphosphate, 3'-diphosphate
pppGpp	Guanosine 5'-triphosphate, 3'-diphosphate
QQ	Quorum Quenching
qRT-PCR	Quantitative Reverse Transcription - Polymerase Chain Reaction
QS	Quorum Sensing
rRNA	Ribosomal RNA

SAA	Schaedler Anaerobe Agar
SAB	Schaedler Anaerobe Broth
SEM	Scannin Electron Microscopy
SM	<i>Streptococcus mitis</i>
SR	Stringent Response
SS	<i>Streptococcus sanguinis</i>
TNF- $\alpha$	Tumor Necrosis Factor Alpha

# **CHAPTER 1: INTRODUCTION**

## 1.1. *Fusobacterium nucleatum*

*Fusobacterium nucleatum* is a Gram negative, anaerobic rod with tapered ends. *F. nucleatum* does not form spores and is non-motile (Brennan and Garrett, 2019). It belongs to the phylum *Fusobacteria* (Signat *et al.*, 2011). Some authors consider it to be a commensal (Han, 2015), while others label it as an opportunistic pathogen (Brennan and Garrett, 2019). *F. nucleatum* is one of the most numerous species found in the oral cavity of humans. It is a well-known resident of dental biofilms, playing a very important structural role (Huang, Li and Gregory, 2011).

The Atlas of Oral Microbiology states that the length of *F. nucleatum* is 0.4-0.7  $\mu\text{m}$  x 3-10  $\mu\text{m}$ . The size of colonies is 1-2 mm in diameter. The shape of the colonies is rounded or slightly irregular, translucent, and the bacteria produce a typical foul odour on blood agar plates. Haemolysis is not observed on blood agar. Despite being an anaerobe, it was shown that *F. nucleatum* can survive exposure to an oxygen containing environment for at least 100 minutes (Atlas of Oral Microbiology, 2015, p.77-80).

*F. nucleatum* species include five known subspecies to date: *animalis*, *fusiforme*, *nucleatum*, *polymorphum* and *vincentii*. *F. nucleatum* ssp. *nucleatum* further includes two strains, ATCC 25586, which is the type strain, and ATCC 23726, which is the most genetically tractable subspecies to date (Brennan and Garrett, 2019). It has been reported that ssp. *fusiforme* and ssp. *vincentii* are mostly found in healthy sites while ssp. *animalis* and *nucleatum* are associated with diseased state (Han, 2015), not only in the oral cavity.

### 1.1.1. *F. nucleatum* and human diseases

*F. nucleatum* has been associated with oral and periodontal disease of varying seriousness – from halitosis through gingivitis to periodontitis (Fig. 1.1.). Halitosis, or bad breath, is unpleasant and might affect an individual's self-confidence and relationships (Aylikci and

Çolak, 2013; Liu *et al.*, 2013). Gingivitis, inflammation of the gums, is caused by the build-up of dental plaque and is usually a reversible state. However, when left untreated, it can progress to periodontitis, a chronic inflammation of the gingival (gum) tissue linked with the irreversible damage of the tissues supporting the tooth, resulting in the loss of the tooth (Erchick *et al.*, 2019). This condition is debilitating and decreases the quality of life of an individual. Moreover, severe periodontitis belongs to the group of diseases affecting the highest number of people being the sixth most common condition worldwide (De Andrade, Almeida-Da-Silva and Coutinho-Silva, 2019).

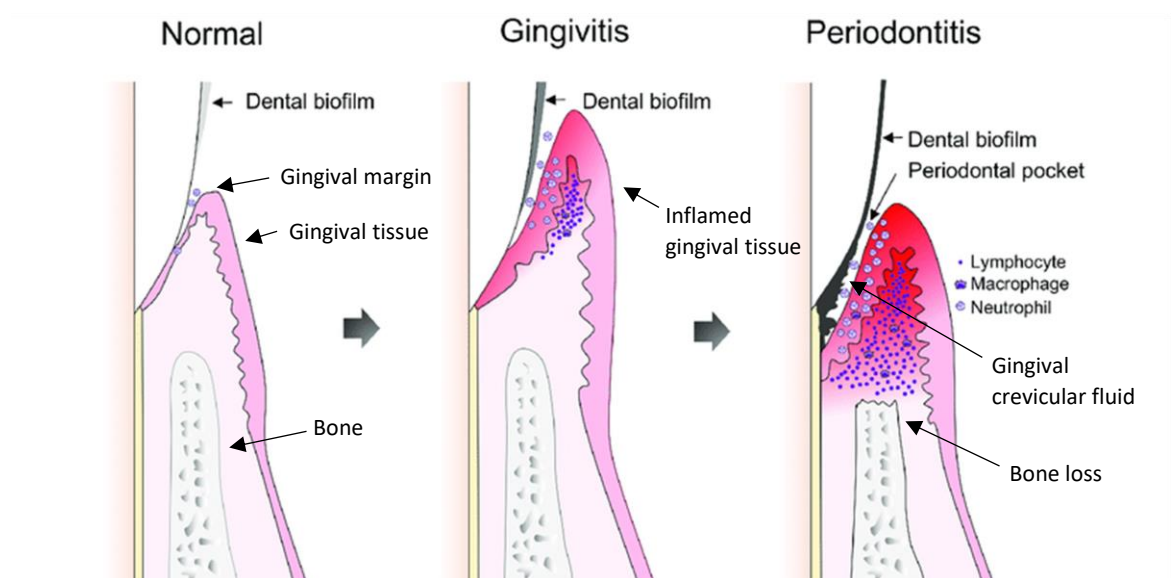


**Figure 1.1. Progression from healthy state through gingivitis to periodontitis.** In the healthy state, the tooth surface is covered with the commensal microbiota. In gingivitis, the inflammation in the gingival tissue is initiated. In periodontitis, a periodontal pocket filled with gingival crevicular fluid is formed and a pathogenic biofilm colonises the site. An aggressive immune response is employed by the host tissue, leading to bone tissue loss. (Adapted from Kriebel *et al.*, 2018)

Apart from its disease-producing activities in the oral cavity, *F. nucleatum* has been found to be involved in infections in multiple extraoral sites. This species is the most common bacterium originating in the oral cavity causing adverse pregnancy outcomes, such as preterm labour,

retardation of the foetus growth in the uterus or miscarriage (Han, 2015) . Reports show that *F. nucleatum* was able to move from the mother's dental plaque to the placenta and foetus and has been confirmed to elicit inflammation leading to the death of the foetus (Han, 2015). The subspecies that has been mostly isolated from intrauterine infections is ssp. *animalis*, followed by a few cases of ssp. *polymorphum* infection (Han, 2015).

Additionally, *F. nucleatum* was found to play a role in gastrointestinal (GI) disorders. To start with, it has recently become the main research subject of cancer scientists studying its relation to colorectal cancer (CRC). *F. nucleatum* was identified in increased numbers in tumours when compared to the adjacent healthy tissues. It was often detected together with other oral microbes, such as *Peptostreptococcus* and *Leptotrichia* species. Surprisingly, multiple studies showed that this species is a driving, causative agent, rather than a passive member of a more complex network (Brennan and Garrett, 2019).

When it comes to the GI tract, *F. nucleatum* has not only been associated with CRC, but also appendicitis and inflammatory bowel disease (IBD) (Han, 2015; Brennan and Garrett, 2019). Biopsies from inflamed colonic tissues from IBD patients confirmed the presence of this oral bacterium (Han, 2015). Moreover, Liu and the collective showed that *F. nucleatum* worsens the tissue damage in ulcerative colitis, a form of IBD, and modulates the localised immune response in the intestine (Liu *et al.*, 2019).

*F. nucleatum* has also been found to be involved in other systemic diseases, such as cardiovascular disease. It is one of the most prevalent oral microbes isolated from ruptured aneurysms in the brain and it is very often found in atherosclerotic plaques. Furthermore, together with *Fusobacterium necrophorum*, it is the main causative agent of Lemierre's Syndrome, an infection of the upper respiratory tract, which can have life threatening complications in young adults, who were previously healthy (Han, 2015).

Interestingly, *F. nucleatum* subspecies also have the ability to actively invade host cells. Active invasion means that they do not rely on a compromised mucosal layer or a viral infection, but they possess specific factors enabling them to invade independently. Based on the available, yet limited literature, the most studied factor facilitating invasion is an outer membrane protein FadA, characterised as an invasin and adhesin. FadA is followed by another adhesin, RadD, which is also associated with invasion into host cells (McGuire *et al.*, 2014). Furthermore, short, membrane-embedded protein domains known as MORN2 (membrane occupation and recognition nexus) were identified and found to be enriched in active invaders, thus considered to be important for invasion (McGuire *et al.*, 2014; Umana *et al.*, 2019). When it comes to the dissemination from the oral cavity, it was proposed that FadA binds to vascular endothelial cadherins, cell-junction molecules. This binding loosens the tight junctions between the endothelial cells, increasing the permeability of the blood vessels and allowing *F. nucleatum* and possibly other microbes to enter the circulation and colonise extraoral sites, such as the placenta. This shows that *F. nucleatum* is disseminated from the human mouth hematogenously (Vander Haar *et al.*, 2018).

*F. nucleatum* originating in the oral cavity does not occupy this niche on its own. It forms complex polymicrobial communities with other microbes present in the oral cavity known as dental plaque. It has been reported that between 700 and 1000 different bacterial species have been identified in the human mouth (Cate, 2006; Larsen and Fiehn, 2017). In individuals with poor dental hygiene, these bacterial species including *F. nucleatum* can aggregate into dental plaque, also known as dental biofilm, creating a perfect environment for the development of periodontal disease, as detailed above (Larsen and Fiehn, 2017). Moreover, the dental biofilm can act as a reservoir of *F. nucleatum* and other invasive species, which can disseminate and cause systemic infections. Taking into account the causative role of *F. nucleatum* in various

systemic diseases and its ability to invade host tissues, it is imperative that the pathogenicity of this bacterial species, when present in dental biofilms, is studied in more detail.

## **1.2. Dental biofilm**

As implicated above, dental plaque is a specific type of biofilm, that it why it is important to understand the general concept of a biofilm before focusing on the dental plaque and the role of *F. nucleatum* in it. A biofilm is defined as a very dynamic, multi-species community of microbes attached to a biotic or an abiotic substrate, embedded in an extracellular matrix (ECM) of polymers, such as polysaccharides, proteins, glycoproteins as well as extracellular DNA (eDNA) provided by the resident microbes (Eroshenko, Vidyaeva and Kuttyrev, 2010; Karunakaran *et al.*, 2011). Some authors use the term “extracellular polymeric substance” (EPS) in place of ECM and these terms are interchangeable. Biofilms can be found as a natural, beneficial element in the human body, such as the intestinal microbiome (De Vos, 2015). However, biofilms can also be harmful when formed on artificial medical devices inserted into the human body, such as heart valves, hip joints, coronary stents or catheters (Orme *et al.*, 2006). Removal of harmful biofilms remains a challenge due to a number of reasons. The presence of the ECM increases the stability of the biofilms and the adhesion to the substrate, making it harder to disrupt the biofilms (Karunakaran *et al.*, 2011). Also, the heterogeneous nature of the polymers forming the ECM complicates the existing enzymatic removal of biofilms, decreasing the efficacy of the enzymatic cleaners (Stiefel *et al.*, 2016). Additionally, an increased antimicrobial resistance prevents the biofilm removal, despite more and more research focusing on these polymicrobial communities. Bacteria in biofilms are resistant to antibiotics due to multiple reasons. Cate (2006) in his review sets forth four main causes of resistance. Firstly, penetration of the antibiotic substance is limited due to the shielding effect

of the ECM. Secondly, the resident microbes are able to turn on the adaptive stress response. Thirdly, a mixed population in the biofilm shows physiological differences, which allow the survival of the bacteria. Additionally, some bacterial cells can exist as persisters, a dormant subgroup highly resistant to antibiotics (Cate, 2006).

Dental biofilm can exist either as a friend or a foe. When it comes to its beneficial role, it hosts commensal bacteria, such as *Streptococci* or *F. nucleatum*, which colonise the tooth surface and the mucosa and protect the tissue from pathogens, which are present as a minority. However, certain factors, such as age, diet, medication, insufficient oral hygiene, weakened local and/or systemic immunity or a combination of these factors can allow the pathogens to outnumber the commensals, thus resulting in the development of a diseased biofilm. Additionally, commensals like *F. nucleatum* can turn into opportunistic pathogens, supporting the build-up of diseased biofilm when the conditions change. A pathogenic biofilm can lead to demineralisation of the tooth tissue causing dental caries (Bowen *et al.*, 2018). Pathogens in the plaque can also cause and exacerbate the abovementioned periodontal disease, namely gingivitis and periodontitis. The pathogenic type of biofilm leading to gingivitis and periodontitis is found on the tooth surface, either above (supragingival biofilm) or below the gingival margin (subgingival biofilm). Subgingival biofilms are found in so-called periodontal pockets, where they are in a close contact with the gingival tissue (Fig. 1.1.) (Kriebel *et al.*, 2018).

Clinicians face multiple challenges when trying to prevent and treat periodontal disease due to the antimicrobial resistance of the dental biofilm. At present, non-surgical treatment of periodontitis involves mechanical removal of plaque, which might harden into calculus, which is not possible to remove with a toothbrush. The plaque removal, also known as scaling, can be performed with hand and ultrasonic instruments. However, bacteria can recolonise the site within a week (Sahni *et al.*, 2012). To lower the recolonization, the use of antimicrobials

disinfecting the oral cavity is added to the mechanical removal. Additionally, depending on the progression of the disease, systemic antibiotics can be prescribed. However, excessive use of antibiotic substances might cause an increase in antibiotic resistance, which is already seen in dental biofilms, and might lead to further side effects (Sahni *et al.*, 2012). This is why alternative modes of treatment of periodontal disease, which do not cause antibiotic resistance, need to be identified. Additionally, key microbes found in the oral biofilm have to be studied in more depth. *F. nucleatum* has been found to be one of these key bacterial species affecting the switch from a helpful to a harmful type of dental biofilm.

#### 1.2.1. Role of *F. nucleatum* in the dental biofilm

*F. nucleatum* has been found to be a very important structural component of the dental biofilm. As discussed earlier, it possesses multiple adhesins, which allow this species to attach to other residents of the dental biofilm as well as to host cells. Thanks to these adhesion molecules, *F. nucleatum* acts like a bridging organism, initially adhering to the Gram-positive early colonisers of the tooth surface, such as *Streptococcus* species. If the equilibrium exists between the microbes and the host's immune response, this bacterial aggregation is considered to be a healthy state. However, if the equilibrium is disturbed and dysbiosis occurs, the attachment of *F. nucleatum* provides an ideal surface for the Gram-negative late colonisers to bind, such as *Porphyromonas gingivalis*, a true pathogen (Lima, Shi and Lux, 2017). In this way, *F. nucleatum* brings together the early and late colonisers that otherwise would not attach to each other (Park *et al.*, 2016). Thus *F. nucleatum* can orchestrate the shift from Gram-positive protective microbiota to a predominantly Gram-negative pathogenic biofilm.

The shape of *F. nucleatum* also makes it an ideal and versatile binding partner. From the studies looking at interspecies interactions in dental biofilms, it was proposed that the length of the

bacterium strengthens the structural relationships in the biofilm. When *F. nucleatum* was co-cultured with *Streptococcus sanguinis*, at least ten *S. sanguinis* cells were found attached to the surface of one *F. nucleatum* cell, creating a corncob-like structure (Brennan & Garrett, 2019). Its importance in the growth and maturation of a dental polymicrobial community was further confirmed by an *in vitro* study of a supragingival biofilm model, in which the total number of colony forming units (CFU) significantly declined when *F. nucleatum* was not present (Thurnheer *et al.*, 2019).

The evidence shows that *F. nucleatum* is essential in the dental biofilm build-up, which makes it an ideal therapeutic target. In order to find the most efficient approach and treatment strategy, it is necessary to discern the multi-step process of dental biofilm assembly.

#### 1.2.2. Pathogenic dental biofilm assembly, structure and virulence of the residents

Dental biofilm is unique in that the microbes do not just randomly adhere to the surface and to each other. Each species has a specific role at a specific stage of biofilm formation.

To initiate the biofilm assembly, the oral microbes need glycoproteins from the saliva of the host to attach to (Fig. 1.2.). The surface of the tooth is naturally covered with saliva, which creates a proteinaceous pellicle on the clean enamel. The early colonisers include *Actinomyces*, *Streptococcus*, *Capnocytophaga*, *Veillonella* and *Haemophilus* species (Huang, Li and Gregory, 2011). These commensals, which are planktonic at this stage, reversibly bind to the glycoproteins in the pellicle. Once the chemical forces aid in the irreversible attachment, the bacteria start producing ECM, which strengthens the structural relationship of the early colonisers and the attachment to the surface. These species have a protective role as they fill in the empty spaces and prevent pathogens from attacking both the soft and hard host tissue (Huang, Li and Gregory, 2011).

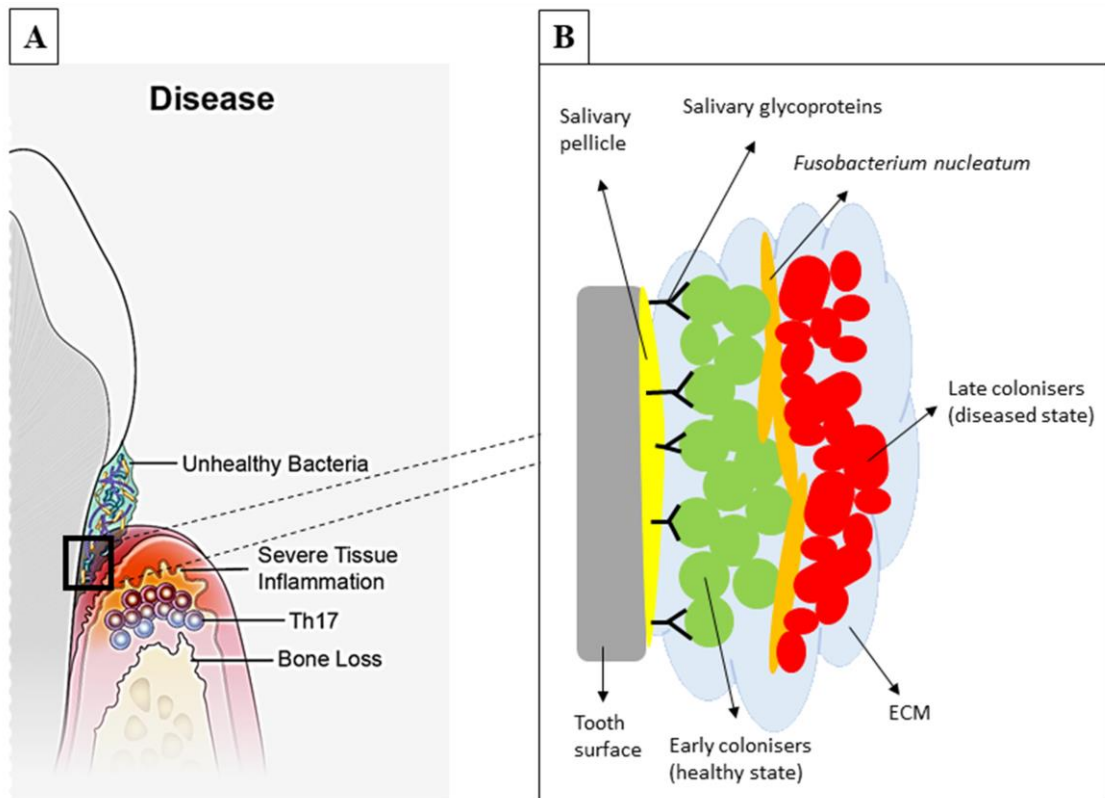


**Figure 1.2. Schematic representation of (A) a periodontal disease site and (B) the subgingival biofilm.** (A) Disease-related dental plaque forms on the surface of the tooth, especially in the periodontal pocket. The presence of pathogens elicits an aggressive immune response, leading to a severe tissue inflammation and bone tissue loss. (B) Enlarged section of the disease-related biofilm (unhealthy bacteria) from panel A adhered to the salivary pellicle on the tooth surface. Early colonisers (green cocci) attach to the glycoproteins in the salivary pellicle. *F. nucleatum* (orange rods) and other intermediate colonisers can attach to the adhesin proteins of the early colonisers and provide binding surface for the late colonisers (red cocci and coccobacilli), pathogens of the red complex. Bacteria are enclosed in the ECM. The biofilm is washed by GCF, which is not present in the figure.

When the first layer of biofilm is anchored, the maturation step can occur. At this stage, intermediate colonisers, such as *Fusobacterium*, *Corynebacterium* species and *Aggregatibacter actinomycetemcomitans*, aggregate with the pioneer colonisers attaching to their adhesion receptors, further enhancing the biofilm's structural stability and maturation (Huang, Li and Gregory, 2011). *F. nucleatum* in periodontitis-related biofilms was found to secrete serine proteases, which damage the host tissue, degrade immunoglobulin A (IgA) and help obtain

nutrients (De Andrade, Almeida-Da-Silva and Coutinho-Silva, 2019). *F. nucleatum*, being the key bridging organism, allows the co-aggregation of the late colonisers, such as *P. gingivalis*, *Tannerella forsythia* and *Treponema denticola*. These species belong to a so-called “red complex”, comprising obligate anaerobes which are key in periodontal disease (Nayak *et al.*, 2018). The microbes of the red complex express specific virulence factors and promote an aggressive immune response by inducing the proinflammatory mediators of the host. The main virulence factors produced by *P. gingivalis* are gingipains, which play a role in nutrient acquisition and damage of host tissues (Dominy *et al.*, 2019). *T. forsythia* expresses cell surface proteolytic enzymes, cell envelope lipoproteins and cell surface (S)-layer suppressing immune clearance, to name a few (Chukkapalli *et al.*, 2015). One of the most versatile virulence factors of *T. denticola* seems to be dentilisin, involved in adherence, suppression of the immune response and degradation of host gingival tissue (Ishihara, 2010). The proinflammatory mediators induced by the red complex microbes are IL-1, IL-6, IL-8 and TNF- $\alpha$  (De Andrade, Almeida-Da-Silva and Coutinho-Silva, 2019). The exacerbated tissue inflammation caused by these cytokines, which is usually not successfully resolved, leads to the irreversible damage of the supportive tissues of the teeth. Based on this knowledge, it is clear that not only bacterial virulence factors are responsible for the development and progression of periodontitis, but also an excessive immune response of the host tissue, which worsens the tissue damage (De Andrade, Almeida-Da-Silva and Coutinho-Silva, 2019).

This highly complex subgingival pathogenic biofilm is located in the periodontal pocket, an environment which favours the growth of pathogenic anaerobes. As the disease progresses, the depth of the pocket increases because the bone tissue is gradually lost, the connective tissue is disorganised and the gingival tissue recedes (Jati, Furquim and Consolaro, 2016). The periodontal pocket site is constantly washed with gingival crevicular fluid (GCF), an exudate

from the inflamed tissues. It contains serum as well as the proinflammatory cytokines and antibodies against the pathogenic microbes. However, it also contains nutrients which the anaerobic bacteria can use for their growth in this niche. (Cate, 2006). Micrographs of mature biofilms revealed distinct channels, which facilitate the distribution of nutrients and removal of waste products. This means that the pathogens have a constant supply of nutrients (Huang, Li and Gregory, 2011). The acquisition of nutrients as well as waste disposal are not random and have to be regulated in such a complex system. Biofilms are indeed very sophisticated, coordinated communities and the resident bacteria have been found to communicate on multiple levels.

### **1.3. Communication in the dental biofilm**

In order for the bacteria to coordinate their metabolic activities in the subgingival biofilms, they communicate using a specific system known as quorum sensing (QS). This type of communication allows individual bacteria to sense the density of bacterial cells around them and adjust their gene expression according to the changes in the environment. This type of communication is considerably well studied in both Gram-positive and Gram-negative bacteria (Plančak, Musić and Puhar, 2015).

In addition to QS, bacteria in the thick layer of dental biofilm have to adapt to changing microenvironments which might induce a stress response, such as nutrient deprivation, undesirable pH and harmful oxygen levels. Communication during this stress response, which is known as a stringent response, is facilitated by alarmones, a set of second messengers involved in biofilm formation, sporulation and production of virulence factors (Ronneau and Hallez, 2019).

The third system that has recently been found in the periodontal biofilms is the use of cyclic dinucleotides (CDNs). CDNs are small molecules used as second messengers by various bacterial species. They are involved in multiple processes, such as cell wall homeostasis, metabolism, sporulation and most importantly, in biofilm formation (Dias da Purificação *et al.*, 2020).

### 1.3.1. *Quorum sensing (QS) in dental biofilms*

QS is a well characterised intracellular type of signalling via the secretion of a signalling molecule. Bacteria living in communities produce and secrete small signalling molecules called autoinducers. The concentration of the autoinducer increases as the number of bacteria in the community increase. When the autoinducer concentration reaches the detection level, bacteria sense it with specific receptors and alter their gene expression depending on survival requirements (Plančak, Musić and Puhar, 2015; Verbeke *et al.*, 2017).

The inter-species communication used by both Gram-positive and Gram-negative bacteria utilises autoinducer-2 (AI-2). The universal AI-2 is synthesised by the enzyme LuxS and binds to a sensor LuxP (Sun *et al.*, 2004). Interestingly, the system using AI-2 has been found to be the primary system used by periodontal pathogens, controlling the aggregation of bacteria and thus biofilm formation (Jang *et al.*, 2013). It was discovered that commensals synthesise AI-2 at very low levels (pM), however pathogenic bacteria synthesise and sense AI-2 at significantly higher concentrations. The increase in the production of AI-2 prevents the growth of a protective microbiota and helps the pathogens to flourish, supporting the build-up of subgingival plaque and the development of periodontitis (Jang *et al.*, 2013). QS inhibitors have been studied and found to reduce biofilm formation as well as the virulence of the bacteria in the biofilm. However, the use of QS inhibitors, also known as Quorum Quenching (QQ) molecules, could interfere with vital regeneration of the tissues. Secondly, numerous studies

listed by Krzyżek, (2019) showed the QQ caused increased virulence, more specifically biofilm formation in bacteria such as *A. actinomycetemcomitans*. Thirdly, it was shown that bacteria such as *Pseudomonas aeruginosa* can develop resistance to the QQ substances by increasing the number of efflux pumps removing the inhibitors from the cells (Krzyżek, 2019). It is highly likely that other bacterial species might react in the same way. This shows that targeting the QS in dental biofilms might not bring the desirable result.

### 1.3.2. *Stringent response and alarmones*

In order to survive challenging conditions, bacteria evolved systems which are employed during stressful conditions. The stress response induced by nutritional and environmental changes is known as the stringent response (SR). This can occur in localised microenvironments such as the subgingival biofilm, when the amount of nutrients supplied by the GCF sharply decreases or when the waste products of certain species change the pH of the ECM. Communication in the SR follows a similar pattern to that observed in QS: communication molecules are synthesised, their concentration increases, bacteria sense the accumulation and remodel the gene expression based on the stress perceived. The SR uses small molecules known as alarmones, hyperphosphorylated nucleosides ppGpp (guanosine 5'-diphosphate, 3'-diphosphate) and pppGpp (guanosine 5'-triphosphate, 3'-diphosphate) (Germain *et al.*, 2019; Ronneau & Hallez, 2019). Because these alarmones occur together, they are collectively known as (p)ppGpp. Enzymes which regulate the concentration of (p)ppGpp are RelA-SpoT homologues (RSH). These enzymes are bifunctional. The synthase domain produces (p)ppGpp from either GTP or GDP and ATP and the hydrolase domain degrades (p)ppGpp to pyrophosphate and either GTP or GDP (Hauryliuk *et al.*, 2015; Kim and Davey, 2020). The genes encoding RelA-SpoT are highly conserved across bacterial species, that is why multiple

groups study these homologues in various bacteria, such as *Escherichia coli*, *Bacillus subtilis*, *Streptococcus pneumoniae* and *Enterococcus faecalis* (Abranches *et al.*, 2009). Alarmones regulate multiple cellular responses related to nutrient and environmental changes, such as resistance to antibiotics, expression of virulence factors, persistence, colonisation and formation of biofilms. That is why researchers became interested in the function of alarmones in periodontal pathogens, such as *P. gingivalis*. It was recently discovered that *P. gingivalis* mutants lacking the genes for RSH enzymes produced significantly more biofilm mass as well as an increased amount of ECM (Kim and Davey, 2020). The effect of alarmones in *F. nucleatum* biofilms has not been studied yet.

### 1.3.3. Cyclic di-nucleotides (CDNs)

Apart from the abovementioned communication systems, bacteria in biofilms were also found to communicate using cyclic di-nucleotides (CDNs). CDNs belong to the group of nucleotide-based second messengers. These small molecules were reported to be very important in processes leading to bacterial attachment and maturation of biofilms (Gürsoy *et al.*, 2017). Two second messengers have been identified in biofilm regulation to date: cyclic di-GMP and cyclic di-AMP.

Cyclic di-GMP (cyclic dimeric guanosine monophosphate) is the more characterised CDN. It is believed that it coordinates the biofilm formation by regulation of EPS, adhesins and fimbriae synthesis. C-di-GMP is produced by diguanylate cyclases (DGCs) and degraded by phosphodiesterases (PDEs). Generally, DGCs have a specific GGD/EEF domain, characteristic for these enzymes. PDEs have an EAL or HD-GYP domain. Interestingly, these domains have been found to be absent in *F. nucleatum*, which makes it more challenging to identify and study the activity of these enzymes in this organism (Gürsoy *et al.*, 2017).

Cyclic di-AMP (cyclic dimeric adenosine monophosphate) has only recently become a molecule of interest when it comes to the study of biofilm formation (Gürsoy *et al.*, 2017). It was initially found in association with the DisA (DNA integrity scanning) protein looking for double-stranded DNA breaks. The N-terminal of DisA was confirmed to be a diadenylate cyclase, synthesising c-di-AMP from two molecules of ATP. C-di-AMP is hydrolysed by PDEs as it is in the case of c-di-GMP (He *et al.*, 2020).

Gürsoy and colleagues (2017) reported that increased levels of intracellular c-di-GMP in general cause the build-up of the biofilm. A similar effect was seen when the level of c-di-AMP was studied in *Streptococcus mutans* (Peng *et al.*, 2016). This indicates that inhibition of production and decreasing the level of CDNs could lead to biofilm reduction. Studies showed that the deletion of PDE enzymes increases the biofilm formation in *S. mutans* (Peng *et al.*, 2016) and *Streptococcus pyogenes* (Fahmi *et al.*, 2019). Additionally, mutant *S. pyogenes* lacking DacA, diadenylate cyclase, did not form any biofilm *in vitro* (Fahmi *et al.*, 2019).

The effect of CDNs was studied in periodontal pathogens such as *P. gingivalis* (Chaudhuri *et al.*, 2014) and *T. denticola* (Bian *et al.*, 2013). The studies confirmed that *P. gingivalis* lacking diguanylate cyclase had a significantly lower ability to adhere to surfaces coated with saliva. *T. denticola*, lacking the c-di-GMP binding protein, produced a decreased amount of biofilm.

Although the effect of CDNs in biofilm formation and virulence has been partly elucidated in the true periopathogens, their function in *F. nucleatum*, a key player in the periodontitis-related biofilm, remains elusive.

#### **1.4. Aims and objectives**

It is clear that pathogenic dental biofilms, more specifically the subgingival type causing periodontitis, is a worldwide problem. The patients affected with this disease experience

multiple issues, such as problems with speaking and chewing, subsequently decreasing the quality of their life. Moreover, it was suggested that periodontitis might be related to multiple systemic diseases and worsen the prognosis of the patients suffering from CRC, IBD or cardiovascular diseases. Multiple periopathogens were studied in the context of bacterial communication using CDNs and biofilm disruption. Considering that *F. nucleatum* is a key organism in the formation of periodontitis-related biofilms, it is surprising that the amount of literature focusing on the communication of this microbe in biofilms and potential biofilm disruption is, to date, very limited.

That is why this project aimed attention at characterisation of *F. nucleatum* communication by means of CDNs in all known subspecies.

#### 1.4.1. Objectives

- Initially, all subspecies were characterised in detail.
- Secondly, their ability to grow in single-species biofilms was assessed.
- Additionally, the growth of two subspecies, namely *F. nucleatum* ssp. *nucleatum* and *F. nucleatum* ssp. *polymorphum* was analysed in a model of multi-species, periodontitis-related biofilm.
- The expression of genes related with synthesis and hydrolysis of CDNs and alarmones was analysed using qRT-PCR. In order to identify the target genes analysed in this project, a curated repository of corrected *Fusobacterium* genomes called FusoPortal (Sanders *et al.*, 2018; Todd *et al.*, 2018) was used.
- Lastly, the amount of CNDs produced by each subspecies grown on agar plates and in single-species biofilms was quantified.

Understanding the involvement of CDNs in the aggregation of *F. nucleatum* and in the formation of subgingival biofilm might provide new therapeutical targets for the treatment and prevention of periodontitis as well as related systemic diseases.

## **CHAPTER 2: MATERIALS AND METHODS**

## 2.1. Growth of bacteria

All bacteria used in this study were obtained from the Oral Microbiology Group culture collection and are listed in table 2.1. The following species were grown at 37°C in an anaerobic chamber (80% N<sub>2</sub>, 10% CO<sub>2</sub> and 10% H<sub>2</sub>; Don Whitley DG250 Anaerobic Workstation, Don Whitley Scientific, Bingley, UK): *Fusobacterium nucleatum* ssp. *animalis* ATCC 51191, *fusifforme* ATCC 49256, *nucleatum* ATCC 23726, *nucleatum* ATCC 25586, *polymorphum* ATCC 10593 and *vincentii* ATCC 49256; *Porphyromonas gingivalis* W83. All *F. nucleatum* subspecies were grown on Schaedler anaerobe agar (SAA; Sigma-Aldrich, 91019) for 48 hours.

*P. gingivalis* was grown on Blood agar plates (Oxoid, PB0114) for at least 96 hours.

*Escherichia coli* ATCC 10536 and *Streptococcus sanguinis* ATCC 10556 were grown at 37°C in 5% CO<sub>2</sub> on Brain Heart Infusion agar (Oxoid, CM1136) overnight. *Streptococcus mitis* ATCC 49456 and *Aggregatibacter actinomycetemcomitans* ATCC 43718 were grown at 37°C in a 5% CO<sub>2</sub> incubator (Heracell™ 150i, Thermo Scientific) on Blood agar plates.

Liquid cultures for experiments were grown as follows: the abovementioned anaerobic bacterial species were grown stationary in an anaerobic chamber at 37°C in Schaedler anaerobe broth (SAB; Oxoid, CM0497) overnight. *E. coli*, *S. sanguinis*, *S. mitis* and *A. actinomycetemcomitans* were grown in Brain Heart Infusion broth (Oxoid, CM1135) in a shaking incubator (100 rpm; NB-205, N-BIOTEK) at 37°C overnight.

Bacterial species	Strain	Growth conditions	Growth media	
			Agar	Broth
<i>Aggregatibacter actinomycetemcomitans</i>	ATCC 43718	5 % CO <sub>2</sub>	Blood	Brain Heart Infusion
<i>Escherichia coli</i>	ATCC 10536	5 % CO <sub>2</sub>	Brain Heart Infusion	Brain Heart Infusion
<i>Fusobacterium nucleatum</i> ssp. <i>animalis</i>	ATCC 51191	Anaerobic	Schaedler anaerobe	Schaedler anaerobe
<i>Fusobacterium nucleatum</i> ssp. <i>fusiforme</i>	ATCC 49256			
<i>Fusobacterium nucleatum</i> ssp. <i>nucleatum</i>	ATCC 23726			
<i>Fusobacterium nucleatum</i> ssp. <i>nucleatum</i>	ATCC 25586			
<i>Fusobacterium nucleatum</i> ssp. <i>polymorphum</i>	ATCC 10593			
<i>Fusobacterium nucleatum</i> ssp. <i>vincentii</i>	ATCC 49256			
<i>Porphyromonas gingivalis</i>	W83		Blood	Schaedler anaerobe
<i>Streptococcus mitis</i>	ATCC 49456	5 % CO <sub>2</sub>	Blood	Brain Heart Infusion
<i>Streptococcus sanguinis</i>	ATCC 10556		Brain Heart Infusion	Brain Heart Infusion

**Table 2.1. List of bacterial species used in this study.** This table summarizes specific strains used for experiments together with their optimal growth conditions and growth media. All strains are stored in the Oral Microbiology Group culture collection, School of Dentistry, University of Birmingham.

## 2.2. Growth curves of *Fusobacterium nucleatum* subspecies

### 2.2.1. Miles and Misra method

This method was using enumeration of bacterial colonies on agar plates representing the colony forming units in liquid bacterial culture developed by Miles and Misra (1938). Each *F. nucleatum* subspecies was inoculated into 10 ml of SAB and incubated in anaerobic conditions at 37°C for 15 hours. The overnight culture was diluted 100-fold in 10 ml of SAB to give a new sub-culture. 200 µl of the sub-culture was transferred to a 96-well plate and serially diluted

(dilution factor of 10) 7 times in PBS. 20 µl of the sub-culture (neat) and each dilution were plated on SAA plates in triplicate. The sub-culture was incubated in anaerobic conditions at 37°C for 48 hours. The dilution and plating procedure were performed at the time of the initial dilution (T0), after 2, 4, 6, 8, 24 and 48 hours (T2, T4, T6, T8, T24, T48). Agar plates were incubated in anaerobic conditions at 37°C for 48 hours, colonies were enumerated and the final number of bacteria was calculated using the following formula:

$$CFU/ml = \text{Average number of colonies for a dilution} \times 50 \times \text{dilution factor.}$$

### 2.2.2. Automated spectrophotometric method

This method was using the automatic microplate reader (Spark®, Tecan). *F. nucleatum* ssp. *nucleatum* was inoculated into 10 ml of SAB and incubated for 15 hours. The overnight culture was then diluted 10-fold in 1.5 ml SAB. 200 µl of the suspension was added to 5 wells of a transparent 96-well plate. Sterile SAA was used as a negative control/blank. The microplate was then sealed using non-breathable transparent foil and transferred from the anaerobic chamber into the pre-heated microplate reader (37°C). The instrument kept the temperature constant and measured the absorbance of the bacterial culture hourly for 48 hours, gently shaking the plate before each measurement.

### 2.3. Growth of *Fusobacterium nucleatum* subspecies in the presence of oxygen

FN subspecies were grown in SAB in anaerobic conditions for 15 hours and a sub-culture was prepared by serial dilution from approximately  $1 \times 10^8$  CFU/ml (determined previously) to  $1 \times 10^3$  CFU/ml. The sub-culture was further diluted and plated as stated in Miles and Misra method (section 2.2.1.) It was then removed from the anaerobic chamber and incubated with a loose lid in a shaking incubator at 37°C (100 rpm; NB-205, N-BIOTEK) to ensure the access of oxygen.

Dilution and plating were performed at the time of the initial dilution (T0) and then after 2, 4, 6, 8, 24 and 48 hours (T2, T4, T6, T8, T24, T48). The sub-culture was transferred to the anaerobic chamber for a short time at the time of each plating and then returned back to the shaking incubator. SAA plates were incubated at 37°C under anaerobic conditions for 48 hours, bacterial colonies were counted and the growth curves were plotted as described previously (see section 2.2.1. for calculation).

#### 2.4. Conventional polymerase chain reaction (PCR)

Conventional PCR was used to confirm *F. nucleatum* subspecies, as well as to confirm purity of RNA extracts and for primer validation. A mastermix was prepared as follows: 10 µl Q5® High-Fidelity 2X Master Mix (M0492, New England Biolabs), 5 µl nuclease-free water, 2 µl 10-fold diluted forward primer and 2 µl 10-fold diluted reverse primer. 19 µl mastermix were then combined with 1 µl either RNA or DNA sample. Samples were transferred to the thermal cycler (Veriti™ 96-well thermal cycler, 4375786, Applied biosystems) and incubated as per cycling conditions detailed in table 2.2. Amplified samples were run on a 1.5% agarose gel (BIO-41025, Biorline, Meridian Bioscience) either for 30 or 60 minutes at 120 V. Gels were visualised using a G:BOX (Syngene) and Gene Snap software (Syngene).

Temperature	Time	Cycles
98°C	30 s	1
98°C	15 s	
55°C	30 s	40
72°C	30 s	
72°C	5 min	1
15°C	∞	1

**Table 2.2. Cycling conditions for conventional PCR as used for all primers in this study.** Number of cycles or annealing temperature may differ during the course of PCR optimisation, modifications are stated in the results section at the corresponding PCR result.



## 2.6. Mono-species biofilm setup

Biofilms were set up using a well-established protocol (Millhouse *et al.*, 2014), which has been modified to suit the needs of this study. *F. nucleatum* subspecies were inoculated into 10 ml SAB and grown overnight in anaerobic conditions at 37°C. The culture was then centrifuged at 3000 x g for 10 minutes and the pellet washed once with 5 ml phosphate buffered saline (PBS). Bacteria were then resuspended in 10 ml PBS and the optical density of the culture was measured at 550 nm (Jenway 7315 Spectrophotometer). The optical density of the culture was then adjusted to a final OD<sub>550</sub> of 0.2 in artificial saliva (AS) (porcine stomach mucins 0.25% w/v [Sigma, M1778], sodium chloride 0.35% w/v [Fisher Scientific, BP358-1], potassium chloride 0.02% w/v [Sigma, P-9541], calcium chloride dihydrate 0.02% w/v [Sigma, C7902], yeast extract 0.20% w/v [Sigma, Y1001], lab lemco powder 0.10% w/v [Oxoid, L29], proteose peptone 0.50% w/v [Sigma, 82450]; urea added after autoclaving to a final concentration of 0.05% v/v [Sigma, U5378]) to reach a concentration of 1 x 10<sup>8</sup> CFU/ml of bacteria. The bacterial suspension was then transferred into multi-well plates - 5 ml per well in a 6-well plate for quantification of cyclic di-nucleotides, 500 µl per well in a 24-well plate with Nunc™ Thermanox™ 13 mm coverslips (174950, Thermo Scientific) for scanning electron microscopy and 200 µl per well in a 96-well plate for biofilm biomass quantification. Biofilms were then incubated stationary at 37°C in anaerobic conditions for 3, 5 and 7 days. AS was replaced every 24 hours and the biofilms were monitored for contamination (see Fig. 2.1.)

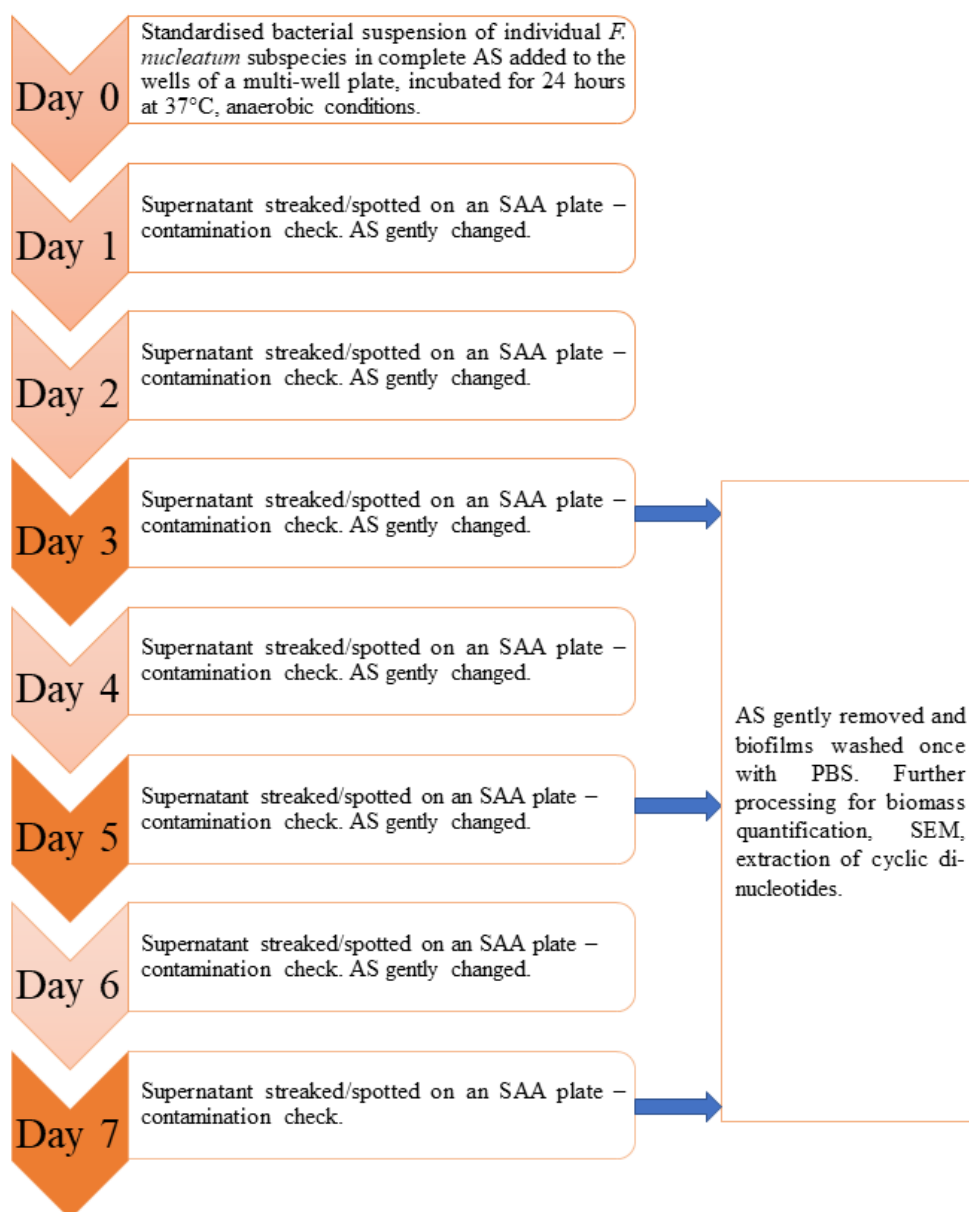


**Figure 2.1. Setup of mono-species *F. nucleatum* biofilm.** Biofilms were analysed after three, five and seven days of incubation. Adapted from Millhouse *et al.*, 2014.

## 2.7. Multi-species biofilm setup

The original protocol for multi-species biofilm setup was followed (Millhouse *et al.*, 2014; Ramage *et al.*, 2017). Two sets of biofilms were grown: the first set contained *F. nucleatum*

ssp. *polymorphum*, the second set contained *F. nucleatum* ssp. *nucleatum* ATCC 23726. Additionally, each biofilm set contained *S. mitis*, *P. gingivalis* and *A. actinomycetemcomitans*.

Standardisation of bacteria: each bacterial species was grown in a corresponding broth overnight (see section 2.1.), the culture was centrifuged at 3000 x g for 10 minutes and the pellet washed once with 5 ml PBS. The bacterial pellet was resuspended in 10 ml PBS, the OD of the suspension was measured and adjusted to OD<sub>550</sub> 0.5 (*S. mitis*) or 0.2 (*F. nucleatum*, *P. gingivalis*, *A. actinomycetemcomitans*) corresponding to 1 x 10<sup>8</sup> CFU/ml of bacteria. Each suspension was then diluted to the final concentration of 1 x 10<sup>7</sup> CFU/ml of bacteria in AS and transferred into multi-well plates – 200 µl per well in a 96-well plate for biofilm biomass quantification and 500 µl per well in a 24-well plate with Nunc™ Thermanox™ 13 mm coverslips for scanning electron microscopy.

Biofilm development: the standardised *S. mitis* suspension was incubated for 24 hours in multi-well plates at 37°C in 5% CO<sub>2</sub>. Biofilms were transferred to an anaerobic chamber, the AS was removed and standardised *F. nucleatum* was added. Biofilms were incubated for further 24 hours at 37°C in anaerobic conditions. Finally, the AS was removed and a combined, standardised suspension of *P. gingivalis* and *A. actinomycetemcomitans* was added. Resulting multi-species biofilms were then incubated for further 4 days, replacing the AS every 24 hours (see fig. 2.2.).

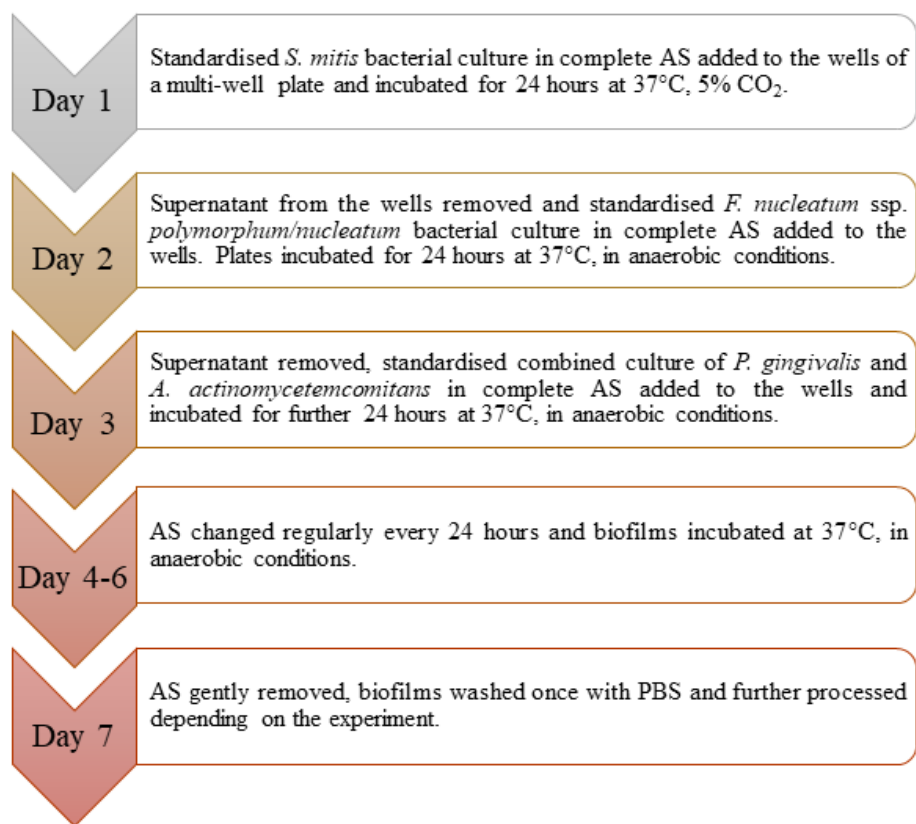


**Figure 2.2. Setup of multi-species biofilms.** Adapted from Millhouse *et al.*, 2014.

## 2.8. Preparation of biofilms and scanning electron microscopy (SEM)

Biofilms were grown in 24-well plates on Nunc™ Thermanox™ 13 mm coverslips for a desired time period. On the day of the preparation, biofilms were gently washed once with 500 µl PBS and subsequently treated with 500 µl fixative: 2.5% glutaraldehyde (electron microscopy grade, Agar Scientific, R1012) in 0.1M sodium cacodylate (Sigma, C0250) buffer, pH 7.3, for 10 minutes at room temperature. The fixative was removed and the biofilms were dehydrated with increasing ethanol concentrations: 20%, 30%, 40%, 50%, 60%, 70%, 90%, 95% two times and 100% two times, incubation time was 10 minutes at each step. Biofilms were then completely

covered with hexamethyldisilazane (HMDS), which was left to evaporate overnight. On the next day the coverslips were mounted onto aluminium specimen stubs (Agar Scientific, G301), sputter-coated with gold (Emitech K550x, Quorum technologies, Ltd.) and visualised using the scanning electron microscope (Zeiss EVO MA10).

## **2.9. Preparation of planktonic bacteria for scanning electron microscopy**

### *2.9.1. Bacteria visualised on Nunc™ Thermanox™ coverslips*

*F. nucleatum* subspecies were grown in SAB overnight in anaerobic conditions at 37°C. 100 µl of the overnight culture was pipetted onto a coverslip placed in a 24-well plate and the bacteria were allowed to adhere for 60 minutes. The liquid was then removed and the coverslips gently washed with 500 µl PBS to remove any non-attached bacteria. 200 µl of fixative was added to each well and incubated for 10 minutes at room temperature. Samples were then dehydrated, mounted, sputter-coated and visualised using the SEM in the same manner as biofilms (see 2.8.).

### *2.9.2. Bacteria visualised on Isopore™ membranes*

*F. nucleatum* subspecies were grown in SAB overnight in anaerobic conditions at 37°C. 1 ml of each overnight bacterial culture was pelleted at 2500 x g for 10 minutes and pellets were washed with 1 ml PBS. Samples were centrifuged, pellets resuspended in 400 µl fixative and incubated at room temperature for 10 minutes. After centrifugation at 2500 x g for 10 minutes, supernatants were discarded and bacterial pellets were incubated for 10 minutes in 400 µl of progressively increasing concentrations of ethanol (20%, 30%, 40%, 50%, 60%, 70%, 90%, 95% two times and 100%), undergoing centrifugation at 2500 x g for 10 minutes after each ethanol step. Pellets were then resuspended in 100% ethanol one more time, incubated for 10

minutes and 15 µl of each suspension were transferred onto an Isopore™ membrane mounted on an aluminium specimen stub. Membranes were then covered with 15 µl of HMDS, which was left to evaporate overnight. Samples were sputter-coated and visualised using the SEM in the same manner as biofilms (see section 2.8.).

## **2.10. Extraction and quantification of cyclic di-nucleotides from bacteria grown on agar plates**

Cyclic di-nucleotides were extracted according to a previously published protocol (Burhenne and Kaefer, 2013). Briefly, all *F. nucleatum* subspecies were grown on SAA for 2 days. The bacterial content of each plate was transferred and resuspended with a 10 µl loop into 1 ml SAB. Samples were centrifuged for 10 minutes at 3000 g, 4°C (Fisherbrand accuSpin Micro 17R, Fisher Scientific). Each pellet was resuspended in 900 µl SAB, divided into 3 Eppendorf tubes (300 µl each) and centrifuged 10 minutes at 3000 g, 4°C. The pellet was subsequently resuspended in 300 µl extraction solvent (acetonitrile/methanol/HPLC water – 2/2/1) and incubated on ice for 15 minutes. The suspension was then heated for 10 minutes at 95°C, centrifuged for 10 minutes at 16 000 g, 4°C, and the supernatant transferred into a 2 ml Eppendorf tube. The extraction was repeated 2 more times with 200 µl of the extraction solvent but omitting heating the samples at 95°C. Samples of a total volume of 700 µl were incubated overnight at room temperature, then centrifuged at 16 000 g, 4°C, the supernatant was transferred into a new 2 ml tube and the liquid left to evaporate in a fume hood. Protein pellets obtained after centrifugation were used for BCA protein assay.

## **2.11. Extraction and quantification of cyclic di-nucleotides from single-species biofilms**

The protocol described in section 2.10. was modified to suit the needs of the metabolite extraction from biofilms. Biofilms were grown for five and seven days. AS was removed slowly and carefully not to detach the biofilm layer. Biofilms were washed with 1 ml PBS by slowly dripping onto the wall of the well. PBS was gently removed, 2 ml of SAB were added into each well and biofilms were detached by vigorous pipetting. At this stage, biofilms were checked for contamination by Gram staining and streaking onto SAA plates. When purity was confirmed, biofilm suspensions were collected into a universal tube and centrifuged at 3000 x g for 10 minutes. The pellet was resuspended in 1 ml of SAB, transferred into an Eppendorf tube and centrifuged at 3000 x g, 4°C for 15 minutes. The pellet was resuspended in 900 µl, the suspension was divided into 3 Eppendorf tubes and centrifuged at 3000 x g, 4°C for 15 minutes. Each pellet was resuspended in 300 µl of extraction solvent and incubated on ice for 15 minutes. CDNs were then extracted as described in section 2.10.

## **2.12. Bicinchoninic acid (BCA) protein assay**

Protein content in samples used for quantification of cyclic di-nucleotides was measured using the Pierce™ BCA Protein Assay Kit (Thermo Scientific, 23227), following the manufacturer's instructions. In short, Albumin (BSA) standards were diluted in RNase/DNase free water according to the protocol and transferred into a 96-well plate in triplicates. Protein pellets of the samples were resuspended in 75 µl of RNase/DNase free water and 25 µl of each sample were transferred into a 96-well plate in triplicates. Each sample and standard were mixed with 200 µl of Working Reagent prepared by mixing 50 parts of Reagent A with 1 part of Reagent B. Plates were mixed on a plate shaker (R100/TW Rotatest Shaker, Luckham Ltd.; speed level

3) for 30 seconds, incubated at 37°C for 30 minutes and the absorbance was measured at 562 nm (Microplate reader, Spark, Tecan).

### **2.13. Biomass quantification using crystal violet stain**

The amount of biofilm formed was quantified as follows: biofilms were grown in a 96-well cell culture plate for a desired time period and on the day of the quantification washed once with 200 µl PBS. Biofilms were then air-dried for one hour at 37°C. 200 µl of a crystal violet (CV) solution (0.05 % w/v) were added to each well and incubated for 30 minutes at room temperature. The CV solution was removed, biofilms were rinsed once with 200 µl of PBS to remove excess stain and air-dried for one hour at 37°C. 200 µl of 100% ethanol were added to each well to de-stain the biofilms and the plate was gently shaken for one hour on a plate shaker (R100/TW Rotatest Shaker, Luckham Ltd.; speed level 3). The content of each well was transferred into a new 96-well plate and the absorbance was measured at 600 nm using a spectrophotometer (Universal microplate reader ELx800, BioTek Instruments, Inc; software Gen5 1.11, BioTek Instruments, Inc).

### **2.14. RNA extraction**

RNA extractions were performed according to manufacturer's instructions included in each kit with minor modifications stated below. Centrifugation steps when using kits in sections 2.14.1. and 2.14.2. were performed at 16 000 x g, in section 2.14.3. and 2.14.4. at 8000 x g. The number of bacterial cells used for each extraction was  $1 \times 10^9$ , unless stated otherwise in the results section. Quality and concentration of the eluted RNA was checked by nanodrop (Genova Nano, Jenway) after each elution step. Purity of RNA samples and possible gDNA contamination was tested by conventional Polymerase Chain Reaction (PCR) and agarose gel electrophoresis.

#### *2.14.1. Quick-RNA™ Fungal/Bacterial Miniprep Kit (Zymo Research, R2014)*

The pellet of bacterial cells was resuspended in 800 µl of RNA lysis buffer and transferred into a ZR BashingBead™ Lysis tube. The tube was vortexed for one minute and centrifuged for one minute. 400 µl of the supernatant were transferred into a Zymo-Spin™ IICG column and centrifuged for 30 seconds. The flow-through was mixed with 100% molecular grade ethanol (VWR, 437433T), transferred into a Zymo-Spin™ IIC column and centrifuged for 30 seconds. The flow-through was discarded, the column was washed with 400 µl of RNA Wash buffer and centrifuged for 30 seconds. 80 µl of DNase I Reaction Mix (5 µl of DNase I + 75 µl of DNase Digestion buffer per sample; [RNase-free DNase I, M0303S, New England Biolabs, Inc.]) was applied on the column and incubated for 15 minutes at room temperature. Subsequently, the column was washed with 400 µl of RNA Prep buffer and 700 µl of RNA Wash buffer, centrifuged for 30 seconds after each buffer addition. The column was then washed with 400 µl of RNA Wash buffer, centrifuged for two minutes and transferred into an RNase-free Eppendorf tube. 50 µl of RNase/DNase free water was applied directly onto the column and centrifuged for 30 seconds. Eluted RNA was used for downstream analysis.

#### *2.14.2. Monarch® Total RNA Miniprep Kit (T2010, New England Biolabs)*

The bacterial pellet was resuspended in 800 µl 1X RNA/DNA Protection Reagent and transferred into a ZR BashingBead™ Lysis tube (from the kit described in section 2.14.1). The tube was vortexed for one minute and centrifuged for one minute. Lysate was transferred to a nuclease-free Eppendorf tube and centrifuged for two minutes at room temperature. Supernatant was transferred to a nuclease-free tube, mixed with an equal volume of RNA Lysis buffer and vortexed briefly. Up to 800 µl of the sample was transferred to a gDNA removal column and centrifuged for 30 seconds. The flow-through was mixed with an equal amount of

molecular grade ethanol ( $\geq 95\%$ ). The sample was transferred to an RNA purification column and centrifuged for 30 seconds. The column was washed with 500  $\mu\text{l}$  RNA Wash Buffer and centrifuged for 30 seconds. Subsequently, on-column DNase digestion with 80  $\mu\text{l}$  of DNase I mix included in the kit was performed for 15 minutes at room temperature. 500  $\mu\text{l}$  Wash Buffer was added and the column was centrifuged for 30 seconds. 500  $\mu\text{l}$  Wash Buffer was added again, the column was centrifuged for two minutes and transferred into an RNase-free tube. RNA was eluted by adding 50  $\mu\text{l}$  of nuclease-free water directly onto the column and centrifuging for 30 seconds.

#### *2.14.3. RNeasy® Mini kit (Qiagen, 74104)*

The bacterial pellet was resuspended in 700  $\mu\text{l}$  Buffer RLT and transferred into a ZR BashingBead™ Lysis tube (from the kit described in section 2.14.1). The tube was vortexed for one minute and centrifuged for one minute. The lysate was transferred into a nuclease-free Eppendorf tube and centrifuged for three minutes at top speed. The supernatant was mixed with an equal amount of 70% molecular grade ethanol, up to 700  $\mu\text{l}$  was transferred to an RNeasy Mini spin column and centrifuged for 15 seconds. The column was then washed with 350  $\mu\text{l}$  Buffer RW1 and centrifuged for 15 seconds. 80  $\mu\text{l}$  DNase I mix (see section 2.14.1) was applied onto the column and incubated at room temperature for 30 minutes. The membrane was then washed with 350  $\mu\text{l}$  Buffer RW1 and centrifuged for 15 seconds. The column was subsequently washed two times with 500  $\mu\text{l}$  Buffer RPE and centrifuged for 15 seconds and two minutes, respectively. Additionally, the column was centrifuged at full speed for one minute to remove any remaining buffer. RNA was eluted by adding 50  $\mu\text{l}$  of nuclease-free water directly onto the column and centrifuging for one minute. The sample was treated with DNase I once again in liquid (off-column) by adding 80  $\mu\text{l}$  DNase I mix, incubating for 30 minutes at room

temperature. The sample was then loaded onto an RNeasy Mini spin column and the RNA was cleaned up following the steps described above. The RNA was eluted into a final volume of 50  $\mu$ l.

#### *2.14.4. Phenol/chlorophorm – RNeasy Mini kit hybrid*

This protocol was kindly provided by Dr Helen Wright (School of Dentistry, University of Birmingham). The bacterial pellet was homogenised by vigorous pipetting in 1 ml TRI Reagent (T9424, Sigma-Aldrich) and incubated at room temperature for five minutes. 200  $\mu$ l chloroform (C2432 Sigma – Aldrich) was added and the sample was vortexed for 30 seconds. It was then incubated at room temperature for three minutes and centrifuged for 15 minutes at 12 000 x g. The top aqueous phase was carefully transferred into a new tube and an equal volume of 70% molecular grade ethanol was added. Up to 700  $\mu$ l of the sample was transferred onto an RNeasy column and the sample was centrifuged for 30 seconds.

- gDNA digestion not included – the column was washed with 700  $\mu$ l RW1 Buffer and centrifuged for 30 seconds.
- gDNA digestion included – the column was washed with 350  $\mu$ l RW1 Buffer and centrifuged for 30 seconds. The sample was then treated for 30 minutes at room temperature with 80  $\mu$ l DNase I mix in an on-column reaction (see section 2.14.1). The column was washed again with 350  $\mu$ l RW1 Buffer.

500  $\mu$ l RPE Buffer was added two times and the sample was centrifuged for 30 seconds after each buffer addition. The empty column was then centrifuged for two minutes to remove the remaining buffer. RNA was eluted by adding 50  $\mu$ l of nuclease-free water, incubating the membrane for two minutes at room temperature and centrifugation for one minute.

#### 2.14.5. RNA isolation from *Brucella* species adapted to *Fusobacterium nucleatum*

The original protocol was kindly provided by Dr Daniel Slade (Virginia Tech, Virginia, USA) and modified as follows: the bacterial pellet was resuspended in 1 ml ice cold mixture of molecular grade ethanol:acetone (1:1) and stored at -80°C for 30 minutes. The suspension was centrifuged for three minutes at 17000 x g. The pellet was resuspended in 500 µl Tris-EDTA (TE) Buffer (1 mM EDTA [E5134, Sigma], 10 mM Tris-HCl [Trizma hydrochloride, T6666, Sigma], pH 7.5) and centrifuged for three minutes at 17000 x g. The pellet was resuspended in 200 µl 0.04 M sodium acetate, pH 5.2 (71196, Sigma), 200 µl 1% zwittergent (693017, Millipore) was added and the mixture was vortexed for 15 seconds. The sample was centrifuged for three minutes at 8000 x g, the pellet was washed with 400 µl nuclease-free water and centrifuged again for three minutes at 8000 x g. Cells were resuspended in 200 µl 0.04 M sodium acetate and 160 µl nuclease-free water and 40 µl 10% sodium dodecyl sulphate (SDS; L4390, Sigma) were added. The sample was vortexed for 15 seconds and incubated for seven minutes at 90°C. 400 µl of the sample were mixed with 400 µl of phenol:chlorophorm:isoamyl alcohol (125:24:1, pH 4.5, 77619, Sigma-Aldrich) in a 2 ml phase-lock tube (2302830, 5 PRIME, Quanta Bio), vortexed for one minute and centrifuged at the top speed for two minutes. The upper aqueous phase was mixed with an equal volume of chloroform (C2432 Sigma – Aldrich) in a new phase-lock tube, vortexed for one minute and centrifuged at the top speed for two minutes. The upper aqueous phase was mixed with 0.1 volume of 3M sodium acetate (pH 5.2) and 1 volume of isopropanol (327272500, Acros Organics, Fisher Scientific) in an Eppendorf tube, incubated on ice for five minutes and centrifuged at the top speed for ten minutes. The resulting pellet was washed with 1 ml of 70% molecular grade ethanol and centrifuged at the top speed for ten minutes. The pellet was air-dried and resuspended in 80 µl nuclease-free water<sup>+</sup>. Up to 30 µg of extracted nucleic acid was subsequently treated with 15 µl

of Ambion DNase I (AM2222, Invitrogen) in a 100  $\mu$ l reaction in solution (15  $\mu$ l of Ambion DNase I, 10  $\mu$ l of 10X DNase I Buffer,  $n$   $\mu$ l of extracted nucleic acid,  $n$   $\mu$ l nuclease-free water). The sample was incubated at 37°C for 60 minutes, mixed with 100  $\mu$ l 70% molecular grade ethanol, loaded onto the RNeasy column (from kit used in section 2.14.3) and centrifuged at 8000 x g for 30 seconds\*. The column was washed\*\* with 700  $\mu$ l RW1 Buffer and twice with 500  $\mu$ l RPE Buffer, centrifuged at 8000 x g for 30 seconds after each wash. Centrifugation at 8000 x g for two minutes followed to dry the column. RNA was then eluted by adding 80  $\mu$ l of nuclease-free water, incubating the column at room temperature for two minutes and centrifuging for one minute at 8000 x g.

+ If the sample was treated on-column with Qiagen DNase I (79254, Qiagen) (Section 3.3.9., table 3.2.), an aliquot was removed from the RNA sample resuspended in nuclease-free water and the aliquot was mixed with an equal volume of 70% molecular grade ethanol, loaded onto the RNeasy column and treated with 80  $\mu$ l of DNase I Mix (10  $\mu$ l DNase I + 70  $\mu$ l RDD Buffer) for 15 minutes at room temperature. The column was then washed\*\* and RNA eluted as stated above.

\*If a second, on-column DNase treatment with Ambion DNase I was added (Table 3.2.), Ambion DNase I mix (15  $\mu$ l DNase I + 10  $\mu$ l Buffer +75  $\mu$ l nuclease-free water) was applied onto the column at this point. The column was incubated at 37°C for 60 minutes, then washed\*\* and the RNA was eluted as state above.

## **2.15. Complementary DNA (cDNA) synthesis**

Reverse transcription of extracted RNA into cDNA was performed according to the following instructions (Tetro cDNA kit, BIO-65042, Bionline, Meridian Bioscience): priming premix was prepared on ice as per protocol. Samples were incubated at 45°C for 60 minutes followed by

the termination of the reaction at 85°C for 5 minutes and then chilled on ice (Veriti™ 96-well thermal cycler, 4375786, Applied biosystems).

## **2.16. Reverse transcription – quantitative polymerase chain reaction (RT-qPCR)**

RT-qPCR was performed using the LightCycler480 system (Roche Diagnostics). A mastermix was prepared by mixing 5 µl LightCycler® 480 SYBR Green I Master (04707516001, Roche Diagnostics), 0.05 µl of a neat forward primer, 0.05 µl of a neat reverse primer (see table 2.3. for all primers used in this study) and 3.9 µl nuclease-free water per reaction. 9 µl of the mastermix was mixed with 1 µl cDNA in each well of the qPCR plate (LightCycler® 480 Multiwell Plate 96, 04729692001, Roche Diagnostics). Cycling conditions for each RT-qPCR are detailed in table 2.4. All samples were analysed in duplicate and 2 negative controls were included in every RT-qPCR for each set of primers. Efficiency of each set of primers as well as the relative expression of each target gene were analysed using LightCycler480 software, version 1.5. The software computed Cp values using the second derivative maximum method and these values were used to calculate the relative expression levels of the target genes. The efficiency of each set of primers was determined using dilutions of each *F. nucleatum* subspecies cDNA (100%, 50%, 10%, 1%, 0.1%, 0%).

Gene	Primer sequence	Amplicon size (bp)	Accession number/source
<i>disA</i> 1 (set 1 – c-di-AMP cyclase)	F-ttaaagttgcacctggaagtc R-aagaatcccccatctctaacc	124	23726_FusoPortal_Gene_776
<i>disA</i> 2 (set 2 – c-di-AMP cyclase)	F-tgaaaaggtagagatggggg R-gcagttctatgtcttgtccac	189	
<b>FN-specific</b>	F-ggatttattgggcgtaaagc R-ggcattcctacaaatatctacgaa	162	Zhou <i>et al.</i> , 2016
<i>pde2</i> (phosphodiesterase)	F-agagataggacaggagaaactg R-atgcttctgccactgaaag	190	23726_FusoPortal_Gene_1366
<i>relA/spoT</i> psh 1 [(p)ppGpp synthetase/hydrolase set 1]	F-tcaccaaggacaatacagaaag R-ccatcaacaagagtagcaacag	198	23726_FusoPortal_Gene_2100
<i>relA/spoT</i> psh 2 [(p)ppGpp synthetase/hydrolase set 2]	F-aaagaaagagcagcctcaac R-caaagcctccaatatcatctcc	172	
<i>relA/spoT</i> smh A (Small (p)ppGpp hydrolase set A)	F-gaagcttgagtgaaatagacc R-catctgctgaacctacaatagc	109	23726_FusoPortal_Gene_1455
<i>relA/spoT</i> smh B (Small (p)ppGpp hydrolase set B)	F-tcagaagaagagtgaaaaagcc R-cgtggtgaatattttgccagtc	171	
<i>rpoA</i> (DNA-directed RNA polymerase subunit alpha)	F-cctggagcagcaataaaagg R-tgcgacaatatctgctgctt	198	GenBank: CP028109 REGION: 1187589..1188569
16S bacterial rRNA universal primers I (Uni 16S I)	F-agagttgatcatggctcag R-cggttacctgttacgactt	1465	Lane, 1991
16S bacterial rRNA universal primers II (Uni 16S II)	F-ctaaatacgtgccagcagcc R-cgaccccaacacctagtaa	334	Külekçi <i>et al.</i> , 2001
16S FNN 23726 specific	F-aaaaccagctgtggtttt R-atcccaaggagaacctctgc	151	23726_FusoPortal_Gene_1526

**Table 2.3. List of primers used in this study.** Primers were obtained from Sigma-Aldrich. Accession numbers from GenBank and FusoPortal provide access to specific gene sequences which were used to design the primers.

RT-qPCR step	Temperature	Time	Number of cycles
Pre-incubation	95°C	5 min	1
Amplification	95°C	20 sec	60 (Primer efficiency)/ 45 (Gene expression)
	60°C	20 sec	
	72°C	30 sec (involves 1 sec fluorescence measurement step)	
Melt curve generation	60°C → 95°C	Automatic	1
Cooling	→ 4°C	Automatic	1

**Table 2.4. Cycling conditions for RT-qPCR.** When the efficiency of primers was tested, the protocol was set to 60 cycles of amplification. When the changes in gene expression were analysed, the protocol was set to 45 cycles.

## 2.17. Statistical analysis

Statistical analysis of the obtained results was performed using IBM SPSS Statistics, version 26. If the data sets analysed conformed to a normal distribution, one-way ANOVA with the Bonferroni correction was used to calculate the statistical significance between groups. If the data sets analysed were found not to conform to a normal distribution, non-parametric analyses were employed. Differences between two independent groups were assessed by Mann-Whitney U test, while the differences between multiple independent groups were computed using Kruskal-Wallis H test. The type of analysis used is specified at each result section. The results were considered to be statistically significant if  $p \leq 0.05$ , unless stated otherwise. Graphs were produced using GraphPad Prism, version 5.

## **CHAPTER 3: RESULTS**

### **3.1. Characterisation of *Fusobacterium nucleatum* subspecies**

In order to fulfil the aims of this thesis and to study complex bacterial interaction and communication in biofilms, it is essential to understand the basic characteristics and behaviour of individual *F. nucleatum* subspecies first.

All five *F. nucleatum* subspecies, namely *animalis*, *fusiforme*, *nucleatum*, *polymorphum* and *vincentii* (FNA, FNF, FNN, FNP and FNV), were characterised in this study. Two FNN strains were used for the purposes of this project – FNN ATCC 25586 (abbreviated to FNN25), being the type strain, and FNN ATCC 23726 (abbreviated to FNN23), which is the only genetically tractable strain to date (Wu *et al.*, 2018).

The subspecies were characterised to establish the base for the experiments performed in this study. Firstly, the colony and the cell morphology of the subspecies was investigated to identify whether variations among the subspecies exist. Additionally, the pattern of growth in anaerobic as well as microaerophilic conditions was evaluated. Lastly, the identity of all five subspecies was confirmed using 16S rRNA gene sequencing.

#### *3.1.1. Colony and cell morphology*

In order to understand the differences between the subspecies and to be able to readily recognise possible contaminants during this study, all five subspecies were characterised on a macroscopic as well as a microscopic level. All subspecies were grown on SAA plates for 48 hours in anaerobic conditions. Colony morphology varied among the subspecies. FNA, FNF and FNV produced round colonies with irregular, flower-like edges (Fig. 3.1. B, D, L). FNN23, FNN25 and FNP produced round colonies with smooth edges (Fig. 3.1. F, H, J). Additionally,

colonies of FNV exhibited slightly elevated, umbonate centres. The colour of all colonies was creamy.

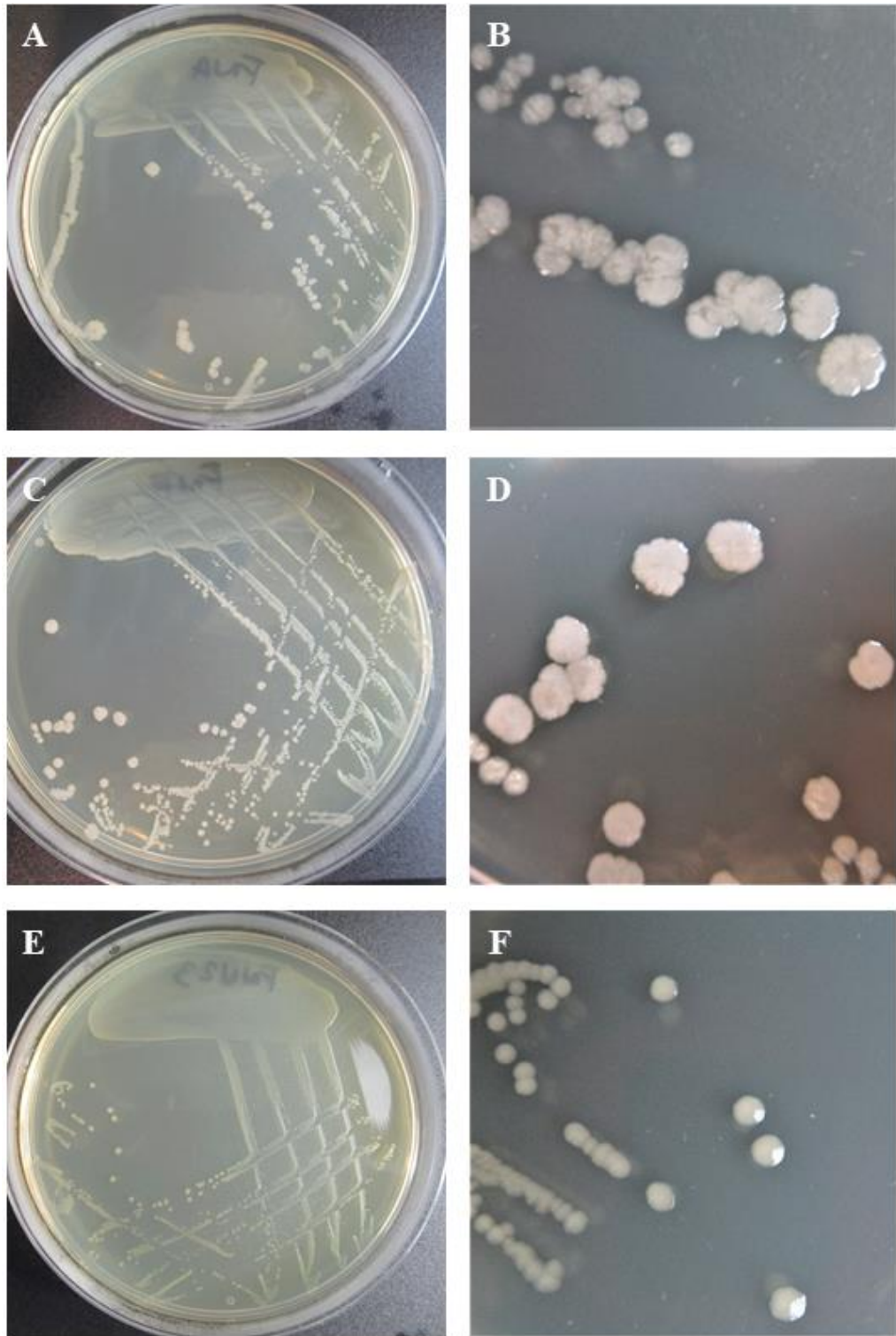


**Figure 3.1.** Colony morphology of *F. nucleatum* subspecies. Pictures and legend continued on the next page.

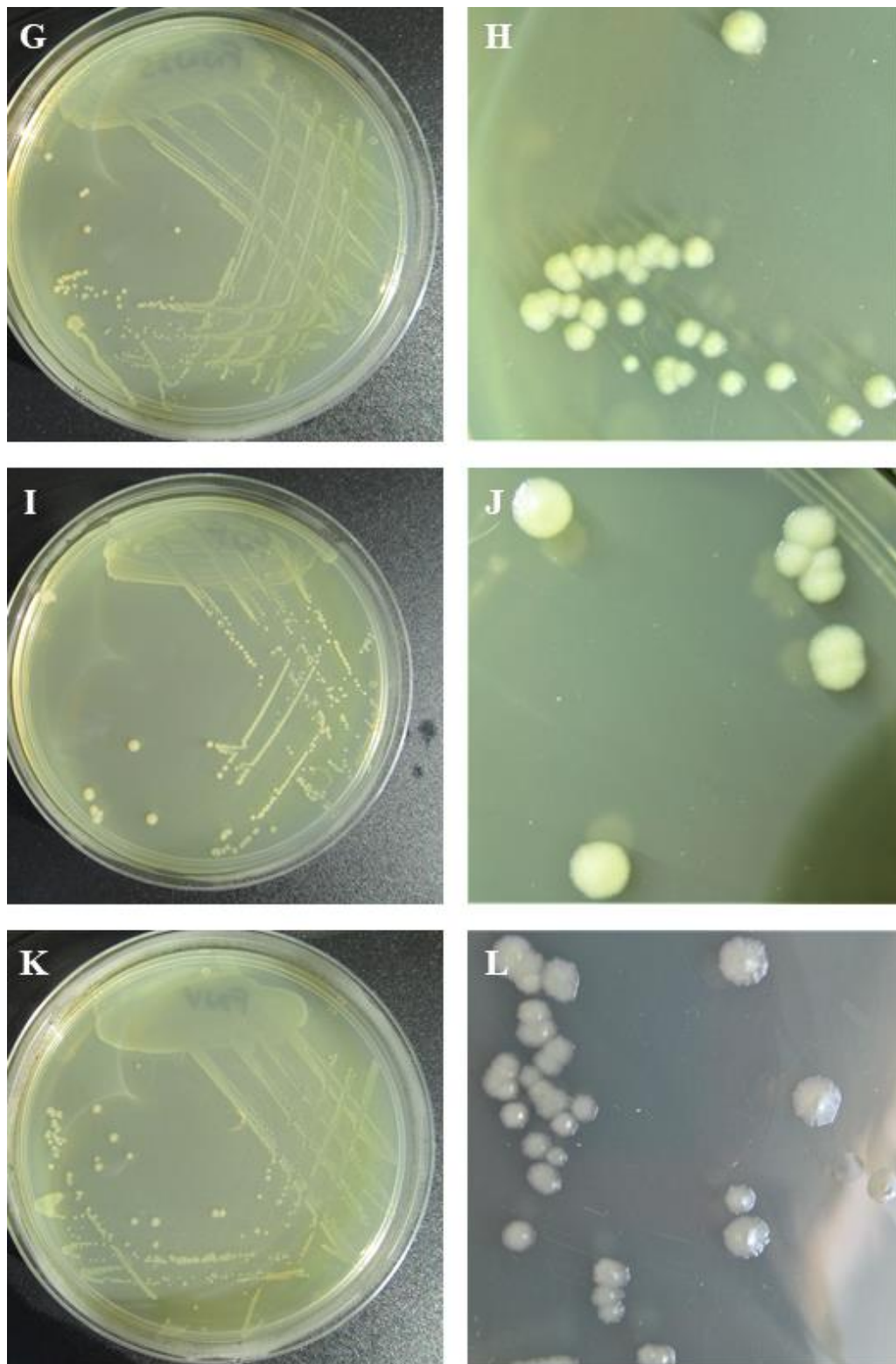


**Figure 3.1. Colony morphology of *F. nucleatum* subspecies.** Growth of the subspecies on SAA plates (A, C, E, G, I, K) and detailed colony morphology differences (B, D, F, H, J, K). A, B – FNA; C, D – FNF; E, F – FNN23; G, H – FNN25; I, J – FNP; K, L – FNV.

On a microscopic level, all subspecies were confirmed to be Gram-negative elongated rods. Interestingly, the length of the bacterial cells varied significantly (Fig. 3.2.). Upon visual examination, FNP cells seemed most elongated, whereas FNV seemed to be the shortest cells.

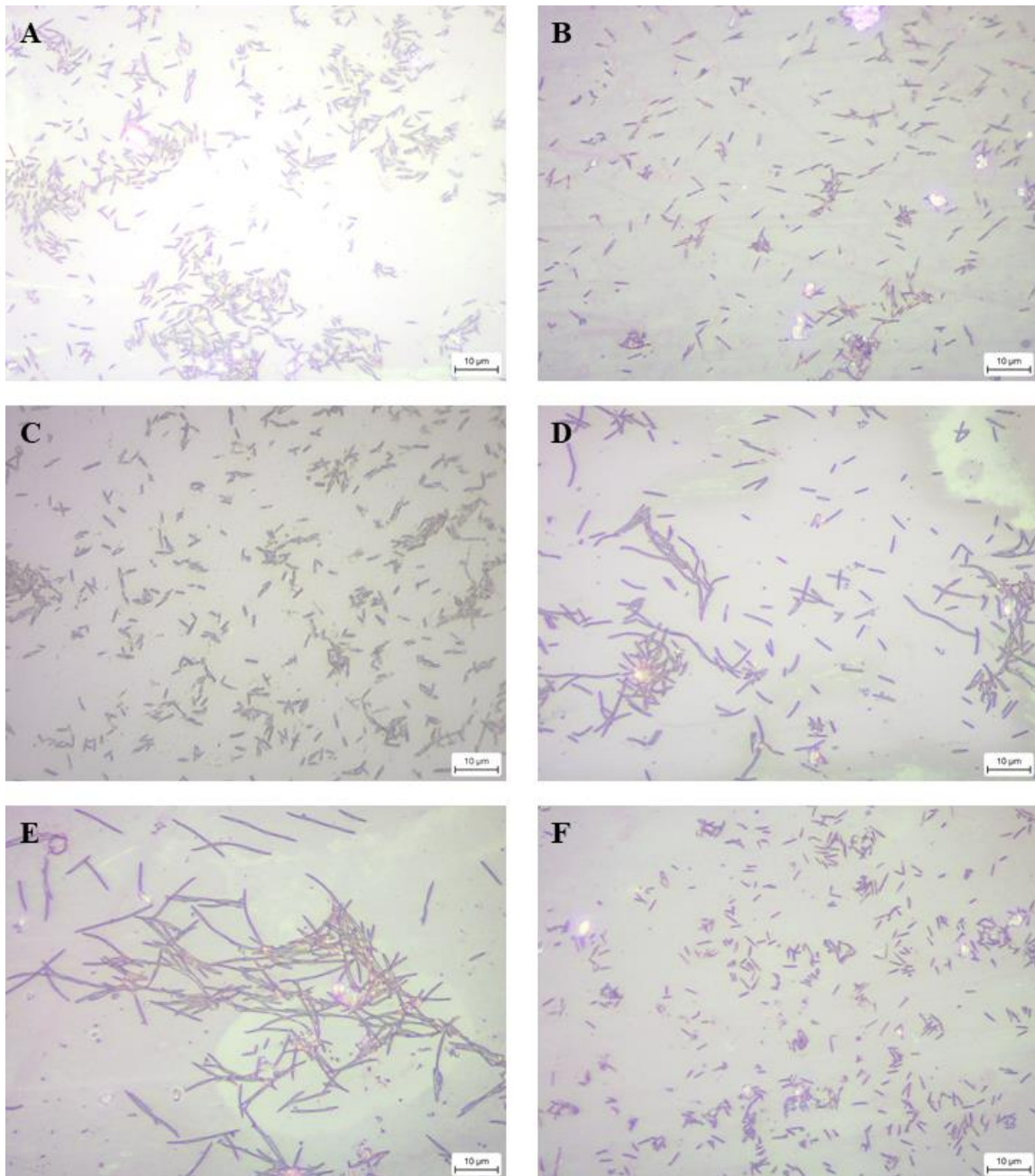


**Figure 3.2. Gram staining of *F. nucleatum* subspecies.** All subspecies were confirmed to be Gram negative long rods of varying length. Magnification 100x. A – FNA, B – FNF, C – FNN23, D – FNN25, E – FNP, F – FNV.

To confirm the visual estimate as well as to accurately determine the differences in the length of the subspecies, individual bacterial cells were analysed using SEM. Zeiss EVO MA 10 software was used to measure the length of individual bacterial cells at 20 000x magnification (Appendix 1). FNP cells were confirmed to be the longest (11.74  $\mu\text{m}$ ) with a high significance value ( $p < 0.0001$ ), however FNA cells were shown to be the shortest rods (2.85  $\mu\text{m}$ ) (Fig. 3.3; 3.4.). The length of FNF, FNN23, FNN25 and FNV range from 4.00  $\mu\text{m}$  to 4.61  $\mu\text{m}$ .

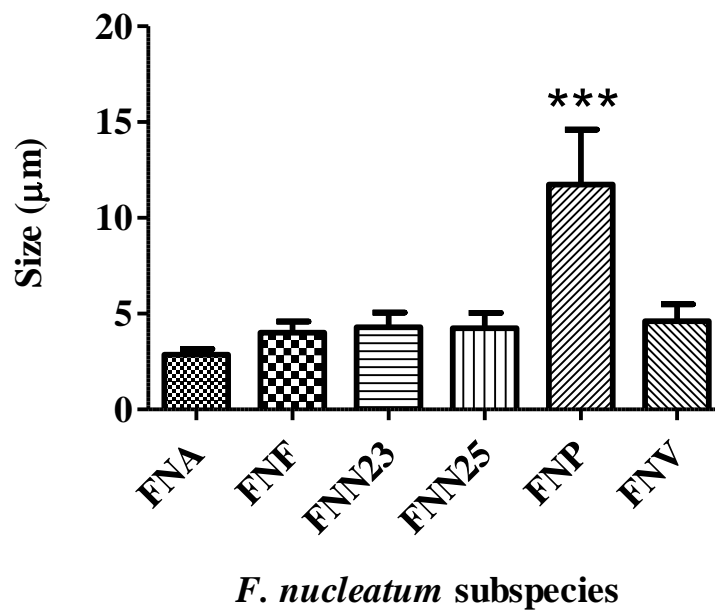


**Figure 3.3. Comparison of bacterial cell length of *F. nucleatum* subspecies.** The size of individual bacterial cells was measured using Zeiss EVO MA 10 software at 20 000x magnification. FNP was shown to be the most elongated subspecies, whilst FNA was the shortest subspecies. One-way ANOVA was used to analyse significant differences among the subspecies and Bonferroni correction was applied. \*\*\*  $p < 0.0001$ . Error bars represent standard deviation,  $n=10$ .

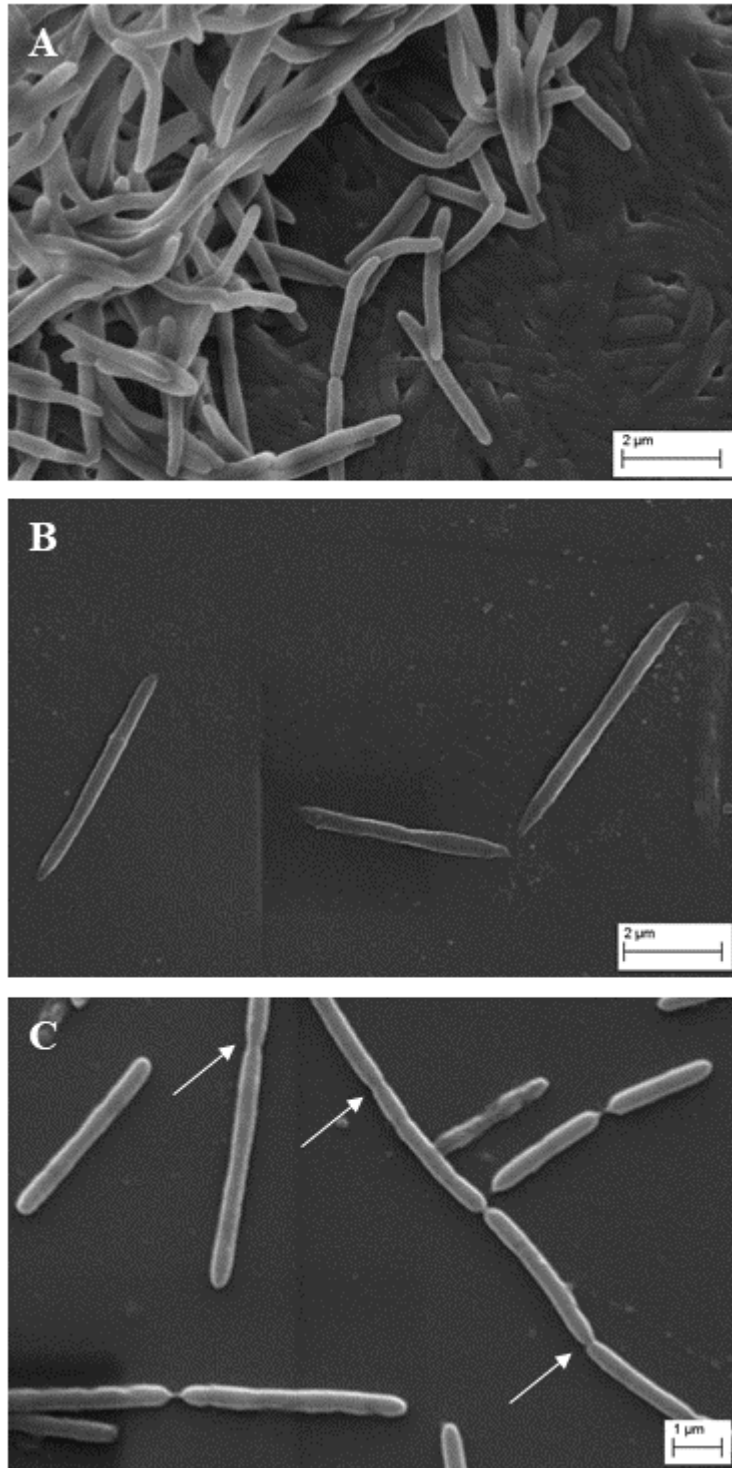


**Figure 3.4.** Scanning electron micrographs of *F. nucleatum* subspecies. Micrographs and legend continued on the next page.

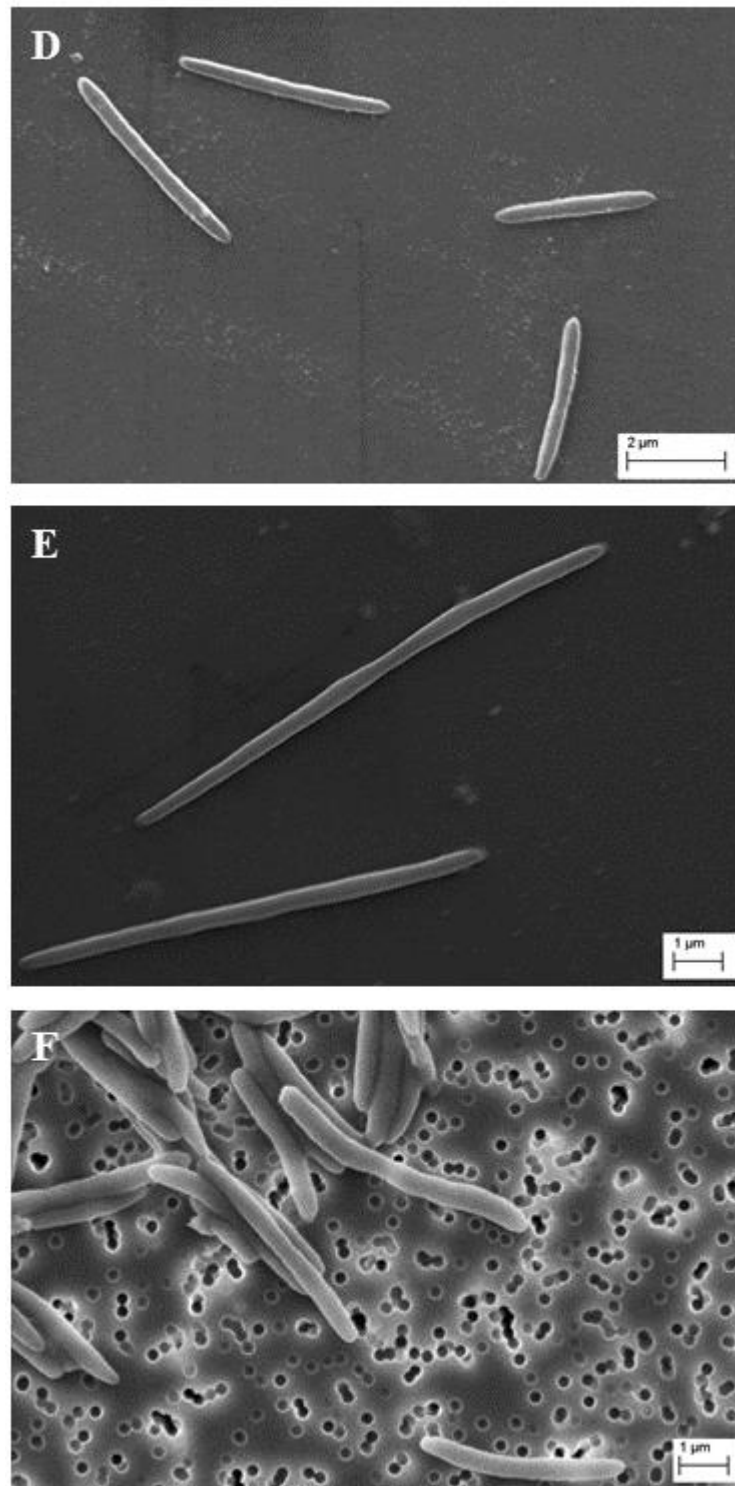


**Figure 3.4. Scanning electron micrographs of *F. nucleatum* subspecies.** Micrographs showing individual bacterial cells. FNP is visibly the longest subspecies (E). Division planes are indicated by the arrows (C). A and F visualised on Isopore™ membranes, B – E visualised on Thermanox™ coverslips. Isopore™ membrane visualised without bacteria can be found in Appendix 1. Magnification 20 000x. A – FNA, B – FNF, C – FNN23, D – FNN25, E – FNP, F – FNV.

FNA and FNV were visualised on Isopore™ membranes containing laser-etched pores, which might be confused with coccal contamination. Membranes without the bacteria were also visualised and the micrographs can be found in the appendix section (Appendix 1). The limitation of this method was visualisation of bacterial cells at different stages of the cell cycle, that is why images were checked for a visible division plane (Fig. 3.4. C) and the cells found to be dividing were excluded from the measurement.

These findings allowed discerning the differences among *F. nucleatum* subspecies, confirming sample purity and identifying the bacteria in mono- and multi-species biofilms at a later stage.

### 3.1.2. *Bacterial growth in anaerobic conditions*

Part of the bacterial characterisation was the growth pattern analysis of each *F. nucleatum* subspecies. These growth profiles are a very useful tool to determine phases of bacterial growth (lag, exponential, stationary and death phase) and their length. Growth curves were generated as detailed in section 2.2. When the growth curves were generated using the Miles and Misra (1938) method (section 2.2.1.), subspecies FNA, FNN23, FNN25, FNP and FNV appeared to already be in the exponential phase at time point 0 as no lag phase was observed (Fig. 3.5.). In the case of FNF, a short lag phase appeared (T0 – T4) followed by the exponential phase. For FNA, FNF, FNN23, FNN25 and FNV, the highest bacterial concentration was observed at T24. Interestingly, FNP reached the highest bacterial concentration at T8, followed by a decrease in the number of bacteria.

Doubling times were calculated based on each growth curve and the results varied across the subspecies. Doubling times longer than one hour were observed for FNA, FNN23, FNN25, FNP and FNV with the values being 1.84 h, 1.33 h, 1.82 h, 1.28 h and 1.60 h, respectively.

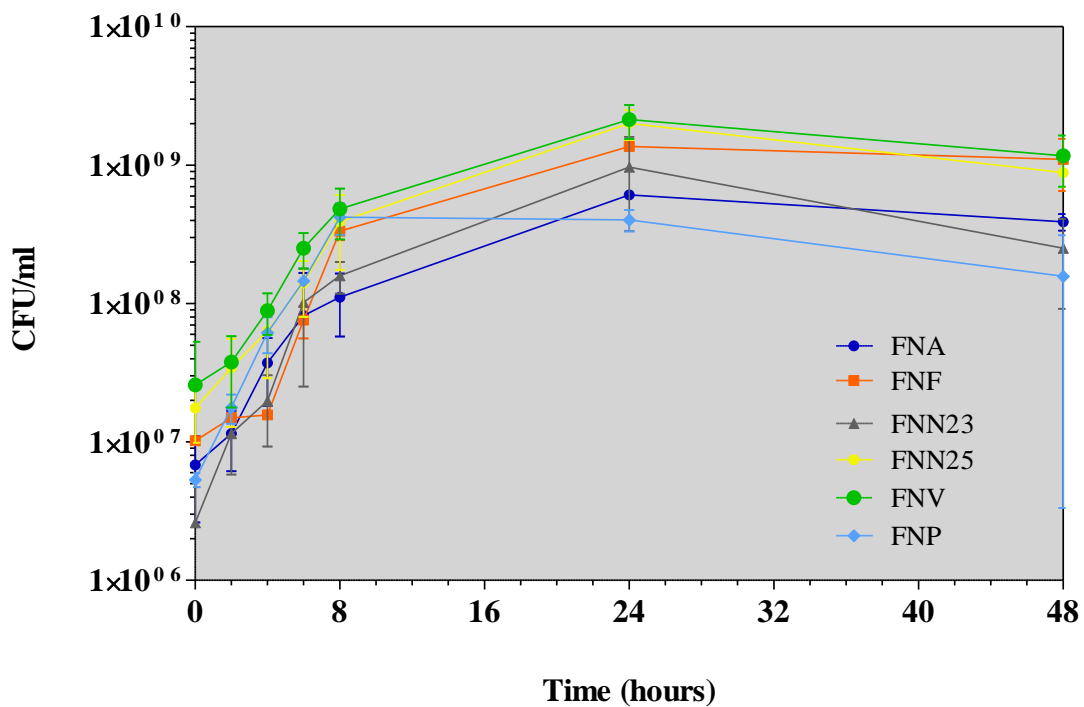


**Figure 3.5. Growth profiles of *F. nucleatum* subspecies grown in anaerobic conditions.** The graph shows mean values of 3 independent experiments. Each experiment involved 3 technical replicates. Error bars represent standard deviation.

Interestingly, doubling time shorter than one hour was that of FNF – 0.91 h.

Bacterial growth can be analysed not only by viable bacterial cell count, using for example the Miles and Misra (1938) method, but also by measuring the optical density of a bacterial culture using a spectrophotometer. The spectrophotometric method provides a relatively easy and quick measurement of bacterial growth based on the increasing turbidity of the culture. Modern sophisticated spectrophotometers can be automated, execute measurements at specified time points and maintain the optimum temperature required for the growth of bacteria studied. In order to compare the viable bacterial cell count method and the spectrophotometric method and to confirm the results obtained using the Miles and Misra (1938) method, an FNN25 growth

curve was generated using an automated spectrophotometer. A microtiter plate containing bacterial culture was sealed with a non-breathable membrane to retain the anaerobic conditions and incubated in the spectrophotometer, which measured the optical density of the culture every hour for 48 hours.

Interestingly, the obtained growth curve differed in multiple aspects. Firstly, a long lag phase was observed for the first 15 hours (Fig. 3.6.). Secondly, considerably high standard deviation values were noted from the beginning of the exponential phase until the end of the experiment. Additionally, only the stationary phase without the death phase was observed based on the shape of the curve and the optical density of the culture was stabilised.

In spite of the exemplary shape of the growth curve, the obtained results were not considered reliable because when the plate was removed from the spectrophotometer after 48 hours, aggregates similar to grains of sand were visible in each well containing bacterial culture. This explained the variation in measurements, as the culture was not uniformly mixed. *F. nucleatum* has been shown to autoaggregate (Merritt *et al.*, 2009), which agrees with this observation. The spectrophotometer was programmed to shake the plate before each measurement, however the intensity of shaking was probably not sufficient to break the aggregates and this resulted in inaccurate optical density measurements. Due to the abovementioned reasons, only the FNN25 growth curve was generated using the automated spectrophotometer and the remaining subspecies were excluded from this analysis.

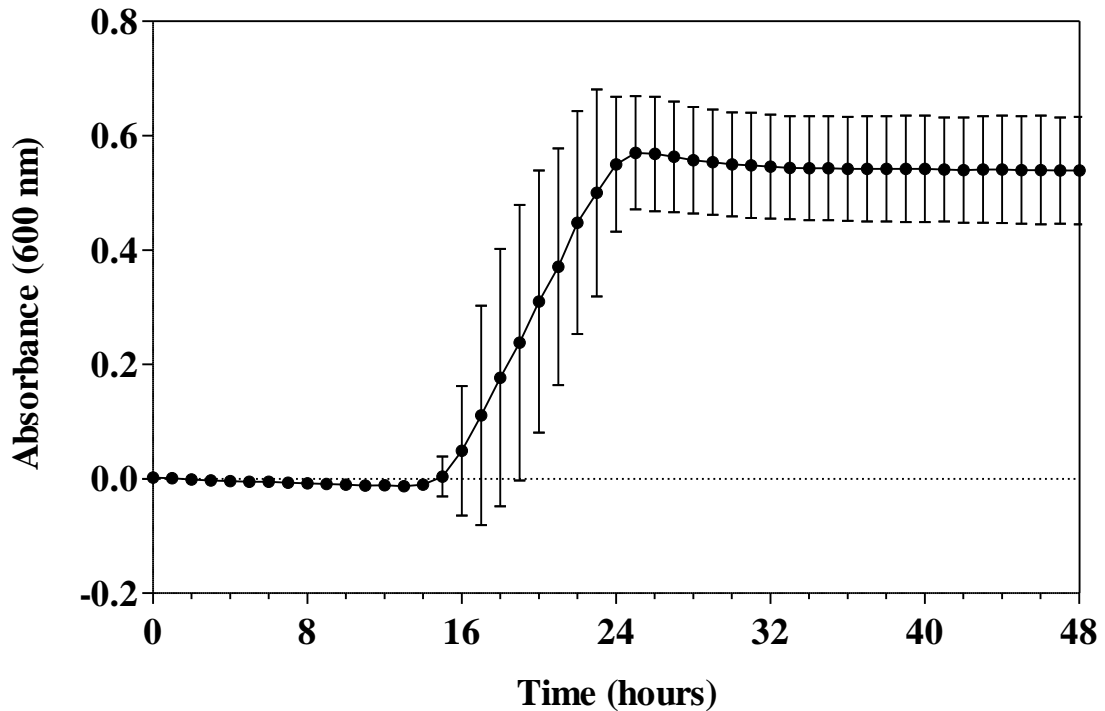


**Figure 3.6. Growth profile of *F. nucleatum* ssp. *nucleatum* 25586 grown in anaerobic conditions.** The growth curve was generated by hourly measurements of optical density of the bacterial culture at 600 nm performed by automated spectrophotometer. Values of the optical density are corrected for the negative control (SAB only). Error bars represent standard deviation, n=5.

Both methods that were used to generate bacterial growth curves contributed towards characterisation of the *F. nucleatum* subspecies and shed more light on the subspecies' growth patterns. Thanks to the Miles and Misra (1938) method, the exponential phase of the growth was identified and it was possible to divide this phase into the early, intermediate and late exponential phase. Acquired information provided a base for a transcriptional analysis of genes involved in synthesis and hydrolysis of signalling molecules at a later stage of this project.

### 3.1.3. Growth of *Fusobacterium nucleatum* subspecies in the presence of oxygen

Some authors classify *F. nucleatum* as an obligate anaerobe (Petri *et al.*, 2019), others place it into a category of facultative anaerobes (Kabwe *et al.*, 2019). In order to address this ambiguity,

it was decided to include the growth of *F. nucleatum* subspecies in the presence of oxygen into the characterisation of these bacteria. Bacterial overnight culture was diluted as stated in section 2.3. It is important to mention that due to problems with FNV culture, it was only possible to repeat the experiment two times, while the growth of all the other subspecies was analysed in three independent experiments.

The sub-culture was then incubated in a shaking incubator with a loose lid to ensure the access of oxygen from the surrounding air. Analysis of the viable cell count showed that all the subspecies were growing well in SAB for at least eight hours (Fig 3.7.).

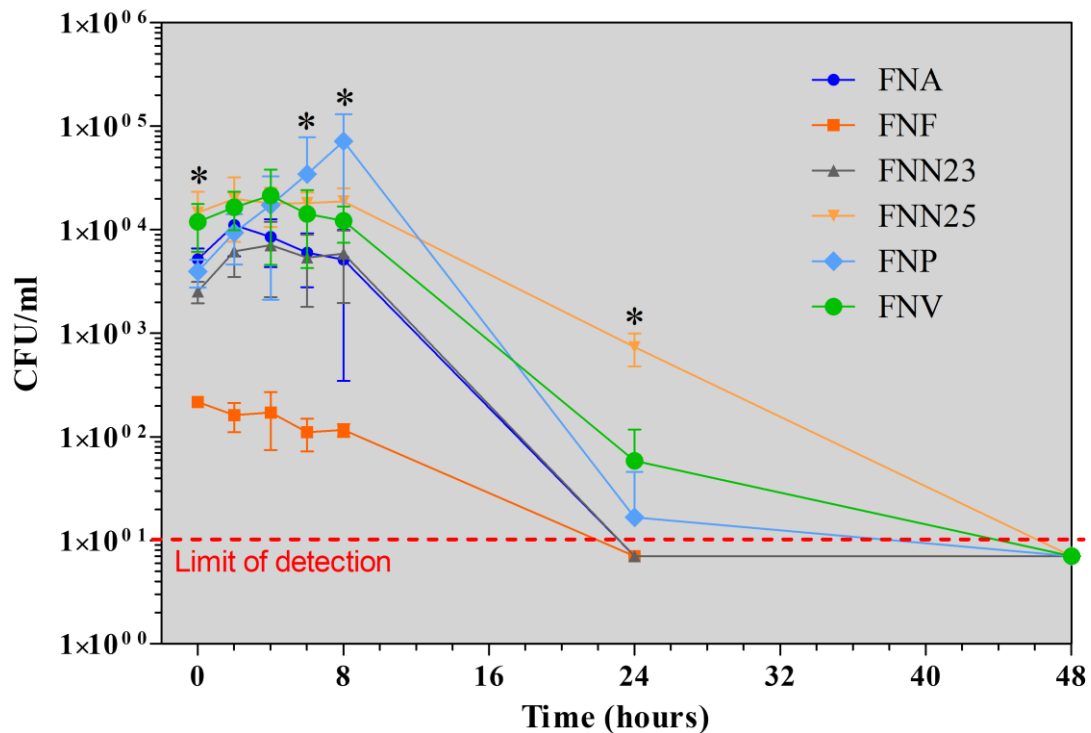


**Figure 3.7. Growth profiles of *F. nucleatum* subspecies grown in oxic conditions.** The limit of detection was arbitrarily selected as 10 CFU/ml. If there was no growth observed at T24 and T48, values were graphed below the limit of detection. The graph shows mean values of three independent experiments apart from FNF, which was repeated two times. Each experiment involved three technical replicates. Asterisks (\* $p \leq 0.050$ ) show the overall significant difference at the time point indicated as calculated by Kruskal-Wallis test. Even if there was no overall significance calculated at T2 and T4, FNF was significantly different in both cases ( $p = 0.050$ ). A more detailed table of statistical results (Appendix 2) shows differences between pairs of subspecies at each time point as calculated by Mann-Whitney test. Error bars represent standard deviation.

During this time period, the bacterial concentration of FNN25 and FNV stayed considerably stable, with the bacterial numbers around  $10^4$  CFU/ml. FNA bacterial concentration slightly increased at T2 from  $5.17 \times 10^3$  CFU/ml to  $1.11 \times 10^4$  CFU/ml and then started decreasing. FNF was the subspecies with the lowest bacterial count recorded throughout the experiment and the growth was gently decreasing from  $2.17 \times 10^2$  CFU/ml (T0) to  $1.17 \times 10^2$  CFU/ml (T8). FNN23 increased in cell number for the first four hours from  $2.53 \times 10^3$  CFU/ml to  $7.11 \times 10^3$  CFU/ml, then the counts slightly decreased. Strikingly, FNP as the only subspecies grew exponentially for the first eight hours from  $3.95 \times 10^3$  CFU/ml (T0) to  $7.13 \times 10^4$  CFU/ml (T8). In the case of FNN25, FNV and FNP, the viability of bacteria was detected even at T24, with values of  $7.33 \times 10^2$  CFU/ml,  $5.83 \times 10^1$  CFU/ml and  $1.67 \times 10^1$  CFU/ml, respectively.

These results suggest that *F. nucleatum* subspecies are not obligately anaerobic *sensu stricto*, as they are not killed by the presence of oxygen immediately.

In order to test the statistical significance between the subspecies when the cultures were incubated in the presence of oxygen, the mean values of CFU/ml of all the subspecies were compared at individual time points. The data did not conform to a normal distribution, that is why non-parametric tests were used. The overall significance was first analysed using Kruskal-Wallis test and subsequently specific differences between pairs of subspecies were evaluated using Mann-Whitney test.

To start with, the growth of FNF was confirmed to be significantly different from FNA, FNN23, FNN25 and FNP for the first eight hours ( $p = 0.050$ ). At T24, it was different only from FNN25, which still contained viable bacteria, while FNF did not. Interestingly, the FNP growth was found to be significantly different only from FNN23 and FNN25 at T0 ( $p = 0.050$  in both cases) and then from FNN25 at T24 ( $p = 0.046$ ). The growth of FNA was significantly different from

FNN23 at T0 ( $p = 0.050$ ) and FNN25 at T6 ( $p = 0.050$ ), T8 ( $p = 0.050$ ) and T24 ( $p = 0.037$ ). Additionally, a significant difference was observed between FNN23 and FNN25 at T0 ( $p = 0.050$ ), T6 ( $p = 0.050$ ), T8 ( $p = 0.050$ ) and T24 ( $p = 0.037$ ).

Strikingly, FNV was found not to be statistically significantly different from any subspecies at any time point. A more detailed table of the statistical results can be found in the Appendix section (Appendix 2).

Growing *F. nucleatum* subspecies in the presence of oxygen showed that the bacteria can survive a prolonged exposure to an oxygenated environment. The statistical analysis showed that there are significant differences between certain subspecies when the bacterial concentration is considered in detail at each time point.

#### 3.1.4. Confirmation of *Fusobacterium nucleatum* subspecies using 16S rRNA sequencing

While analysing colony morphology and bacterial cell morphology using staining techniques, such as Gram staining, are methods that are inexpensive, easy to perform and are not time-consuming, they do not provide unequivocal results. Some of the limitations are that bacteria might be Gram stain variable, the sample might be over-decolorised, thus giving false results and, additionally, different bacterial species might have very similar morphology (Thairu, Usman and Nasir, 2014). To overcome inaccuracy, more sophisticated methods have been developed, one of them being 16S small unit ribosomal RNA (rRNA) sequencing. This method is used for identification of bacteria based on the sequence of their 16S rRNA gene, which can be found in almost all bacteria and its sequence is highly conserved (Janda and Abbott, 2007). In order to rule out contamination and confirm the purity of bacterial stocks as well as to find differences among the 16S rRNA gene sequences of the subspecies, PCR of the 16S rRNA gene

was performed with generic 16S primers (Table 2.3.), the amplified DNA was isolated from an agarose gel, sequenced and bioinformatics was used to confirm the identity of each subspecies. Firstly, visualisation of the PCR products on an agarose gel indicated the presence of the gene in each subspecies (Fig. 3.8.).

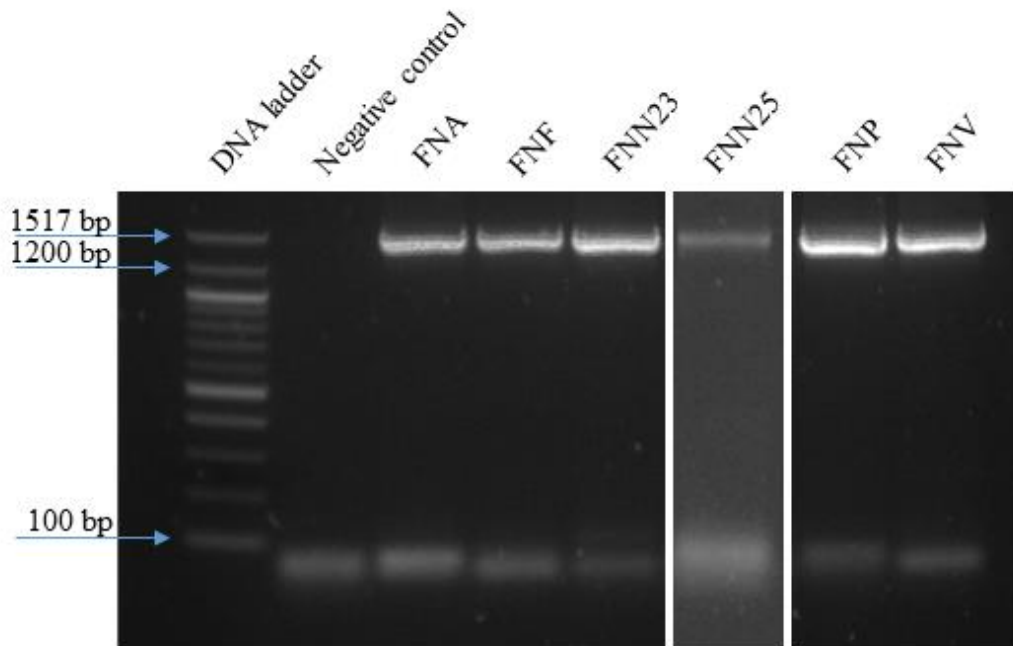


**Figure 3.8. Agarose gel showing amplified 16S rRNA gene fragments.** The 16S rRNA gene was detected in each subspecies and the size was estimated to be approximately 1450 bp. The bands visible in each well smaller than 100 bp are primer dimers. Template in the negative control was nuclease-free water. Electrophoresis conditions: 60 minutes, 120 V. 100 bp DNA ladder was used (N3231, New England Biolabs).

The size of each amplicon was approximately 1450 bp, which agrees with the size of the amplicon calculated based on the specific primer binding sites (1465 bp). When the extracted DNA was sequenced, the resulting sequence was compared against the online database of 16S ribosomal RNA sequences of Bacteria and Archea using Targeted Loci Nucleotide BLAST ([https://blast.ncbi.nlm.nih.gov/Blast.cgi?PAGE\\_TYPE=BlastSearch&BLAST\\_SPEC=TargLociblast](https://blast.ncbi.nlm.nih.gov/Blast.cgi?PAGE_TYPE=BlastSearch&BLAST_SPEC=TargLociblast)). The top hit for each subspecies was checked for identity percentage as well as E value.

In each case the identity percentage was 100%, with the E value being 0, which means that the match is not a result of chance and is highly significant. These results confirmed the identity of each subspecies as well as purity of the bacterial stocks used for this study.

Next, the differences among the subspecies on the level of 16S rRNA sequences were analysed. It was not possible to compare the sequences obtained in this project because the PCR products were only fragments of the 16S rRNA. That is why 16S rRNA genomic sequences were obtained from NCBI repository and a multiple sequence alignment was performed using Clustal Omega (<https://www.ebi.ac.uk/Tools/msa/clustalo/>). The complete sequence alignment can be found in the Appendix section (Appendix 3). The areas where the bases differ among the subspecies were highlighted in yellow, identical bases in all five sequences were shown with asterisks (\*) below the alignment. Columns in which the only differing nucleotide is “N” (undetermined) were highlighted in blue, to separate them from real differences in nucleotides. Gaps, which could have been a result of either nucleotide insertion or deletion, were shown by a dash (–). Strikingly, the identity of the sequences was substantially high (Table 3.1.).

	<b>FNP</b>	<b>FNF</b>	<b>FNN25</b>	<b>FNA</b>	<b>FNV</b>
<b>FNP</b>	<b>100.00</b>	98.18	97.87	97.22	97.54
<b>FNF</b>		<b>100.00</b>	98.70	98.34	99.34
<b>FNN25</b>			<b>100.00</b>	98.37	98.22
<b>FNA</b>				<b>100.00</b>	98.08
<b>FNV</b>					<b>100.00</b>

**Table 3.1. Percentages of identity of 16S rRNA genes from *F. nucleatum* subspecies.** The table shows the percent identity matrix generated by Clustal Omega from the multiple sequence alignment. The highest identity percentage (green) is between FNF and FNV, the lowest identity percentage (red) between FNP and FNA.

Identity percentages as calculated by Clustal Omega based on the sequence alignment were in the range 97.22% - 99.34 %. Based on these results, FNV and FNF are the most related subspecies, whereas FNP and FNA are the least related subspecies. This corresponds with published material of Kook *et al.* (2013), which describes genetic similarity of FNF and FNV and even suggested reclassification of FNF and FNV into one subspecies of FNV based on a high degree of sequence similarity of 22 housekeeping genes.

### 3.1.5. Chapter conclusions

All the findings discussed above contributed towards the characterisation of *F. nucleatum* subspecies necessary for this study. The subspecies were found to differ in both colony and bacterial cell morphology. Understanding the growth pattern of each subspecies provided the foundation for the later phase of this project focusing on differential production of CDNs at different stages of the exponential phase. It was found out that *F. nucleatum* subspecies potentially can survive in oxic conditions for prolonged time periods. The differences between the subspecies were identified also on a molecular level, when 16S rRNA gene sequences were compared and analysed. FNF and FNV were found to be the most related subspecies based on a considerably high percentage of 16S rRNA gene sequence similarity (99.34 %), while FNP and FNA were found to be the least similar subspecies (97.22%).

### **3.2. Characterisation of mono-species *Fusobacterium nucleatum* biofilms and multi-species periodontitis-related biofilms**

*F. nucleatum* is known to be a key organism in the formation of dental plaque leading to periodontitis and in extreme cases to tooth loss. Due to the importance of this species in the disease-associated plaque accumulation, it is important to understand the biofilm formation of *F. nucleatum* in mono-species biofilms as well as its ability to interact with other subspecies in multi-species biofilm models. That is why mono-species biofilms of individual subspecies were characterised by quantification of the biomass produced and the analysis of the biofilm architecture. Additionally, two specific subspecies were studied in a model of multi-species biofilm. The amount of biomass formed and the 3D structure were studied in each type of biofilm.

#### *3.2.1. Evaluation of biomass production in mono-species biofilms*

In order to understand whether there are differences in the amount of biofilm produced as well as in the biofilm stability among the subspecies, the quantity of biomass formed by each subspecies was assessed. Additionally, variations in the biofilm formation were investigated when biofilms were grown for different time periods. Biofilms were grown stationary in microtiter plates for three, five and seven days in artificial saliva (AS) as described in section 2.6. Biomass was then stained with Crystal violet stain and the amount of biofilm formed was inferred from the absorbance values obtained after solubilising the stain. The higher the quantity of the biofilm formed, the higher the value of absorbance measured by the spectrophotometer. The data obtained from the biomass quantification was found not to conform to normal distribution, that is why all the statistical tests used were non-parametric. Statistical analysis was performed in two steps – individual groups were first analysed using Kruskal-Wallis test

to find the overall significance in groups. Significant differences were confirmed in each analysed group, therefore a Mann-Whitney U test was performed in the second step to find specific significance values between specific pairs of data sets.

To start with, biofilm formation of individual subspecies was analysed comparing the amount of biomass quantified at three different time points (Fig. 3.9.). *Streptococcus sanguinis* (SS) was used as a positive control because it has been used as the main biofilm forming oral microbe in many publications and characterised as a reliable biofilm former producing stable biofilms. As expected, the amount of biofilm in the positive control (SS) increased significantly at each time point (Fig. 3.9. G; 3 days vs. 5 days –  $p = 0.009$ ; 5 days vs. 7 days –  $p = 0.016$ ). Biofilm layers were found to be homogeneous and stable when observed visually before the removal of the AS and biofilm washing on the day of the biomass staining.

Interestingly, distinct patterns of biofilm growth were observed in individual subspecies of *F. nucleatum* (Fig 3.9 A-F). The amount of biofilm increased significantly from day three to day five in FNA, FNF, FNN23, FNP and FNV ( $p = 0.009$  for each subspecies). The increase in the amount of biofilm during this period was only not significant in the case of FNN25 ( $p = 0.175$ ), however when the biofilm growth was monitored for two more days, this was the only *F. nucleatum* subspecies which produced significantly higher amount of biomass ( $p = 0.009$ ). When the build-up of biomass was compared between day five and day seven, the amount of biofilm significantly decreased in case of FNA and FNF ( $p = 0.047$  and  $p = 0.009$ , respectively). The quantity of biomass did not significantly change in case of FNN23, FNP and FNV ( $p = 0.754$ ,  $p = 0.076$  and  $p = 0.602$ , respectively). The amount of biomass produced from the beginning of the experiment till the end increased significantly in FNN23, FNN25, FNP and FNV ( $p = 0.009$ ). For a more detailed table of the statistical results see the Appendix section (Appendix 4).

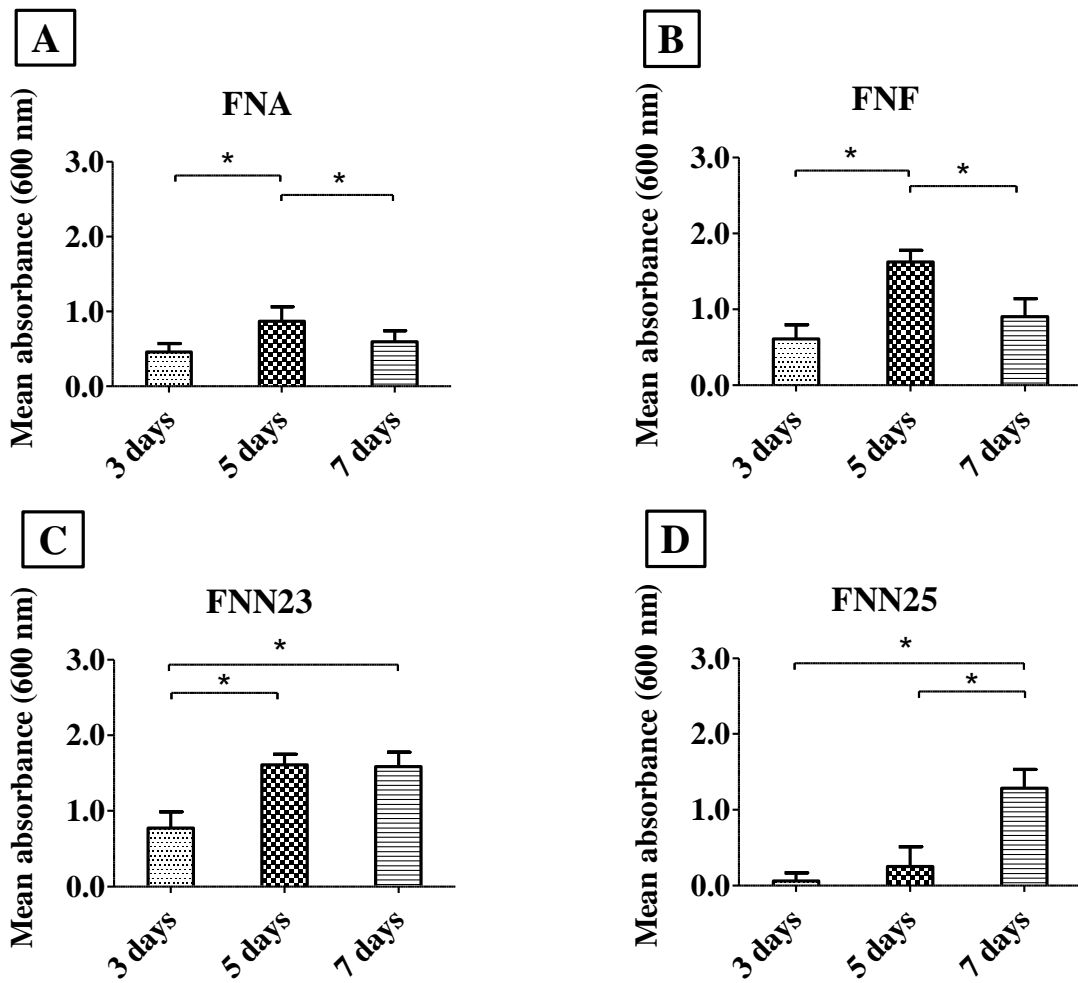


**Figure 3.9. The amount of biofilm formed by individual subspecies.** Graphs and the figure legend continued on the next page.

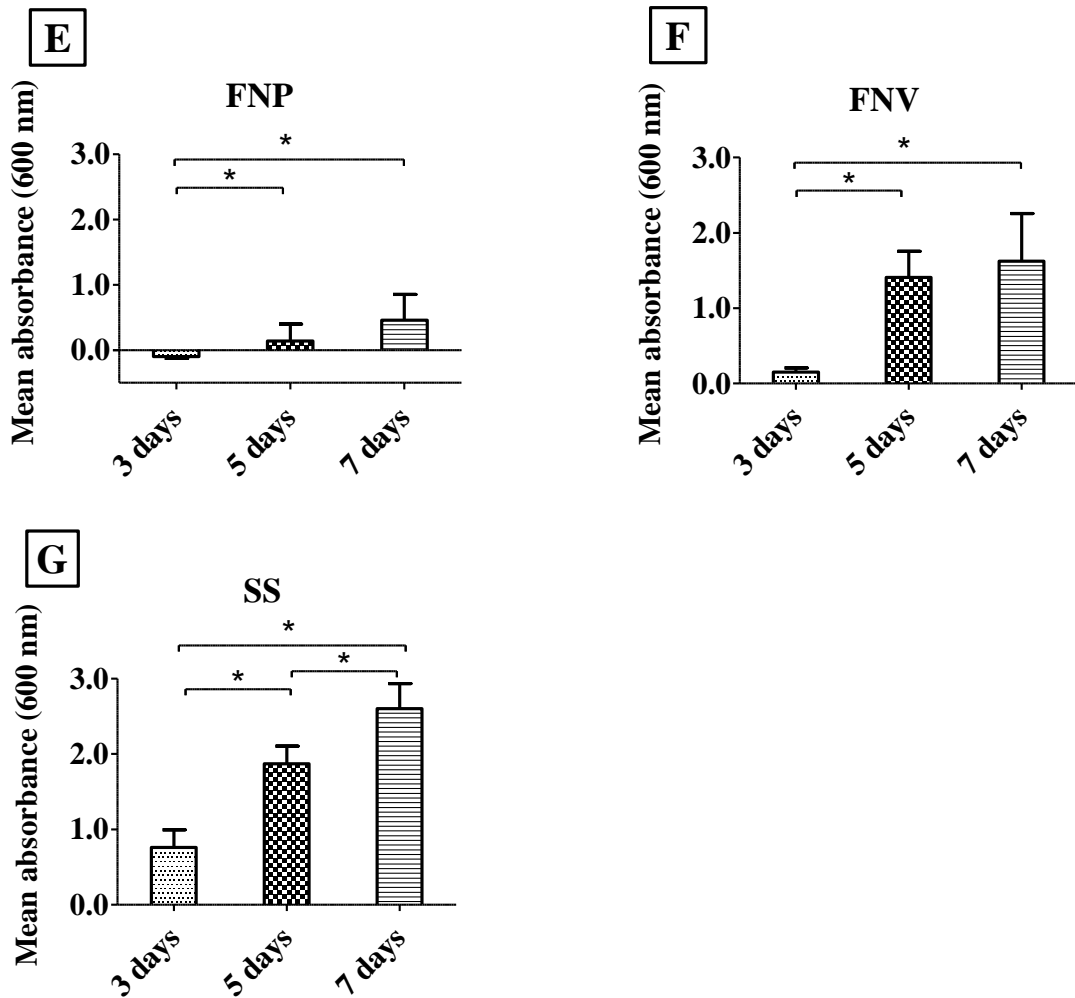


**Figure 3.9. The amount of biofilm formed by individual subspecies.** Each graph shows the biomass quantified at three different time points. Absorbance was measured at 600 nm. Individual groups were analysed using Kruskal-Wallis and Mann-Whitney tests. Asterisks (\*) represent significant difference ( $p \leq 0.05$ ). Error bars show standard deviation,  $n=5$ .

Secondly, the variation in the amount of biofilm formed at specific time points comparing all subspecies was analysed. Strikingly, SS formed the most biomass at each time point. When the biomass was quantified after three days of biofilm growth (Fig 3.10), FNA, FNF and FNN23 were among the strongest biofilm formers (comparison with SS –  $p = 0.076$ ,  $p = 0.251$ ,  $p = 0.754$ , respectively), while FNN25, FNP and FNV formed significantly lower amounts of biofilm (comparison with SS –  $p = 0.009$  for all three subspecies). As the graph in Fig. 3.10 A shows, mean absorbance of FNP is reported as a negative value. This was caused by the fact that absorbance values were corrected for the “blank” – AS without bacteria. These wells were confirmed not to be contaminated during the incubation by daily plating of the media on agar plates (see Appendix 5) as well as by Gram staining. Therefore, it was only the background staining that was detected. The amount of stained biomass in case of FNP was so low that the mean absorbance value was almost equal to the mean absorbance value of the background staining of the wells with the AS only.

When the biofilms were stained after five days of incubation, FNF was the strongest biofilm former when compared to the positive control SS ( $p = 0.076$ ). Subsequently, comparison of FNF with other subspecies showed that also FNN23 ( $p = 1.000$ ) and FNV ( $p = 0.347$ ) were among the strongest biofilm formers as they were not significantly different from FNF. FNN25 and FNP were the weakest biofilm formers, with  $p$  values of 0.009 when compared to the rest of the subspecies. FNA formed an intermediate amount of biofilm significantly different from the highest and the lowest absorbance values of the subspecies ( $p = 0.016$  compared to FNV;  $p = 0.009$  compared to the rest of the subspecies). Detailed results of the statistical analysis can be found in the Appendix section (Appendix 6).

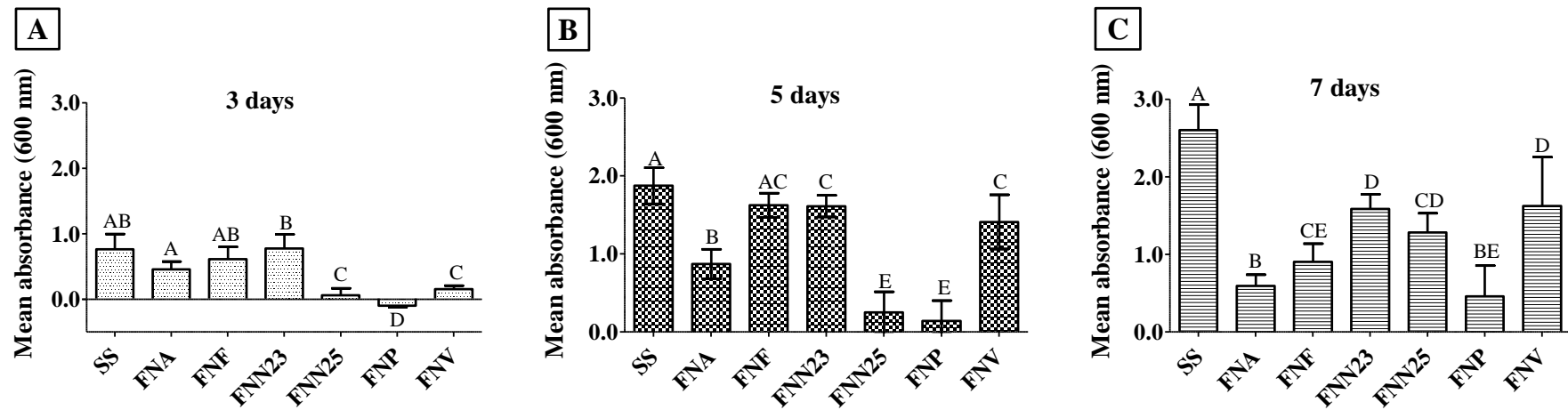


**Figure 3.10. The amount of biofilm formed by all subspecies at specific time points.** Absorbance was measured at 600 nm. Individual groups were analysed using Kruskal-Wallis test and Mann-Whitney test. Different letters indicate significant difference ( $p \leq 0.05$ ). If the groups share the same letter, the difference is non-significant. Error bars show standard deviation,  $n=5$ .

Incubation of biofilms for seven days showed that none of the *F. nucleatum* subspecies reached the level of biofilm formed by the positive control and all of them were significantly lower ( $p = 0.009$ ). FNN23, FNN25 and FNV were found to form the most abundant biofilms out of all *F. nucleatum* subspecies, whereas FNA and FNP formed the least abundant biofilms ( $p = 0.009$  both subspecies). FNF was classified as an intermediate biofilm former due to the fact that it was not significantly different from FNN25 and FNP ( $p = 0.075$  and  $p = 0.076$ , respectively).

Based on the mean absorbance values, it can be concluded that the amount of biofilm varied significantly among the subspecies at different time points. However, it is important to mention that not only the amount of biomass, but also the stability of individual biofilms varied. Microtiter plates with the biofilms were handled daily, when the old medium was replaced with the fresh medium. Biofilms were also washed before the staining procedure. These steps of media replacement and washing were performed slowly and gently, strictly avoiding vigorous pipetting, however it was noticed that the biofilm layer was easily disturbed, especially in the case of FNP. Crystal violet staining suggests that the most stable biofilm layer was formed either as a considerably intense purple ring on the walls of the wells or on the perimeter of the bottom of each well. Fig. 3.11. shows these patterns of stable biofilm formation on the day of staining of seven days old biofilms. A ring lighter in colour was observed on the walls as well as on the bottoms of the wells with the AS only (negative control). This was considered to be background staining. Interestingly, SS seems to form very faint biofilm rings on the walls of the wells when compared to well-defined, sharp biofilm rings of *F. nucleatum* subspecies.

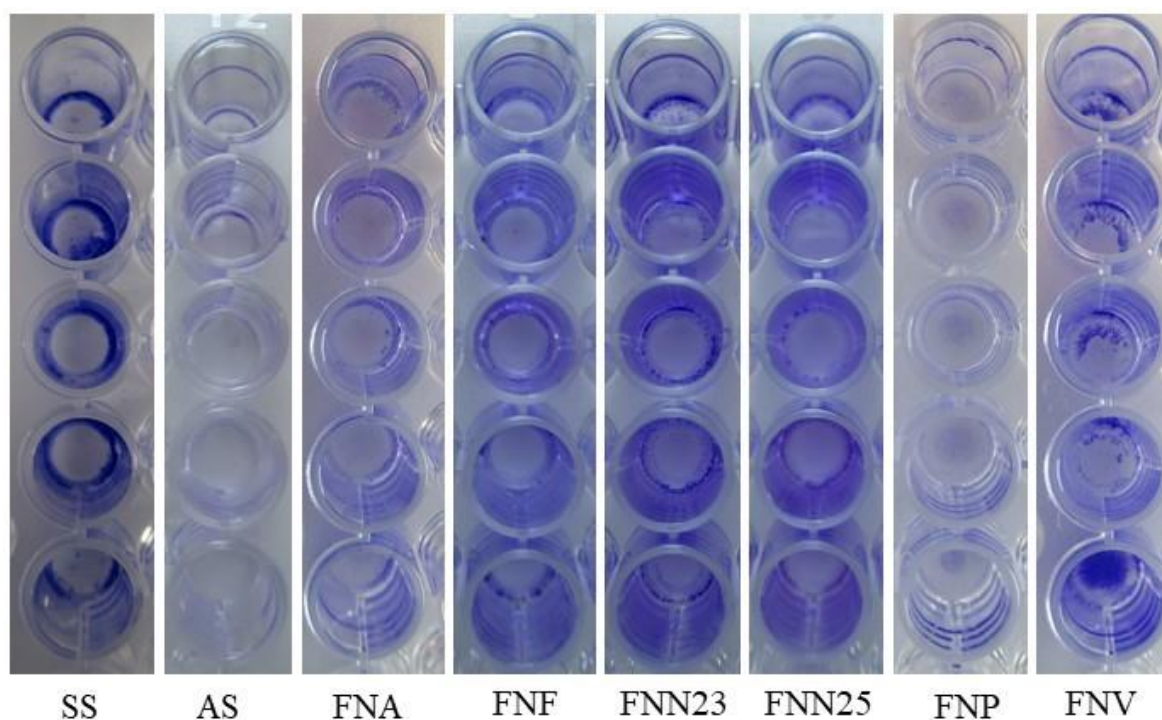


**Figure 3.11. *F. nucleatum* subspecies biofilms stained with Crystal violet.** The staining shows the pattern of stable biofilm formation in the wells of a 96-well polystyrene plate suitable for cell culture. Biofilm is visible either as rings formed around the walls of the wells or as deposits on the perimeter of the bottoms of the wells. The bottom well of FNV was the only example of a thick biofilm layer formed in the centre of the well. FNP exhibits a very faint layer of stained biofilm in the centre of each well. SS – positive control, AS – negative control.

The pictures of the stained biofilms support the claim that the biofilm stability varies among the subspecies. Stained biofilms were observed as uneven patches rather than homogeneous layers, which indicates that the fragile biofilm layers might have been removed during the washing step. The best example is FNV. One well contains biofilm formed in the centre of the well, while the remaining 4 show irregular areas of stained biofilm. This leads to another conclusion stating that mono-species biofilms of *F. nucleatum* subspecies form unstable biofilms when grown in artificial saliva on a polystyrene surface, even if it is treated to promote cell adhesion.

### 3.2.2. *Mono-species biofilm architecture and structure analysed by SEM*

In order to understand the 3D structure of individual mono-species biofilms as well as the pattern of cell-to-cell cohesion, biofilms were grown for SEM analysis in 24-well plates on Nunc™ Thermanox™ coverslips (section 2.6.), which have, similarly to 96-well plates described above, a specially treated surface to support cell attachment. Additionally, the coverslips can be easily removed from the plate and mounted onto the SEM aluminium stubs. Biofilms were grown for three, five and seven days. Biofilms were monitored for contamination by daily plating of the supernatant and the AS on SAA plates and the bacteria growing on the plates after incubation in the anaerobic chamber were identified both by observing colony morphology (Appendix 5) as well as Gram staining. Biofilms were additionally inspected for contaminants during the SEM by looking for bacterial cells with morphologies that did not correspond to *F. nucleatum* morphology (Appendix 7).

To start with, all biofilms shared certain common characteristics. None of the subspecies formed a continuous layer of biofilm covering the majority of the coverslip area. When observed under low magnification (100x), biofilms were seen as patches of biomass rather than a homogeneous layer (Appendix 8). FNN23 and FNN25 grown for seven days seemed to produce a continuous layer of biofilm when observed at 100x (Appendix 8), however when the magnification was increased to 2000x, irregularities in the biomass formed were evident. This agrees with the Crystal violet biomass staining results (Fig. 3.11.) showing stained patches rather than a continuous layer.

Another characteristic that was observed in multiple cases was the formation of water channels (Fig. 3.12). These are characterised as pores that form in the biofilm layer in order for water and nutrients to diffuse through the biomass (Stewart, 2003). The water channels were found in biofilms grown for different time periods, however the most occurrences of the water

channels were in the biofilms grown for seven days (FNA, FNN23, FNP and FNV - Fig. 3.12, C, I, O, S, respectively, yellow circles).

Interestingly, all biofilms contained small irregular particles incorporated into the network of bacteria, which were confirmed not to be contaminants. These particles were inconclusively identified either as the constituents of the AS which aggregated with the bacteria during the biofilm formation or debris of the extracellular matrix.

The amount of biomass formed seems to correspond to the results of crystal violet biomass quantification only in the case of FNP and FNV. When the FNP biofilms were observed visually, there were only a few bacterial cells attached to the coverslips after three days of incubation. The number of bacteria which aggregated into the biofilm increased after five days of incubation and a complex network of interconnected bacteria could be seen after seven days. In the case of FNV, a very small area was covered with biofilm after three days. The amount of biomass significantly increased after five days and interconnected bacteria in the biofilm were observed after seven days.

When it comes to the cell-cell cohesion, two distinct patterns were observed. Firstly, individual bacterial cells were found to cohere to the neighbouring cells side by side. The cells were observed to be either bent and cohere with other cells only partially or they were aligned in a parallel position, cohering with the whole side of the cell. Secondly, the bacterial cells cohered end to end. This can be clearly seen in Fig. 3.12 (B, E, F, H, S), where long, connected structures are seen to be spanning considerably long distances.

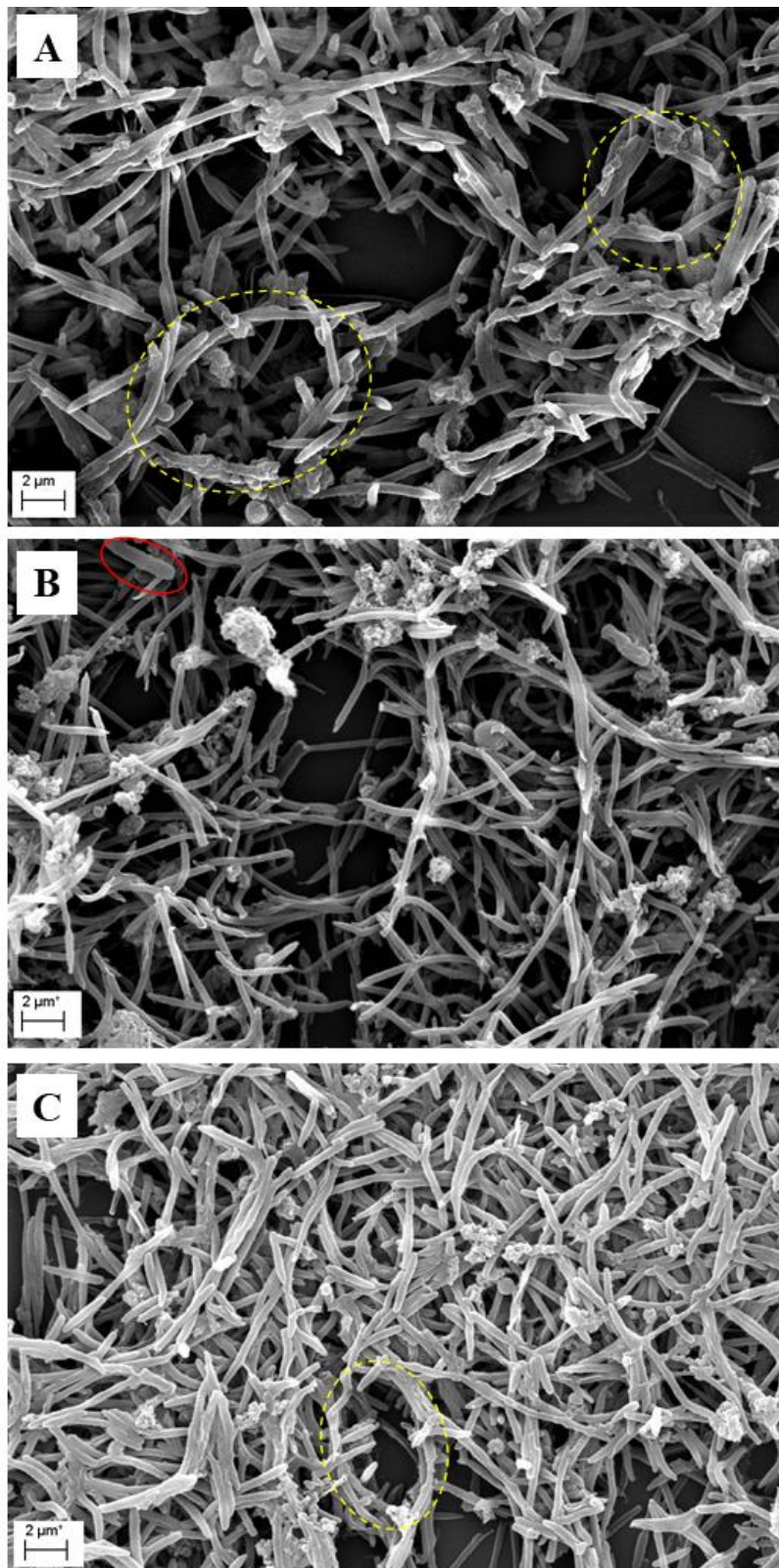


**Figure 3.12. Mono-species FNA biofilms.** Biofilms were grown for three days (A) five days (B) and seven days (C). Yellow circles show water channels formed. Red circle shows a bacterial cell with different morphology. Magnification 8000x.

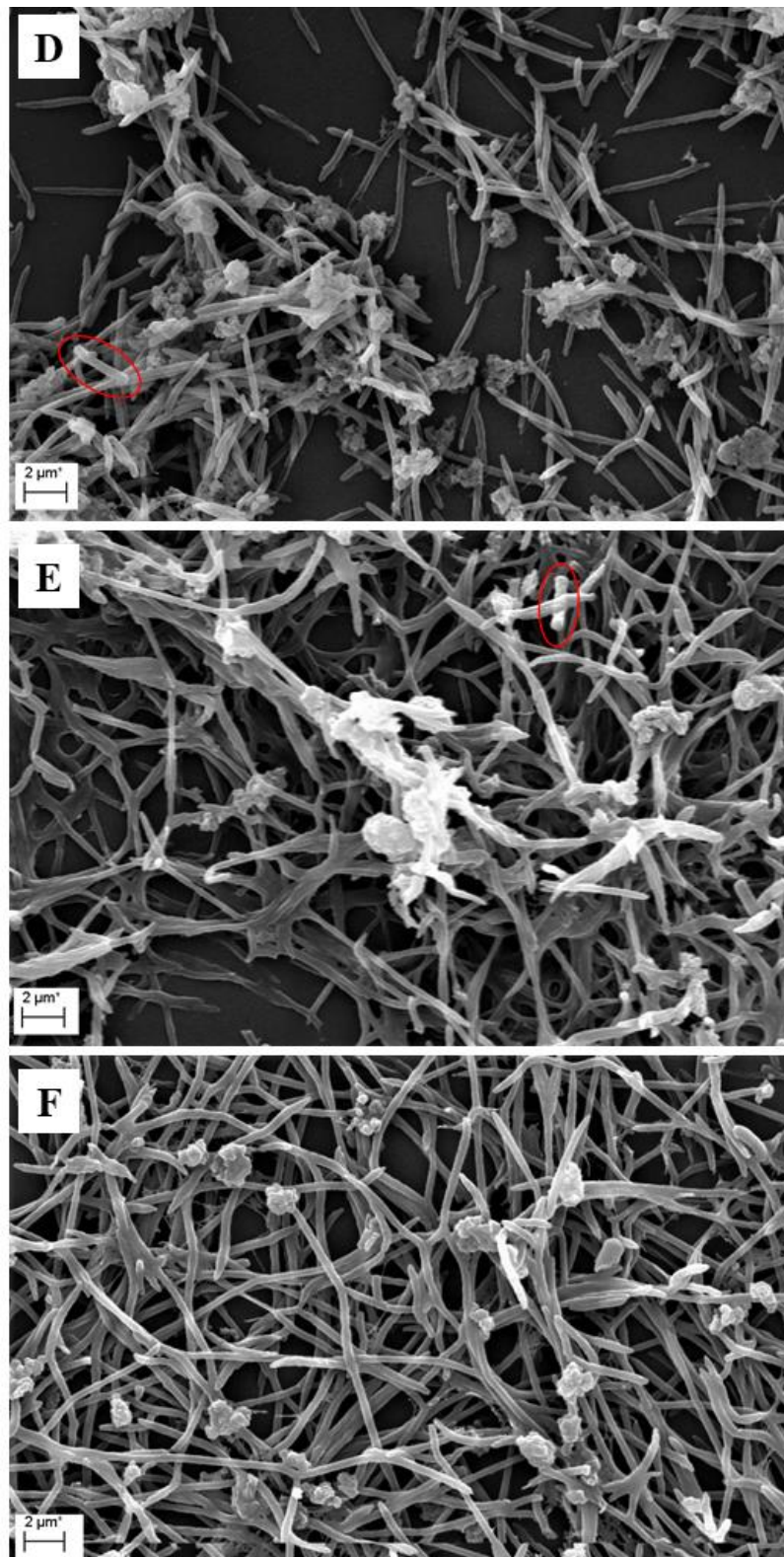


**Figure 3.12. Mono-species FNF biofilms.** Biofilms were grown for three days (D), five days (E) and seven days (F). Red circles show bacterial cells with different morphology. Magnification 8000x.

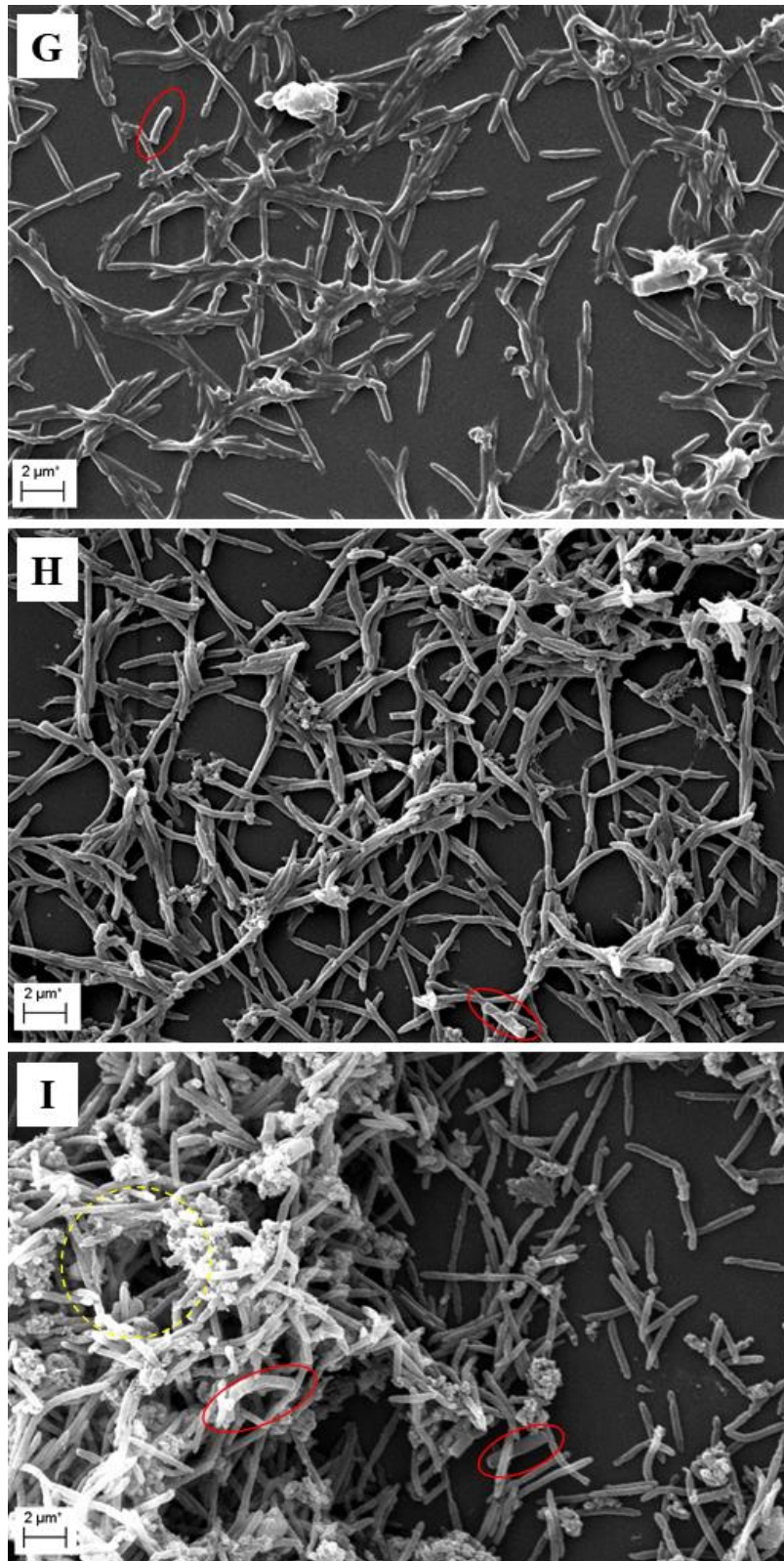


**Figure 3.12. Mono-species FNN23 biofilms.** Biofilms were grown for three days (G), five days (H) and seven days (I). Yellow circle shows a water channels formed. Red circles show bacterial cells with different morphology. Magnification 8000x.

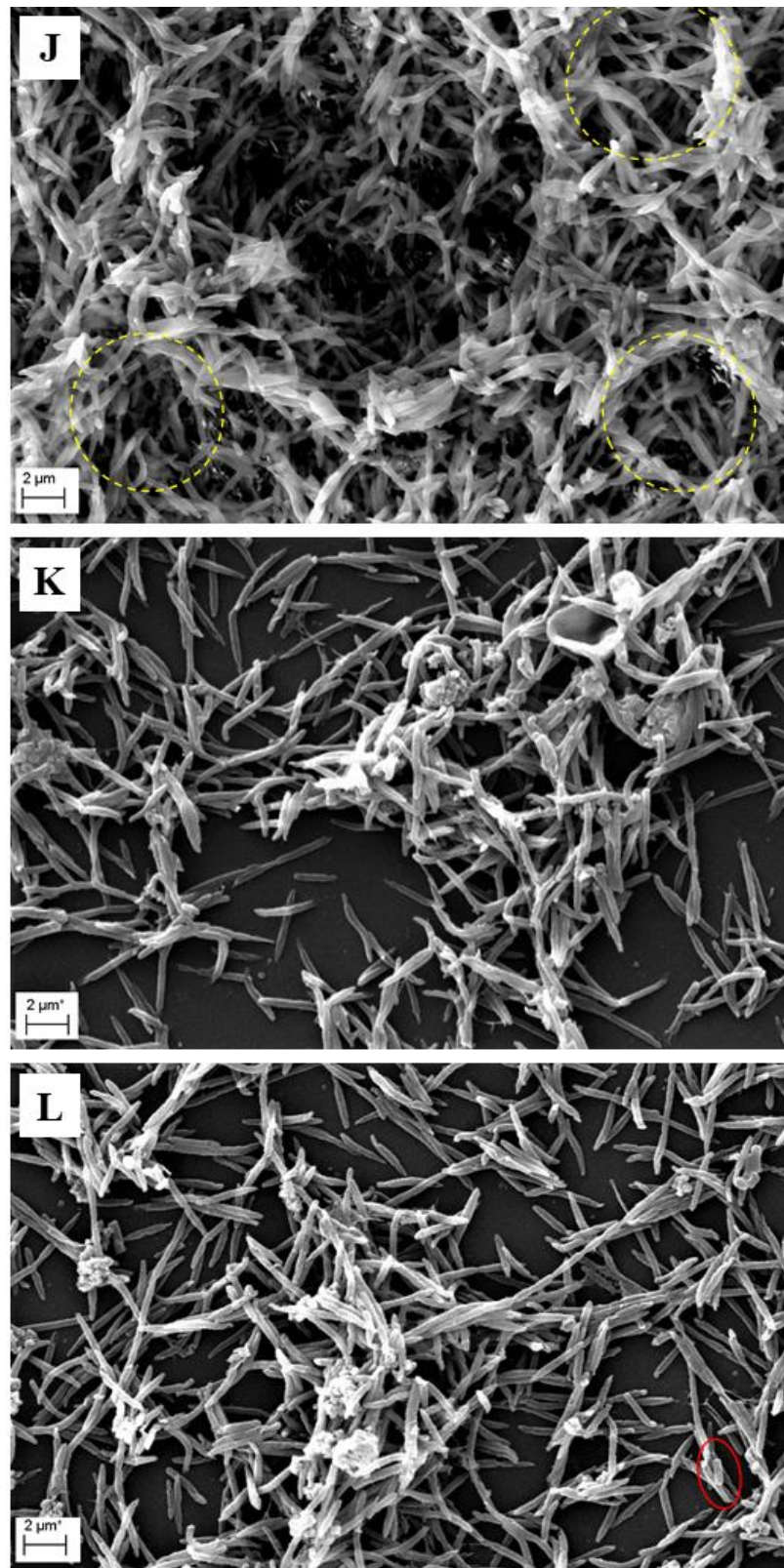


**Figure 3.12. Mono-species FNN25 biofilms.** Biofilms were grown for three days (J), five days (K) and seven days (L). Yellow circles show water channels formed. Red circles show bacterial cells with different morphology. Magnification 8000x.

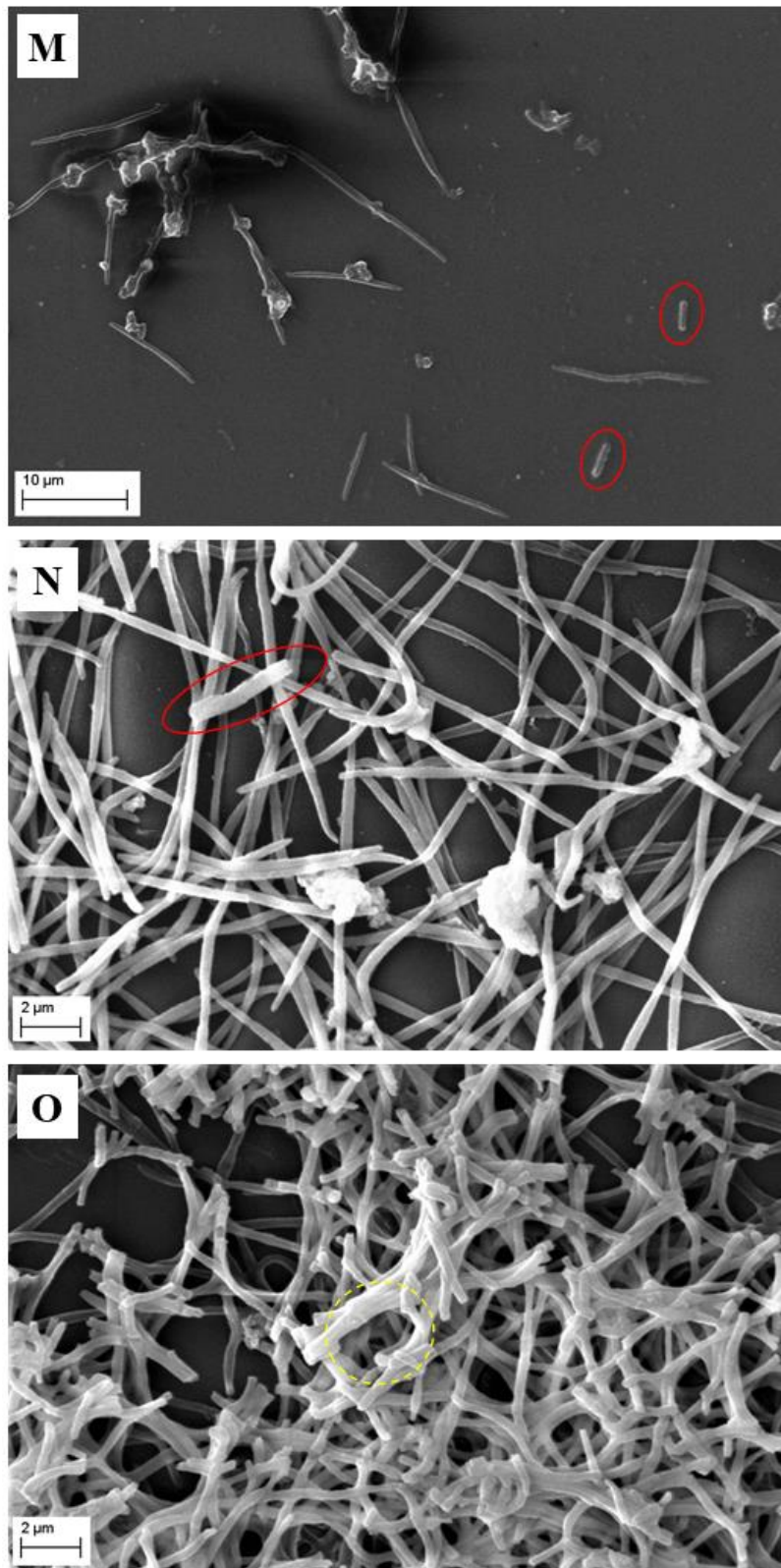


**Figure 3.12. Mono-species FNP biofilms.** Biofilms were grown for three days (M), five days (N) and seven days (O). Yellow circle shows a water channel formed. Red circles show bacterial cells with different morphology. Magnification 8000x.

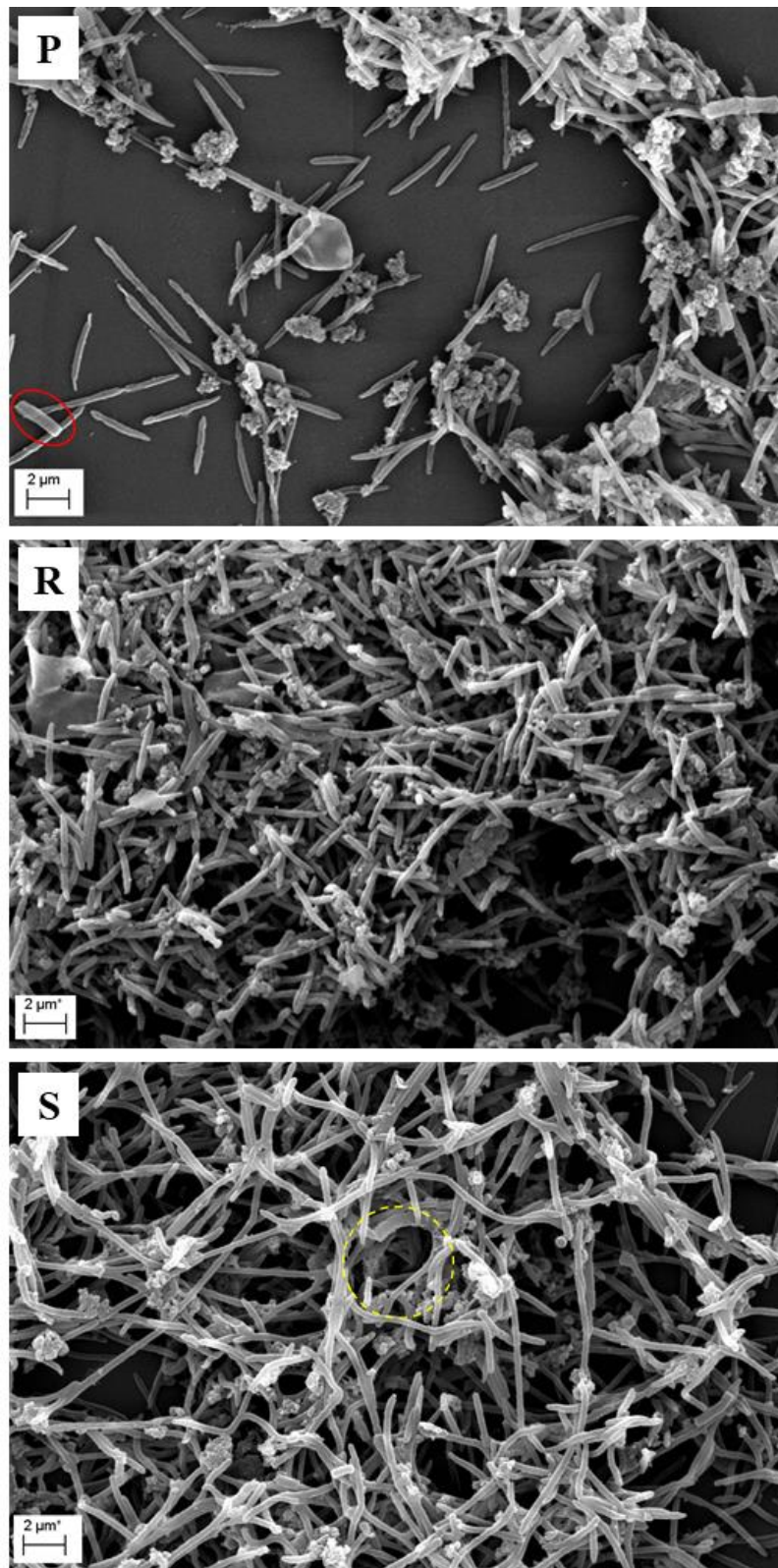


**Figure 3.12. Mono-species FNV biofilms.** Biofilms were grown for three days (P), five days (R) and seven days (S). Yellow circle shows a water channel formed. Red circle shows a bacterial cell with different morphology. Magnification 8000x.

Additionally, a number of biofilms at different time points was observed to contain cells with morphology different from *F. nucleatum*. These cells were both shorter and longer bacilli with bulky, hemispherical caps as opposed to *F. nucleatum* cells with tapered ends (highlighted by red circles in Fig. 3.12, B, D, E, G, H, I, L, M, N, P). The surface of some of the cells seemed to be rougher compared to *F. nucleatum* cells (Fig. 3.12. E, H, I, N, P). Initially the cells were thought to be *E. coli* contamination, however they were confirmed not to be contaminants.

### 3.2.3. Evaluation of biomass production in multi-species biofilms

Biofilm models containing multiple human oral commensals as well as pathogens are used to study different levels of dental and periodontal disease, from caries to gingivitis and periodontitis. Various models incorporate different *F. nucleatum* subspecies (Millhouse *et al.*, 2014; Sherry *et al.*, 2016; Ramage *et al.*, 2017). A “mini” biofilm model, containing four human oral bacterial species including FNP, was used in this study in order to understand *F. nucleatum* interaction with different oral microbes. As this model has been published (Ramage *et al.*, 2017) and used for further studies with epithelial cells, it was considered to form a stable layer of biomass and provide a reliable reference for the experiments performed in this project and in the future investigations. Apart from growing the original version of the biofilm model, FNN23 was incorporated into this model, replacing FNP, to find out whether this subspecies forms equally stable biofilms and whether there are differences observed depending on the subspecies incorporated. Understanding FNN23 behaviour in the multi-species biofilm can provide information for future studies with FNN23 mutants, as FNN23 is the only reliably genetically tractable subspecies to date.

In order to quantify the amount of biomass produced in each biofilm model, the biofilms were grown as described in section 2.7., in 96-well microtitre plates suitable for cell culture for seven

days and the biomass was subsequently stained with crystal violet. Both groups were corrected for the blank – the absorbance values from the wells with artificial saliva (AS) only. The groups were statistically analysed using Mann-Whitney test.

Strikingly, when the groups were compared, the amount of biomass in the biofilm containing FNN23 was significantly higher than in the biofilm containing FNP ( $p=0.000157$ ) (Fig. 3.13.).

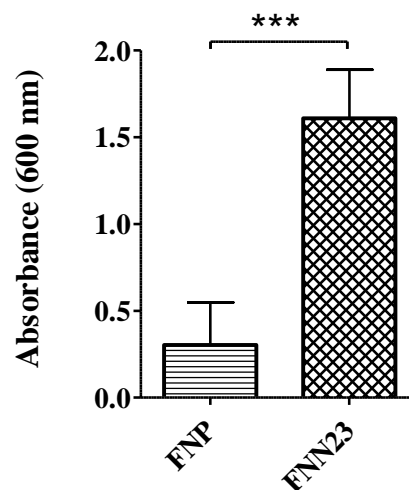


**Figure 3.13. The amount of biomass quantified in the multi-species biofilms.** Absorbance was measured at 600 nm. Individual groups were analysed using Mann-Whitney test. Asterisks (\*\*\*) represent a high level of significant difference ( $p < 0.001$ ). Error bars show standard deviation,  $n=10$ . FNP – multi-species biofilm containing FNP; FNN23 - multi-species biofilm containing FNN23.

This significant difference in the absorbance is supported by the pattern of crystal violet staining when the 96-well plate was visually examined. The wells containing only AS were monitored for microbes introduced during AS changes and were confirmed to be contaminant-free. Rings of varying intensity were observed on the walls of AS only wells, therefore this was considered to be a background staining. As Fig. 3.14. shows, multi-species biofilms containing FNN23 formed a thick layer of biofilm on the perimeter of the bottom of each well, whereas biofilms

containing FNP formed a much thinner layer of biofilm, judging from faint circles observed on the perimeter of the bottom of the wells.

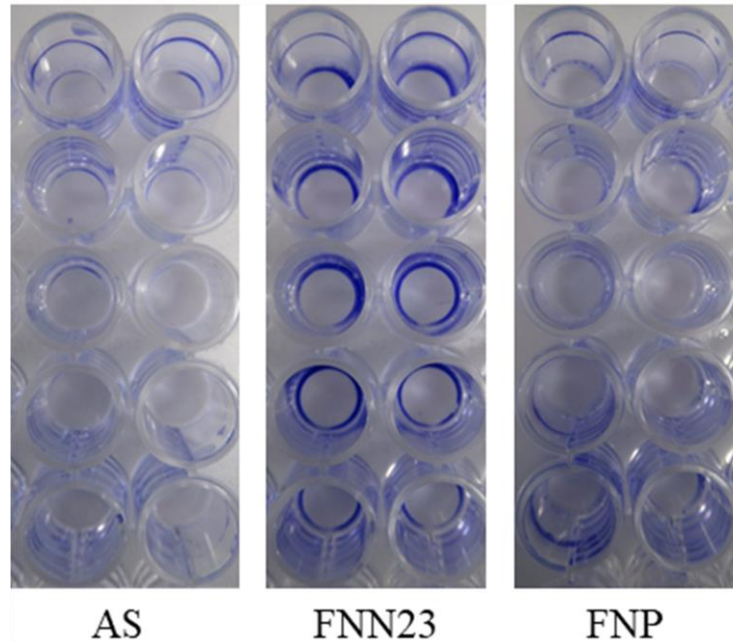


**Figure 3.14. Pattern of biofilm formation in multi-species biofilms.** Crystal violet staining shows significant differences in the amount of biomass formed by each type of multi-species biofilm. AS – Artificial saliva only; FNN23 – multi-species biofilms containing FNN23; FNP – multi-species biofilms containing FNP.

These findings indicate that if FNN23 is incorporated into a multi-species biofilm model, the amount of biomass formed is significantly higher and the biofilm layer is very likely more stable. The results also suggest that FNP can be replaced in a model of multi-species biofilm by FNN23 in order to perform studies with mutant FNN23 subspecies.

#### 3.2.4. *Multi-species biofilm architecture and structure analysed by SEM*

In order to understand how *F. nucleatum* subspecies are interacting with the oral commensal as well as pathogenic bacteria, the aforementioned multi-species biofilm model was analysed using SEM. The biofilms were grown on the Nunc™ Thermanox™ coverslips, fixed and

dehydrated and subsequently visualised thanks to the scanning electron microscope Zeiss EVO MA10.

To start with, when the biofilm containing FNP was visualised, no layer of biofilm was observed, contrary to what was expected based on the literature (Ramage *et al.*, 2017), only individual bacterial cells attached to the substrate and a number of clusters of bacteria. These clusters might be the micro-colonies initiating the biofilm formation (Fig 3.15.).

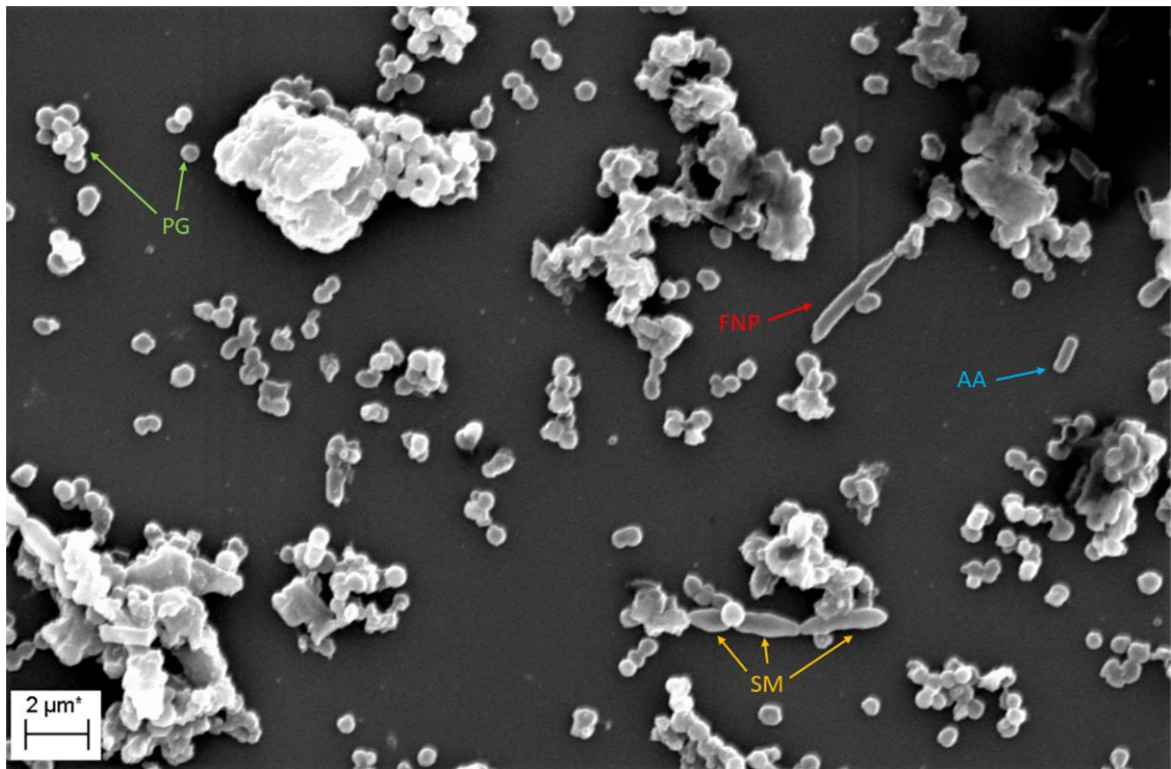


**Figure 3.15. Micrograph of the multi-species biofilm containing FNP.** Individual coloured arrows identify the bacterial species present: AA – *A. actinomycetemcomitans*; FNP – *F. nucleatum ssp. polymorphum*; PG – *P. gingivalis*; SM – *S. mitis*. Magnification – 8000x.

All four species were identified to be present in the visualised sample. The Atlas of Oral microbiology (2015, p. 79, 85 and 91) was used to help identify and confirm the presence of individual species. PG (green arrows) was the most numerous species in the analysed field, characterised as cocci or coccobacilli. The presence of one FNP cell was identified in this field

(red arrow), thanks to its long shape with tapered ends. SM was observed as a chain of prolonged coccobacilli dividing at multiple planes. AA was found as a single cell as it was in the case of FNP.

When the biofilm containing FNN23 was visualised, a much more abundant layer of biofilm with a complex structure was observed (Fig. 3.16.). All four species were also identified in this biofilm model (representatives indicated by the colour-coded arrows).

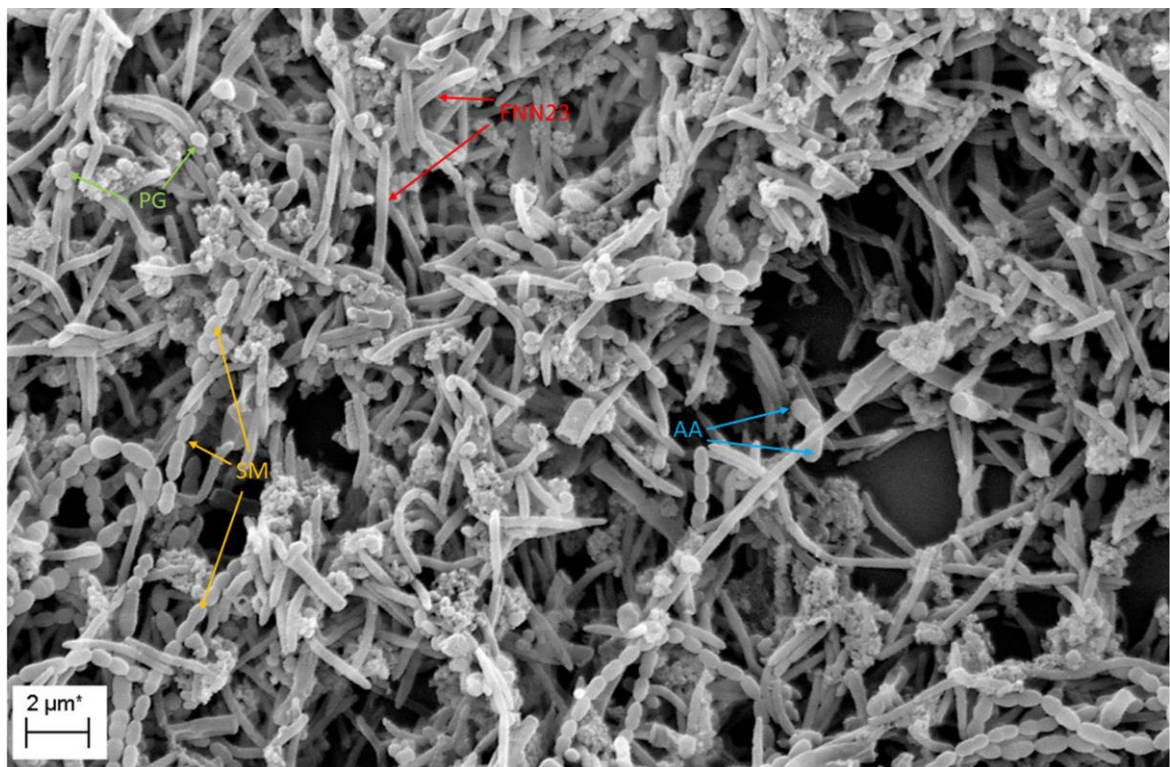


**Figure 3.16. Micrograph of the multi-species biofilm containing FNN23.** Individual coloured arrows suggest the identity of the bacterial species: AA – *A. actinomycetemcomitans*; FNN23 – *F. nucleatum* ssp. *nucleatum* ATCC 23726; PG – *P. gingivalis*; SM – *S. mitis*. Magnification – 8000x.

Thanks to a much higher amount of biofilm formed it was possible to examine the interaction of FNN23 with the other species used in the model. As anticipated, FNN23 cohered to its own subspecies (red arrows) in the same way as it was observed in the mono-species biofilm. FNN23 also cohered with interspersed PG cells (green arrows). Long chains of SM also closely

interacted with FNN23. The cells that were identified as AA (blue arrows) were also in close contact with FNN23.

The results obtained thanks to the SEM analysis support the results of the crystal violet biomass quantification, showing that when FNN23 was incorporated into the biofilm model replacing FNP, the amount of biofilm was significantly higher. The results also indicate that FNP can be replaced in this model by FNN23 without affecting the architecture of the biofilm, when comparing the modified model to the original biofilm shown by the authors (Ramage *et al*, 2017). Lastly, the result suggests that FNN23 can be used in a multi-species biofilm model replacing FNP and the behaviour of a mutated FNN23 can be studied.

### 3.2.5. Chapter conclusions

Significant differences in the amount of biomass of single-species biofilms were observed when individual subspecies were grown for different periods of time as well as when all subspecies were compared at a specific time point. SEM analysis of the architecture of the mono-species *F. nucleatum* biofilms showed that the subspecies do not form a continuous layer of biofilm covering a large surface area, but rather small patches of biomass with irregular thickness, ranging from a layer of single cells to clumps of complex structures of interconnected bacteria. The amount of biomass formed differed significantly when FNN23 was introduced into a multi-species biofilm, replacing FNP. Introducing FNN23 possibly positively affected the bacterial interaction and the biofilm architecture.

### **3.3. Optimisation of RNA extraction from *Fusobacterium nucleatum* subspecies**

One of the aims of this thesis was to analyse the production of CDNs by *F. nucleatum* subspecies at different stages of the exponential phase of growth. In order to understand whether the amount of CDNs produced changes as the bacterial population proceeds through the stages of the bacterial growth, the expression of specific genes responsible for the synthesis and degradation of CDN, cyclases and hydrolases, was analysed using a highly sensitive molecular method known as qRT-PCR. In order to perform the qRT-PCR assay, first it was necessary to extract pure RNA from the studied bacterial samples in order for the qRT-PCR assay to provide true results, as RNA contaminated with genomic DNA (gDNA) could generate false expression results.

The use of a routinely employed kit for RNA isolation proved to be ineffective for RNA extraction from *F. nucleatum* subspecies, it was therefore necessary to find and optimise a method for successful isolation of pure RNA. Multiple RNA isolation kits as well as a conventional phenol-chloroform RNA extraction method were tested during the optimisation process. Thanks to the growth curves generated at the beginning of the project (section 3.1.2., fig. 3.5.), it was possible to find the early, intermediate and the late stage of the exponential phase (EP). Based on these findings, each extraction was performed from bacterial cultures grown for four hours (T4 – early EP), eight hours (T8 – intermediate EP) and 24 hours (T24 – late EP). To illustrate the optimisation process, the results of each RNA extraction will be shown in order to clearly describe specific changes applied after each experiment.

#### *3.3.1. Optimisation of RNA extraction – Extraction n. 1*

To start with, the first RNA extraction was performed from FNN25 using the Quick-RNA™ Fungal/Bacterial Miniprep Kit (for details see section 2.14.1). The number of bacteria used for

the extraction was  $1 \times 10^9$ , which was the maximum advised in the manufacturer's instructions. The lysate was not treated with DNase because the kit contained specialised columns for gDNA removal. The concentration of the eluted RNA was quantified using the nanodrop as follows: T4 – 0.023  $\mu\text{g/ml}$ , T8 – 15.7  $\mu\text{g/ml}$  and T24 – 4.431  $\mu\text{g/ml}$ . The purity of the isolated RNA was tested by conventional PCR using 16S universal primers and the PCR products were visualised on an agarose gel. If the PCR is performed with RNA as the template, no amplification is expected, which means that no bands should be visible on the gel. When the gel was visualised, no bands were observed in the lanes containing RNA samples. However, no band was observed in the positive control either (Fig. 3.17.), which suggests error in the PCR setup.

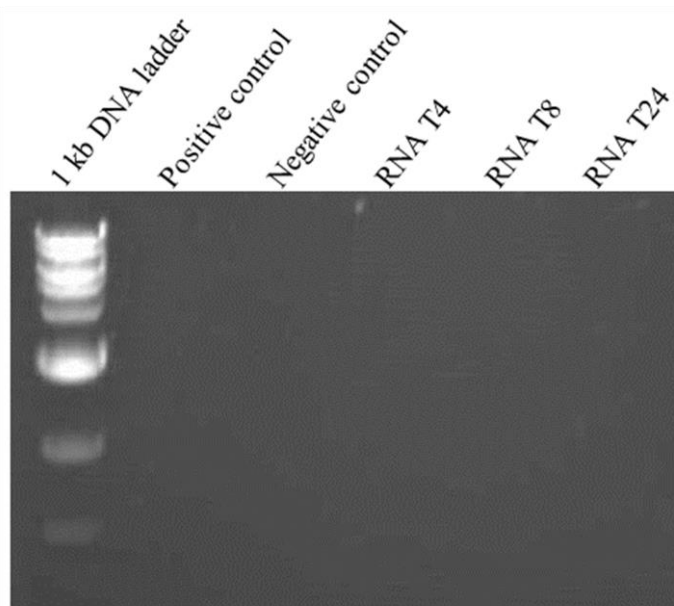


**Figure 3.17. RNA extraction n.1 from FNN25.** RNA was extracted from FNN25 and Uni 16S II primers were used. No visible bands can be observed on the gel, especially in the positive control. Negative control contains nuclease-free water as a template. Electrophoresis settings: 120V, 30 minutes. 1kb DNA ladder used (N3232, New England Biolabs).

Due to the absence of the band in the positive control as well as a very low concentration of the isolated RNA, it was decided that the extraction was to be repeated again. A 10-times higher

number of bacteria was be used for the extraction in order to increase the concentration of the RNA extracted.

### 3.3.2. Optimisation of RNA extraction – Extraction n. 2

This RNA extraction was performed using the same kit as during the extraction n.1. The number of bacteria lysed in this experiment was  $1 \times 10^{10}$  and no DNase treatment of the lysates was involved. The concentration of the eluted RNA increased as follows: T4 – 89.02  $\mu\text{g/ml}$ , T8 – 61.79  $\mu\text{g/ml}$  and T24 – 75.82  $\mu\text{g/ml}$ . The RNA purity was tested using FN-specific primers (FN-spec.) and 16S bacterial rRNA universal primers II (Uni 16S II). When the gel was visualised, bright bands were observed in both tested RNA groups (Fig. 3.18.). This showed that the extracted RNA was contaminated with gDNA.

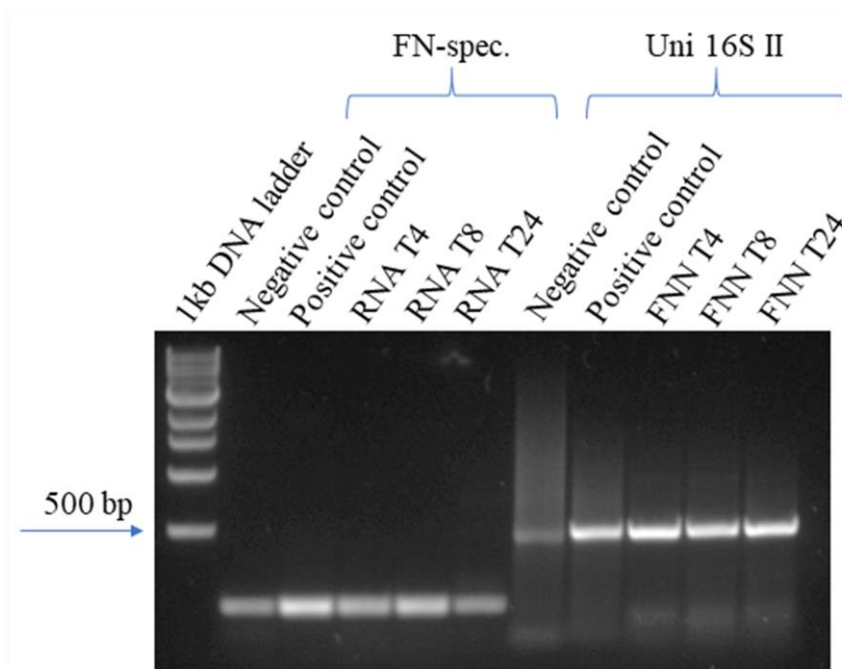


**Figure 3.18. RNA extraction n.2 from FNN25.** Bright bands visible in all lanes containing RNA samples demonstrating gDNA contaminating all RNA samples. Negative controls contain nuclease-free water as a template. Contamination found in both negative controls. Electrophoresis conditions: 120 V, 30 minutes. DNA ladders used: 1 kb DNA ladder (N3232, New England Biolabs); 100 bp DNA ladder (11300, Norgen Biotek).

Additionally, bands were observed in both negative controls. Faint bands with the size of approximately 100 bp in the lanes with Uni 16S II primers were identified as primer dimers. Due to the contamination issues, another RNA extraction was performed and a different kit was chosen. It was also decided to use a new batch of the nuclease-free water to avoid contamination in the negative controls. Gaps between the negative and the positive control were introduced in order to prevent possible leakage of the positive sample into the well with negative sample.

### *3.3.3. Optimisation of RNA extraction – Extraction n. 3*

For this RNA extraction, the Monarch® Total RNA Miniprep Kit was used as described in section 2.14.2. This kit contained gDNA removal columns as well as DNase I enzyme, therefore complete removal of gDNA was expected. In order to maintain the RNA yield considerably higher when compared to the first extraction,  $1 \times 10^{10}$  bacteria were used for lysis. The lysates were treated with DNase on-column for 15 minutes at room temperature. RNA eluted was quantified as follows: T4 – 23.63  $\mu\text{g/ml}$ , T8 – 34.15  $\mu\text{g/ml}$  and T24 – 8.72  $\mu\text{g/ml}$ . PCR contamination check was performed using FN-spec. primers (Fig. 3.19. A) and Uni 16S II (Fig. 3.19. B). When PCR products were observed on the gel, one bright band of the expected size was observed in the positive control in both tested RNA groups (Fig. 3.19.). The negative control was not contaminated and only contained a band corresponding to primer dimers. The extracted RNA was confirmed to be again contaminated by gDNA as very bright bands were visible in both groups of RNA (Fig. 3.19.). The bands visible in gel B, which have approximately 100 bp, were identified as primer dimers. After performing the PCR contamination check, it was found out that the concentration of the DNase I Buffer used was incorrect (10X), that it why it was decided that the samples would be treated with DNase again, using the correct Buffer concentration (1X). However, the second treatment decreased the

concentration of the extracted RNA considerably as follows: T4 – 19 µg/ml, T8 – 1.16 µg/ml and T24 – 0.00 µg/ml. Therefore, no additional PCR contamination check was carried out and another RNA extraction was performed with prolonged on-column DNase treatment and with the addition of the pde2 primers for purity checks.

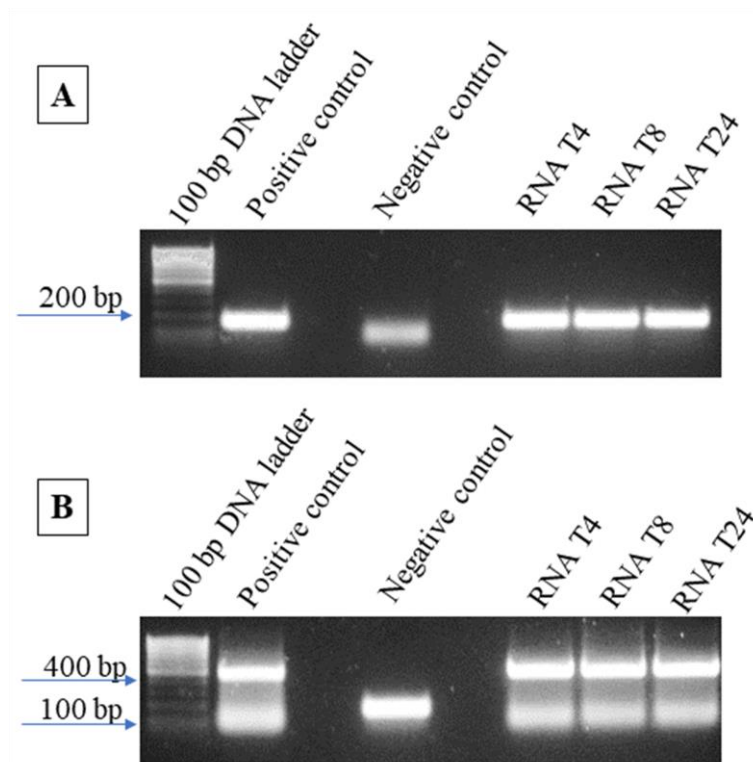


**Figure 3.19. RNA extraction n.3 from FNN25.** Bright bands were visible in all lanes containing RNA samples, gDNA contamination confirmed in all RNA samples. Negative controls contain nuclease-free water as a template. Only primer dimers observed in the negative controls. Gel A) RNA template amplified with FN-spec. primers. Gel B) RNA template amplified with Uni 16S II primers. Electrophoresis conditions: 120 V, 30 minutes. DNA ladder used: 100 bp DNA ladder (11300, Norgen Biotek).

#### 3.3.4. Optimisation of RNA extraction – Extraction n. 4

Extraction n. 4 was performed using the Quick-RNA™ Fungal/Bacterial Miniprep Kit again. The number of bacteria lysed was  $1 \times 10^{10}$ . This time it was decided to increase the time of on-column DNase treatment from 15 minutes to 60 minutes at room temperature with the correct Buffer concentration. RNA extracted at T24 was chosen to be tested with (+) and without (-)

the DNase treatment to find out whether the enzyme is functional. One more set of primers – pde2 – was added. The concentration of the eluted RNA was: T4 – 6.87  $\mu\text{g/ml}$ , T8 – 24.47  $\mu\text{g/ml}$ , T24 (-) – 188.15  $\mu\text{g/ml}$  and T24 (+) – 44.63  $\mu\text{g/ml}$ . When the eluted RNA purity was checked using PCR, very bright bands were observed in all RNA groups tested (Fig. 3.20.), which showed that gDNA contamination was not eliminated with the prolonged DNase treatment.

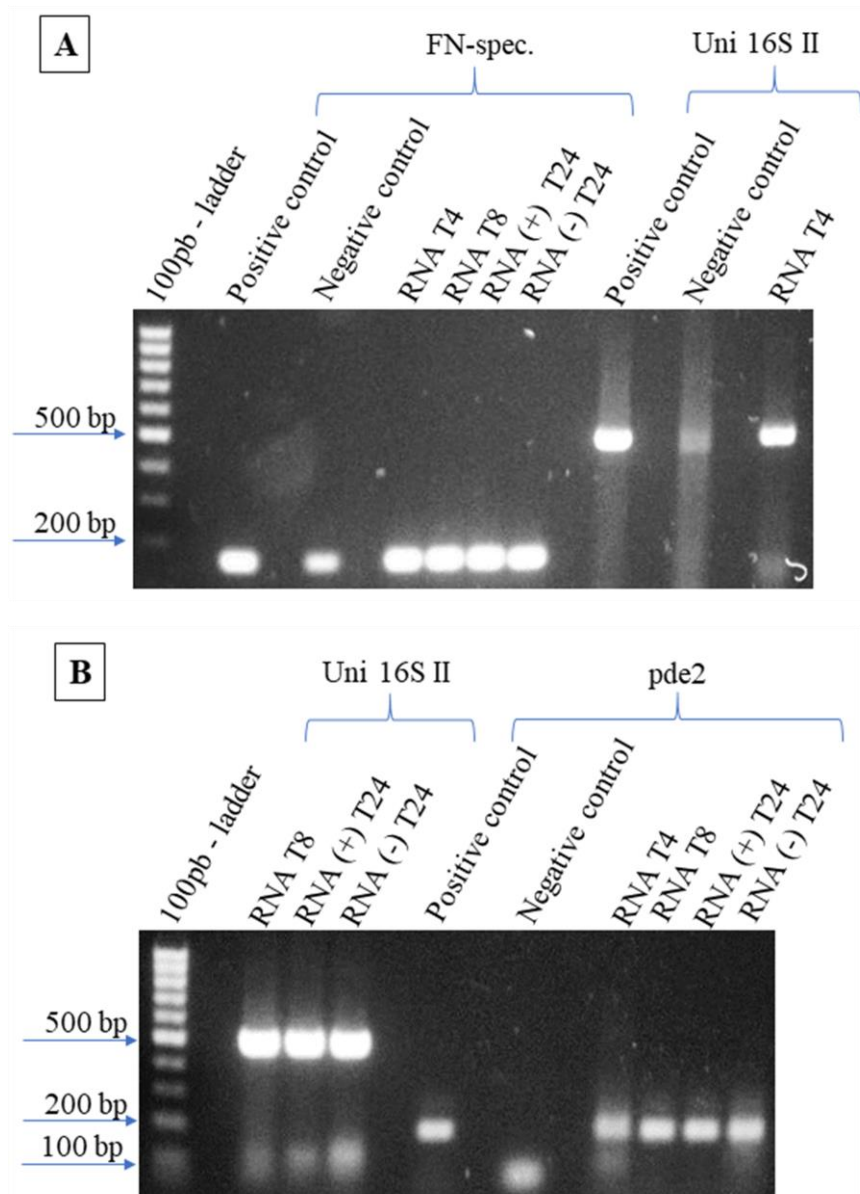


**Figure 3.20. RNA extraction n.4 from FNN25.** Bright bands were visible in all lanes containing RNA samples, gDNA contamination confirmed in all RNA samples. Negative controls contain nuclease-free water as a template. Electrophoresis conditions: 120 V, 60 minutes. DNA ladder used: 100 bp DNA ladder (11300, Norgen Biotek).

A difference in the RNA concentration was noticed between the DNase-treated and non-treated sample, however no difference was observed in the band intensity between the DNase-treated and non-treated samples (RNA (+) T24 vs. RNA (-) T24. This suggests that the DNase enzyme is active, however it does not efficiently remove all the gDNA contamination from the extracts. It was not clear whether the band observed in the negative control for FN-spec. primers was a primer dimer on the same level as the true product observed in the positive control or whether it was contamination. A faint band and smearing appeared in the negative control for Uni 16S I as well, which suggests that the stocks of primers were contaminated. pde2 showed a clear band in the positive control and only primer dimers in the negative control. Based on this result, it was decided not to use FN-spec. primers in the following RNA contamination checks. The possibility of overloading the silica column used during the RNA extraction process with  $1 \times 10^{10}$  bacteria was considered, therefore the following extraction was performed with 10-times less bacteria. It was also decided to add *E. coli* as another control to find out whether the problem lies in the column-based type of kit or in the type of bacteria. *E. coli* was chosen because RNA was successfully isolated from this microbe in a number of publications (Stead *et al.*, 2012; Holmes *et al.*, 2014). The DNase treatment was divided into two phases – on-column and in-solution.

### 3.3.5. Optimisation of RNA extraction – Extraction n. 5

Extraction n.5 utilised a different RNA extraction kit - the RNeasy® Mini kit, Qiagen (see the protocol in section 2.14.3.). The number of FNN25 bacterial cells used for the lysis was  $1 \times 10^9$ . The same number of *E. coli* was included in the extraction. The DNase treatment of the lysates was performed on-column for 30 minutes and after the elution of the RNA, the samples were treated again in-solution for 30 minutes. Both stages were performed at room temperature.

In order to test again whether the DNase enzyme was active, 20  $\mu$ l DNA ladder diluted 1:10 were digested with 20  $\mu$ l of DNase I Mix and run on the agarose gel with the rest of the samples. The extracted RNA was quantified twice – after the first and the second DNase treatment. The first quantification revealed the RNA concentration as follows: T4 – 5.735  $\mu$ g/ml, T8 – 163.5  $\mu$ g/ml, T24 – 7.511  $\mu$ g/ml, *E. coli* – 117.8  $\mu$ g/ml. After the second treatment, the RNA concentration was measured as follows: T4 – 7.964  $\mu$ g/ml, T8 – 2.797  $\mu$ g/ml, T24 – 5.307  $\mu$ g/ml, *E. coli* – 10.03  $\mu$ g/ml. The contamination check was performed after the second treatment using Uni 16S I primers and when the PCR products were visualised on the gel, bright bands were visible in the lanes containing RNA FNN25 T4 and T8. A lighter band was observed in the sample FNN25 T24 and *E. coli* (Fig. 3.21.). A well-defined band was observed in the negative control, which again suggests that the nuclease-free water used was contaminated.

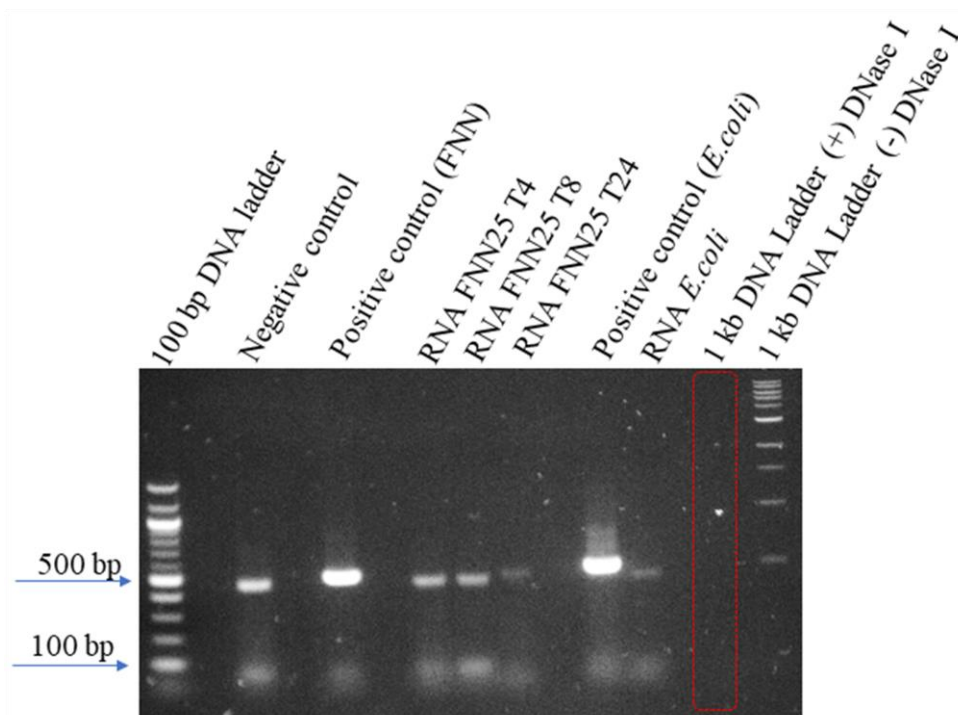


**Figure 3.21. RNA extraction n.5 from FNN25 and *E. coli*.** gDNA contamination was visible in all lanes containing RNA samples, although the bands in the lanes with FNN25 T24 and *E. coli* were considerably lighter. Negative control contains nuclease-free water as a template. Electrophoresis conditions: 120 V, 60 minutes. The main DNA ladder used: 100 bp DNA ladder (11300, Norgen Biotek). Test DNA ladder: 1kb DNA ladder (N3232, New England Biolabs).

It was found out that the DNase enzyme is functional, because there were no bands observed in the 1 kb DNA ladder treated with the DNase (Fig. 3.21., red box), when compared to the non-treated DNA ladder. This again suggests that the enzyme is active, however does not remove the gDNA contamination efficiently.

The extracted RNA was also tested with pde2 primers to check a new aliquot of nuclease-free water as well as to optimise PCR conditions for pde2 primers. The following types of cycling conditions were used: annealing temperature of 59°C and 70°C; and 35 and 40 cycles (for a full set of cycling conditions see table 2.2.). The PCR showed that ideal conditions for pde2 primers are annealing temperature of 59°C with 35 PCR cycles. As the Fig. 3.22.A shows, PCR performed for a shorter time decreases the probability of non-specific binding. An annealing temperature of 70°C was too high as no amplification was observed (Fig. 3.22.B).

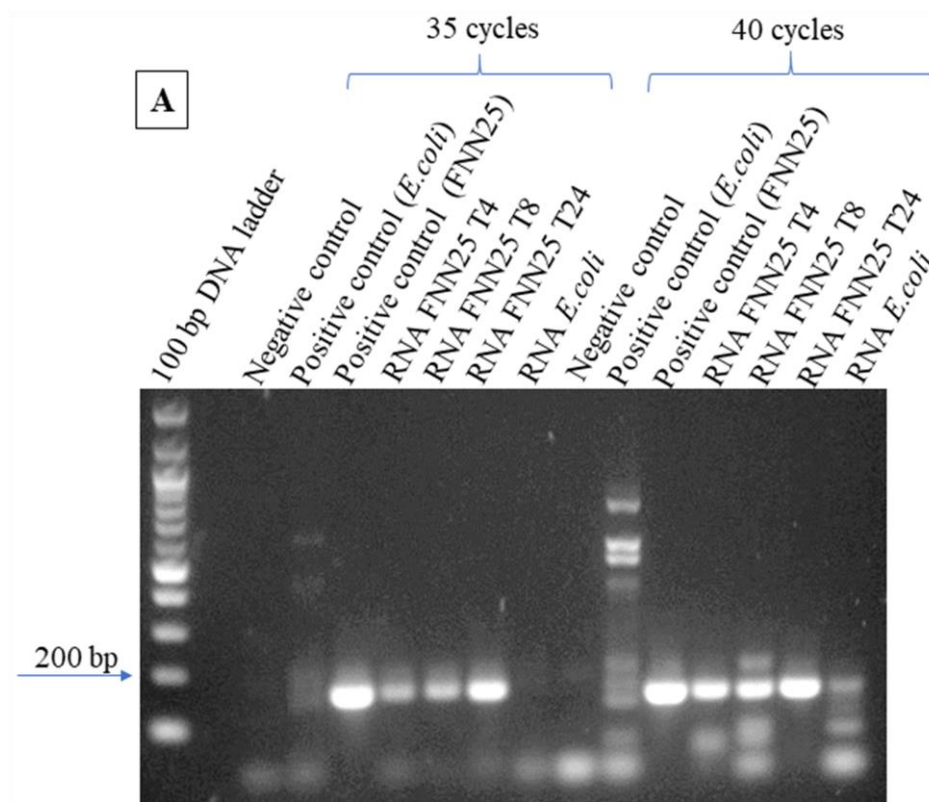


**Figure 3.22. Optimisation of PCR conditions for pde2 primers.** Gel B and the figure legend continued on the next page.

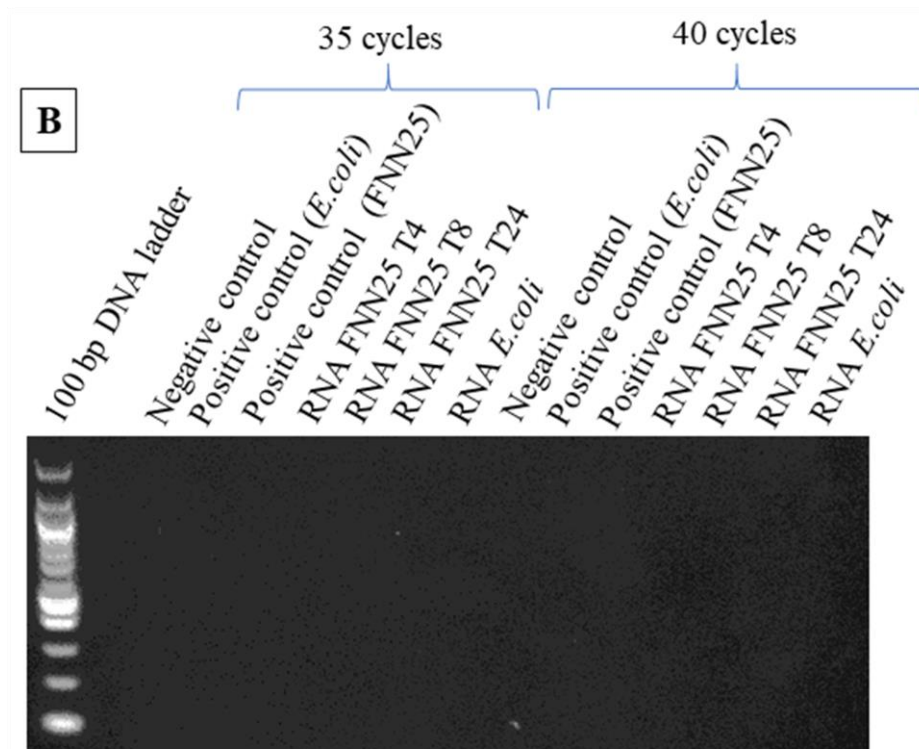


**Figure 3.22. Optimisation of PCR conditions for *pde2* primers.** Gel A) Shorter PCR with annealing temperature of 59°C decreases the probability of non-specific amplification. Contamination with gDNA is still present in all RNA extracts. Gel B) Annealing temperature of 70°C is too high and no amplification occurs. Electrophoresis conditions: 120 V, 60 minutes. 100 bp DNA ladder used (N0467, New England Biolabs).

In gel A, multiple bands are observed in both lanes with *E. coli* positive control, while FNN25 shows one bright band. This was caused by the fact that the *pde2* primers were designed to amplify the *pde2* gene from FNN23, which is not present in *E. coli*. No bands were observed in the negative controls. No band was observed in the *E. coli* RNA extract amplified using 35 cycles (Fig. 3.22.A), however multiple bands were found in the *E. coli* RNA sample amplified using 40 cycles, therefore gDNA contamination of *E. coli* sample cannot be ruled out. Based on these results, neither the change of the RNA extraction kit nor the combination of on-column and in-solution DNase treatment eliminated the gDNA contamination. That is why it was decided to stop using the kits routinely used for other bacteria and perform the RNA extraction using the phenol/chloroform method combined with sample clean-up using silica columns.

### 3.3.6. Optimisation of RNA extraction – Extraction n. 6

A completely different approach has been chosen in order to increase the RNA yield and to completely eliminate the gDNA contamination of the samples. Phenol/chloroform RNA extraction using TRIzol, also known as TRI Reagent, which was utilised in this extraction (section 2.14.4.), is a method in which RNA, DNA and protein from the lysed cells are separated at different phases. TRIzol is a solution of phenol and guanidinium isothiocyanate, which denatures proteins present in the samples and solubilizes biological material. After the addition of chloroform, different components partition to different phases – RNA remains in the upper, aqueous phase and DNA and proteins partition either to the interphase or the organic phase (Tan and Yiap, 2009; Rio *et al.*, 2010). Great care has to be taken in order not to disturb the interphase. Additionally, this hybrid protocol uses the silica columns (RNeasy® Mini kit, Qiagen) to purify the extracted RNA, reducing the handling of the RNA and potentially preventing degradation.

For this method,  $1 \times 10^9$  FNN25 bacterial cells were used. Only one time point (T4) was chosen in order to test whether the method was effective. As the two nucleic acids partition into two different phases, it was expected only RNA would be obtained, hence the DNase treatment was not performed. The concentration of the extracted RNA was 23.01  $\mu\text{g/ml}$ . When the PCR product was visualised on the gel, a bright band was observed in the RNA sample, which again suggests gDNA contamination (Fig. 3.23.). The negative sample did not contain any bands. The result indicates that DNA might remain in the aqueous phase and is removed together with RNA. Moreover, the RNA yield was not increased. In order to prevent gDNA contamination in the samples, it was decided to reintroduce the DNase treatment step in the next phenol/chloroform RNA extraction.

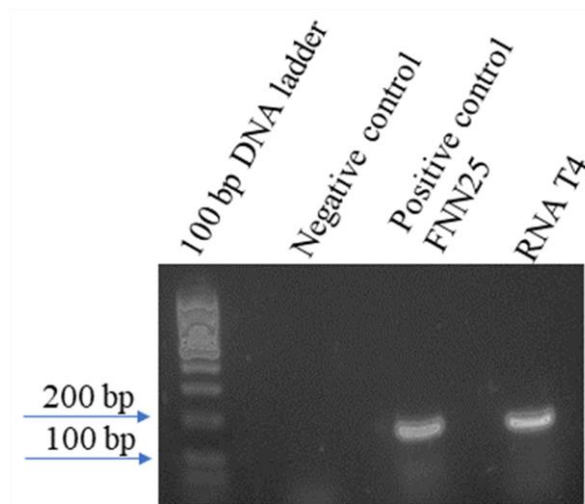


**Figure 3.23. RNA extraction n.6 from FNN25.** Contamination with gDNA was visible in the lane containing RNA sample. Negative control contains nuclease-free water as a template. Electrophoresis conditions: 120 V, 60 minutes. 100 bp DNA ladder used (11300, Norgen Biotek).

### 3.3.7. Optimisation of RNA extraction – Extraction n. 7

The phenol/chloroform RNA extraction was repeated again with  $1 \times 10^9$  FNN25 bacteria harvested at three time points – T4, T8 and T24. Extra care was taken during the removal of the aqueous phase in order not to disturb the interphase layer. The lysates were DNase-treated on-column for 30 minutes at room temperature to eliminate the gDNA contamination. The concentration of the RNA eluted was quantified as follows: T4 – 13.62  $\mu\text{g/ml}$ , T8 – 12.07  $\mu\text{g/ml}$  and T24 – 23.84  $\mu\text{g/ml}$ . The agarose gel showed well-defined, bright bands in all RNA samples (Fig. 3.24.). The negative controls did not show any contamination. The positive control in pde2 showed a well visible band, however the Uni 16S I band was very faint.

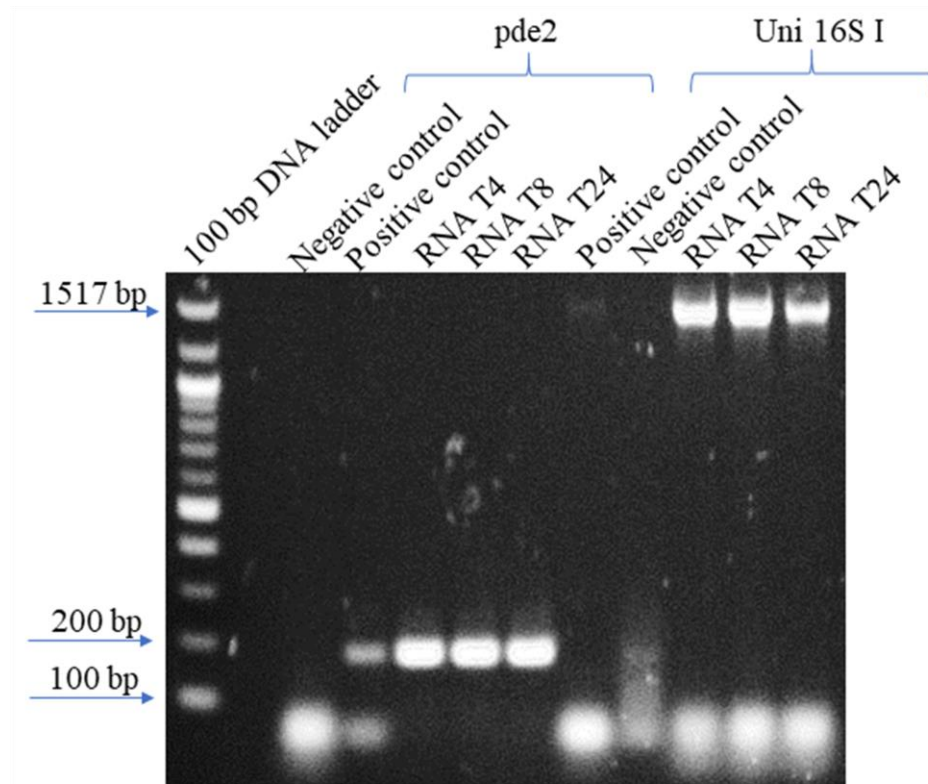


**Figure 3.24. RNA extraction n.7 from FNN25.** The RNA purity was tested using pde2 and Uni 16S I primers. Contamination with gDNA was visible in all RNA samples. Negative control contains nuclease-free water as a template. Electrophoresis conditions: 120 V, 60 minutes. 100 bp DNA ladder used (N0467, New England Biolabs).

Hazy bands at the bottom of the gel smaller than 100 bp were identified as primer dimers. Even after testing multiple methods including silica-based columns as well as conventional phenol/chloroform extraction, together with combinations of on-column and in-solution DNase treatments, it was not possible to remove the gDNA contamination from the extracted RNA samples and increase the RNA yield. The obtained findings, in particular the low RNA yield, indicate that *F. nucleatum* cells are probably not lysed completely during the initial steps of each type of the extraction. To address this issue, a new protocol containing multiple lysing steps was kindly provided by Dr Daniel Slade (section 2.14.5.). This protocol was originally used to extract RNA from *Brucella* species and was modified for the use with *F. nucleatum* subspecies.

### 3.3.8. Optimisation of RNA extraction – Extraction n. 8

During this extraction, the RNA was isolated from  $1 \times 10^9$  FNN23 bacterial cells harvested at T4, T8 and T24. In order to lyse bacteria completely, the bacterial pellets obtained were resuspended in an acetone:ethanol mixture and frozen at  $-80^\circ\text{C}$ . Additionally, bacteria were treated with detergent and subsequently heated at  $90^\circ\text{C}$ . TRIzol reagent was replaced with phenol:chloroform:isoamyl alcohol (125:24:1, pH 4.5) solution and phase-lock tubes were used to decrease the presence of contaminating gDNA. The RNA concentration was quantified immediately after the extraction as follows: T4 – 1321  $\mu\text{g/ml}$ , T8 – 758,1  $\mu\text{g/ml}$  and T24 – 179,6  $\mu\text{g/ml}$ . This result showed that the lysis was considerably more effective as the amount of RNA isolated increased significantly. To completely eliminate gDNA, extracted RNA was treated either with Ambion DNase I for 60 minutes at  $37^\circ\text{C}$  or with Qiagen DNase I for 15 minutes at room temperature (following the manufacturer’s instructions). In order to find the most efficient DNase digestion and RNA purification method, the samples were DNase-treated either once (in-solution or on-column treatment) or twice (combination of in-solution and on-column) as stated in Table 3.2.:

Sample number	Time point	In-solution DNase treatment (Ambion)	On-column DNase treatment (Ambion)	On-column DNase treatment (Qiagen)
1	T4	Yes	Yes	No
2	T4	Yes	No	No
3	T4	No	No	Yes
4	T8	Yes	Yes	No
5	T8	Yes	No	No
6	T24	Yes	No	No

**Table 3.2. List of DNase digestion methods.** Different combinations of in-solution and on-column DNase treatment were created to find the most efficient DNase digestion procedure.

It is important to mention that sample 6 (T24) was cleaned up using the phenol/chloroform extraction protocol and was not loaded onto the RNeasy column. This was done in order to compare the sample clean-up procedures. The RNA concentration was quantified after the DNase treatment and the concentrations of certain samples were found to be considerably higher compared to previous RNA isolation attempts. Table 3.3. states all concentrations after the corresponding DNase treatment(s).

Sample number	Time point	RNA concentration (µg/ml)
1	T4	26.89
2	T4	286.8
3	T4	59.21
4	T8	8.077
5	T8	237.3
6	T24	14.18

**Table 3.3. Final RNA concentration after corresponding DNase treatment(s).** The RNA concentration was significantly higher in sample 2 and sample 5.

RNA extracts 2 and 5 which were treated only once in-solution have significantly higher concentration compared to the rest of the samples. The purity of extracted RNA was tested by PCR with Uni 16S I and pde2 primers (Fig. 3.25). When gel A was visualised, no bands were observed in sample 2, 4, 5 and 6 (Fig. 3.25.A). A very faint band smaller than 1500 bp was visible in the lane containing sample 1 and a brighter band in the lane with sample 3. When PCR products of RNA samples not treated with DNase were visualised on the gel, no bands were observed, however, smearing appeared in RNA T4 and RNA T8. Similarly, a smear appeared in the well with samples 2 and 5. The smears in the wells suggest high concentration of RNA as well as degraded DNA. The negative sample was not contaminated. Primer dimers

were observed in all samples. When gel B was visualised, well-defined bands were visible in sample 3 and untreated RNA T24 extract. Very faint smears were visible in samples 2 and 5.

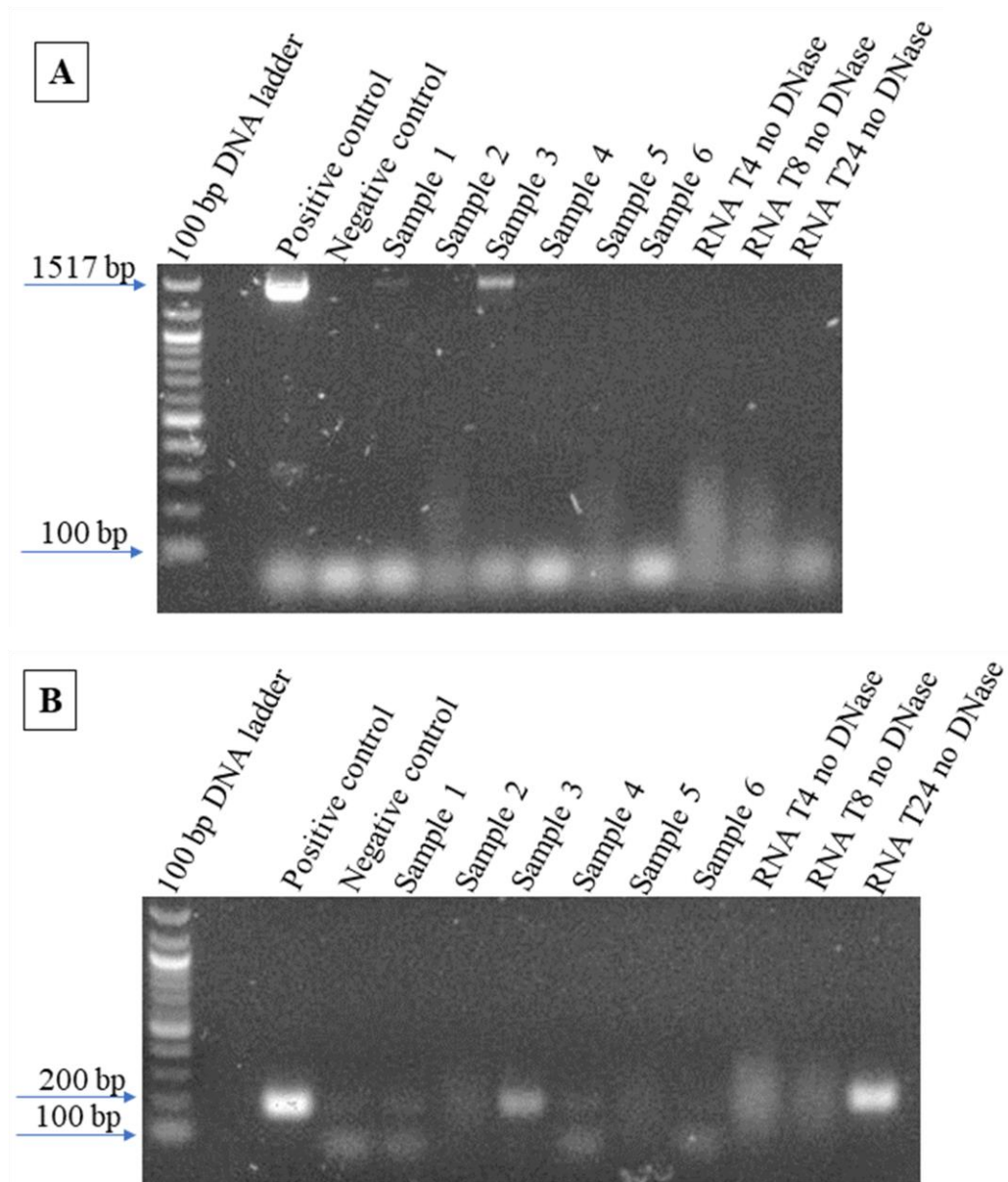


**Figure 3.25. RNA extraction n.8 from FNN23.** The RNA purity was tested using Uni 16S I primers (gel A) and pde2 primers (gel B). A) Contamination with gDNA was visible only in sample 3. A low level of gDNA contamination was observed in sample 1. B) Clear gDNA contamination was visible in sample 3 and non-treated RNA T24. Very faint smears were visible in the treated samples 2 and 5. Negative control contains nuclease-free water as a template. Electrophoresis conditions: 120 V, 60 minutes. 100 bp DNA ladder used (N0467, New England Biolabs).

The PCR gDNA contamination check together with RNA quantification showed that the most efficient DNase treatment is a one-step in-solution DNA digestion with Ambion DNase I enzyme performed at 37°C for 60 minutes. One in-solution treatment seems to completely remove gDNA contamination as well as to preserve the RNA concentration considerably high. The test with Qiagen DNase I confirmed that on-column gDNA digestion performed at room temperature for a short period of time is not sufficient to remove the gDNA contamination from FNN23 RNA extracts.

While the use of the silica columns has been found not to be effective in the gDNA removal, their use for the clean-up of the extracted, DNase-treated sample has proven to provide better results compared to a traditional phenol/chloroform extraction clean-up. When sample 6 was cleaned-up after the DNase treatment, it was perceived that a noticeable amount of sample was lost due to handling low volumes.

Thanks to the success of this protocol, it was possible to proceed to another round of RNA extractions in order to obtain pure RNA from the remaining *F. nucleatum* subspecies.

### 3.3.9. RNA extraction from all *Fusobacterium nucleatum* subspecies

Once the protocol for the RNA extraction was confirmed to yield high amounts of RNA from FNN23, the remaining subspecies FNA, FNF, FNN25, FNP and FNV were grown in liquid culture and the bacteria were harvested at T4, T8 and T24, with the exception of FNP, which was harvested at T4 and T8. FNF failed to grow in the liquid culture even after multiple attempts, thus it was excluded from the RNA extraction and gene expression analysis.

The number of bacteria harvested at each time point was  $1 \times 10^9$ . The concentration of the RNA extracted was quantified before and after the in-solution DNase treatment with Ambion DNase I enzyme. The values are stated in Table 3.4. overleaf.

Sample	RNA concentration before DNase treatment ( $\mu\text{g/ml}$ )	RNA concentration after DNase treatment ( $\mu\text{g/ml}$ )
FNA T4	1723.5	92.60
FNA T8	1451.3	68.63
FNA T24	318.3	93.36
FNN25 T4	680.1	186.6
FNN25 T8	420.1	174.6
FNN25 T24	107.5	35.9
FNP T4	376.4	132.7
FNP T8	366.5	93.22
FNV T4	217.1	95.26
FNV T8	346.9	129.4
FNV T24	64.04	14.33

**Table 3.4. RNA concentration of the remaining *F. nucleatum* subspecies.** The concentration of most samples remained considerably high even after the DNase treatment. Each value is a mean of three measurements.

The purity of each extracted RNA was tested by PCR using Uni 16S I primer. All extracts from FNA, FNP and FNV were shown not to be contaminated with gDNA. The RNA extracted from FNN25 was confirmed to be pure in the case of T4 and T8 sample, however the T24 sample was found to be contaminated with gDNA as a bright band was observed on a visualised gel (Fig. 3.26.)

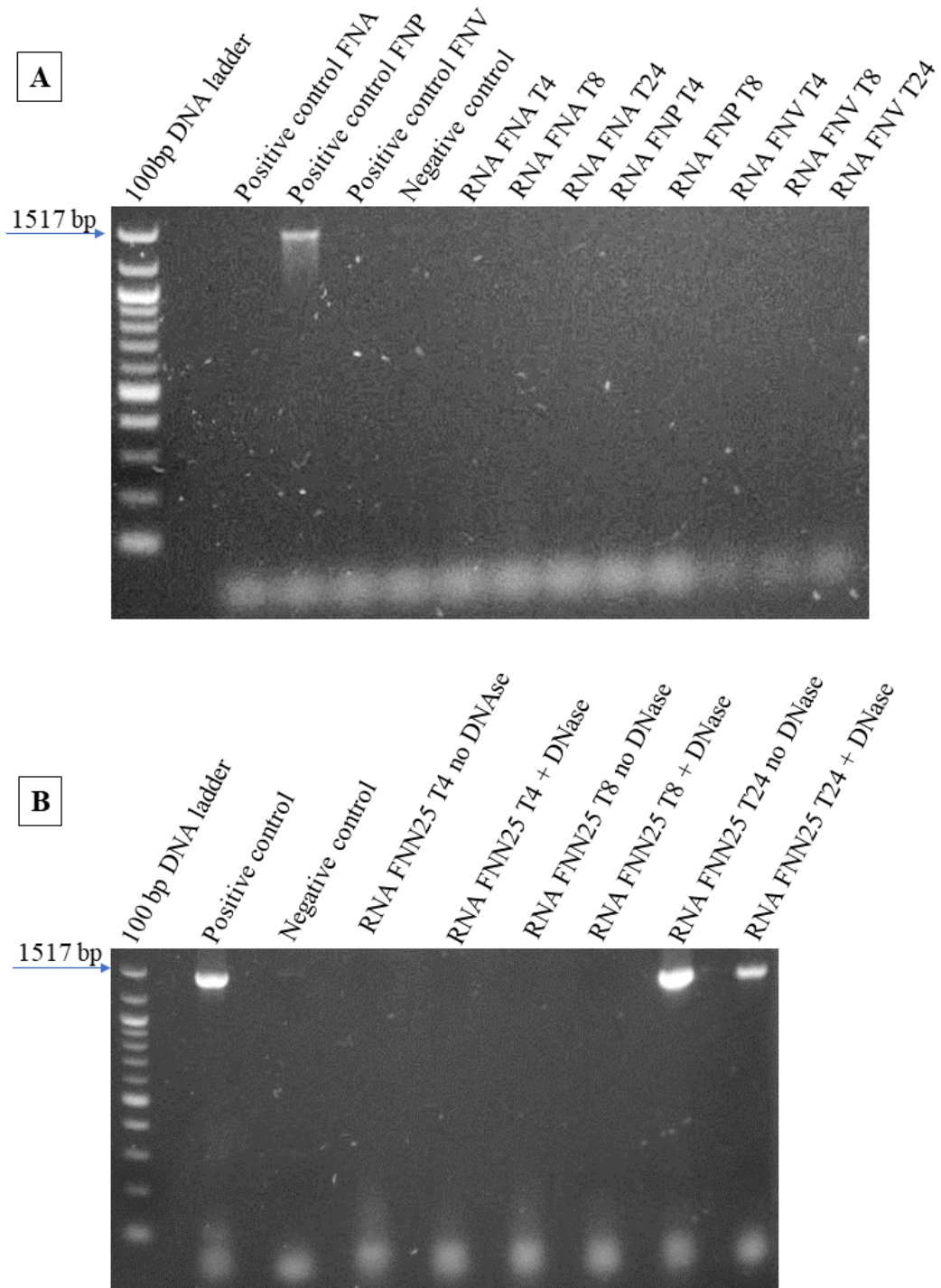


**Figure 3.26. RNA extracted from FNA, FNN25, FNP and FNV.** The RNA purity was tested using Uni 16S I primer. Gel A shows that all extracted RNA was pure. Gel B shows that FNN25 T24 sample was contaminated with gDNA even after DNase treatment. Negative control contains nuclease-free water as a template. Electrophoresis conditions: 120 V, 60 minutes. 100 bp DNA ladder used (N0467, New England Biolabs).

Fig. 3.26, gel A, shows that no bands are visible in positive control FNA and FNV. This was probably caused by a mistake made during the PCR sample preparation. The presence of the band in the FNP positive control confirmed that PCR worked and none of the FNA, FNP and FNV samples were contaminated with gDNA.

FNN T24, which was not pure even after the DNase treatment, was re-digested with Ambion DNase I enzyme and the sample was confirmed to be pure after the second treatment (Fig. 3.27.)

The concentration of the RNA sample after the second DNase treatment was 15.92 µg/ml.

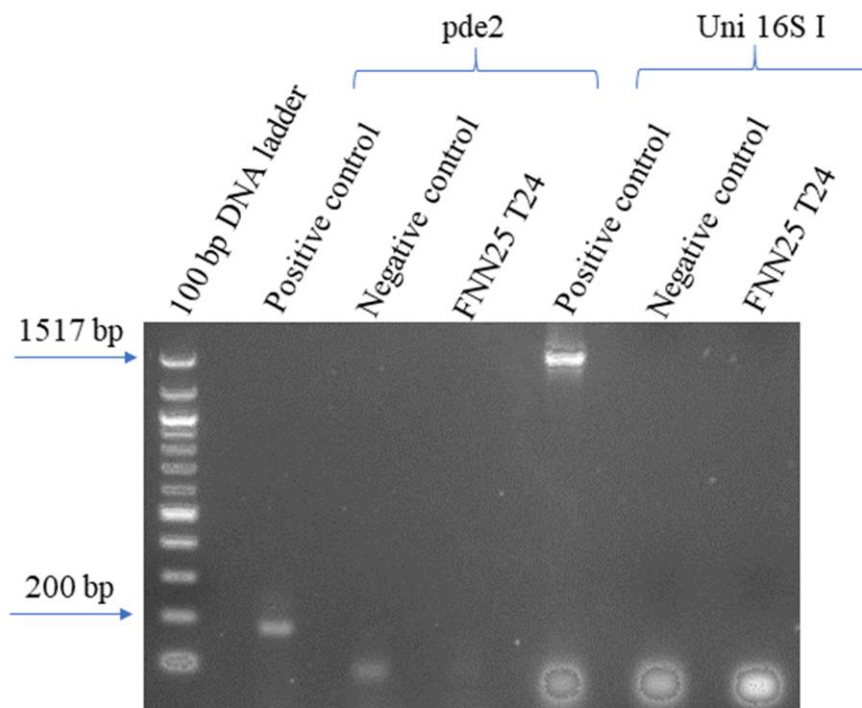


**Figure 3.27. RNA extracted from FNN25 re-treated with Ambion DNase I.** The RNA purity was confirmed after the second DNase I treatment. Negative control contains nuclease-free water as a template. Electrophoresis conditions: 120 V, 60 minutes. 100 bp DNA ladder used (N0467, New England Biolabs).

Once the RNA from all the subspecies was extracted and confirmed to be pure, it was possible to reverse-transcribe each sample and proceed to the next step of the analysis – qRT-PCR.

### 3.3.10. Chapter conclusions

The optimisation of the RNA extraction from the *F. nucleatum* subspecies showed that commercially available kits for RNA extraction are not effective in the case of this bacterium, even if specialised disruption beads were used in the first step of the extraction. The concentration of the extracted RNA was considerably low, regardless of the kit used. Each RNA sample was heavily contaminated with gDNA and neither gDNA removal silica columns, nor DNase I enzyme applied onto the columns removed the gDNA contamination completely to ensure a high quality of the RNA extracted. Successful extraction of RNA with significantly higher concentration was achieved by multi-step disruption of the bacterial cells and subsequent phenol/chloroform/isoamyl alcohol nucleic acid extraction. The purity of the RNA was accomplished by in-solution DNase I treatment.

### **3.4. Analysis of differential expression of genes involved in synthesis and hydrolysis of cyclic di-nucleotides (CDNs) and quantification of CDNs**

Successful extraction of RNA with high concentration and subsequent complete purification with DNase I enzyme made it possible to proceed to the qRT-PCR assay in order to analyse the differential expression of genes involved in production and degradation of CDNs in *F. nucleatum*. The first step towards qRT-PCR involved specificity confirmation of primers designed for this study. The primer confirmation was performed using both conventional PCR and qRT-PCR. Conventional PCR was used to find out the specificity of primer pairs binding, while qRT-PCR was utilised to determine the efficiency of primer binding. Efficiency values for each primer set were then used in the gene expression analysis. This study was interested in the expression of the following genes: c-di-AMP cyclase (*disA*) producing c-di-AMP from two molecules of ATP; phosphodiesterase (*pde2*) hydrolysing c-di-AMP into non-cyclic constituents and two homologues of *relA/spoT* gene products which modulate the concentration of guanosine pentaphosphate/tetraphosphate ((p)ppGpp), also known as alarmone, playing an important role in the stringent response in bacteria.

Additionally, the CDNs were extracted from bacteria grown on agar plates as well as from biofilms to find out whether different lifestyles of *F. nucleatum* subspecies affect the amount and the type of CDN produced.

#### *3.4.1. Primer validation - specificity*

All primers that were used in this study are stated in table 2.3. Before commencing qRT-PCR, it was important to test the specificity of all sets of primers. Primers specific for the genes encoding enzymes involved in synthesis and hydrolysis of c-di-AMP as well as (p)ppGpp were designed based on the sequences obtained from the FNN23 genome published on FusoPortal.

Each set of primers was tested by conventional PCR (full protocol see section 2.4.), using heat-killed FNN23 bacterial culture to provide the DNA template. The PCR products were run on 1.5% agarose gel, showed clear bands (Fig. 3.28.) and the size of the products agreed with the predicted amplicon size, which is stated for each set of primers in table 2.3.

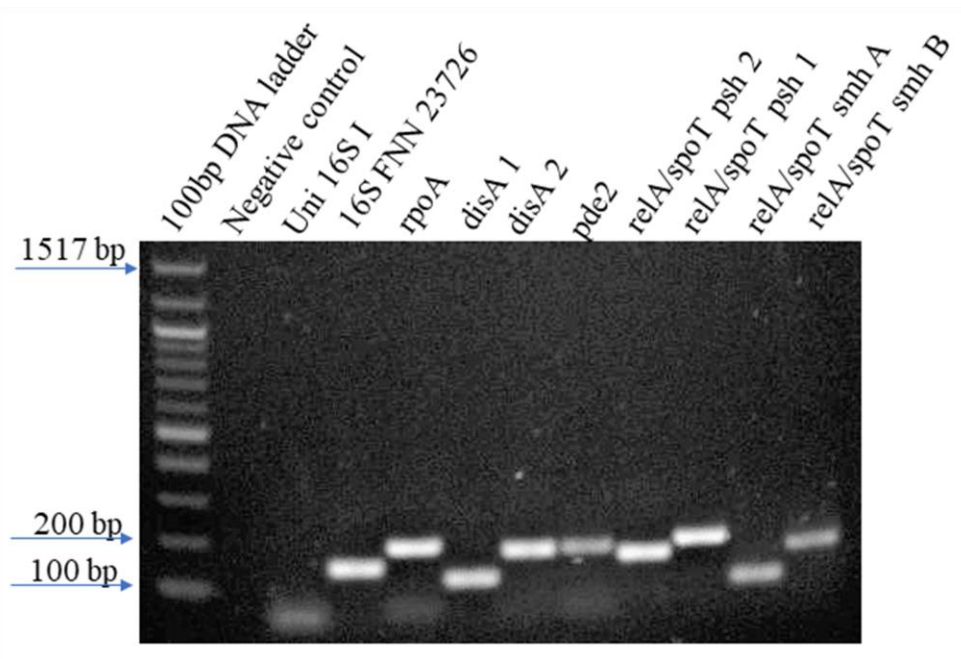


**Figure 3.28. Validation of primers used in this study.** FNN23 was used to provide DNA template for the PCR. All primers were confirmed to produce specific products except for Uni 16S I. 100 bp DNA ladder used (N3231, New England Biolabs). Electrophoresis settings: 120V, 60 minutes.

The only set of primers which did not seem to work was Uni 16S I (amplicon 1465 bp), as there was no band observed, only primer dimers smaller than 100 bp. However, this set of primers was used for the identity confirmation of *F. nucleatum* subspecies and it produced well defined PCR products, therefore it was decided not to exclude this set of primers from this analysis. No non-specific amplification was observed. This showed that the most relevant sets of primers amplified the corresponding genes of interest with high specificity.

### 3.4.2. Primer validation – efficiency

In order to determine the efficiency of each set of primers, cDNA of each *F. nucleatum* subspecies was pooled, diluted as described in section 2.16. and samples with the corresponding primers were run for 60 cycles using LightCycler® 480 SYBR Green I Master. The efficiency values were then calculated by the LightCycler480 software based on the standard curves produced in each run. The level of efficiency was considered to be high if the value was between 1.8 and 2.2.

Interestingly, it was found out that only in the case of FNN23 and FNN25, the majority of primers annealed and amplified the gene of interest with high efficiency (Table 3.5.)

Gene	FNA	FNN23	FNN25	FNP	FNV
<i>rpoA</i>	<b>2.222</b>	<b>2.059</b>	<b>1.986</b>	<b>2.204</b>	3.117
<i>disA</i> 1	0.861	<b>1.956</b>	<b>2.003</b>	0.717	16.07
<i>disA</i> 2	1.431	<b>2.003</b>	<b>1.870</b>	114.6	0.691
<i>relA/spoT smh</i> A	0.860	<b>2.098</b>	<b>1.978</b>	<b>2.031</b>	0.865
<i>relA/spoT smh</i> B	50.39	<b>2.028</b>	<b>1.831</b>	X	0.803
<i>relA/spoT psh</i> 1	X	<b>2.175</b>	<b>1.871</b>	X	X
<i>relA/spoT psh</i> 2	7.395	<b>1.987</b>	<b>1.903</b>	0.174	2.858
<i>pde2</i>	8.080	<b>2.103</b>	6.986/0.4 48	0.384	1.549

**Table 3.5. Efficiency values of primers used in this study.** Each subspecies was tested with each set of primers. Green bold values indicate a high level of efficiency, with the value in the range of 1.8 – 2.2. “X” indicates that the software was not able to calculate the standard curve and thus the efficiency values are missing. Red box highlights the primers with the highest level of efficiency chosen for further analysis. Efficiency testing in FNN25 was performed twice.

The primer set for the housekeeping gene *rpoA*, which serves as a reference gene, worked efficiently in all subspecies but FNV. The primer set targeting *relA/spoT smh A* (small (p)ppGpp hydrolase) also worked with high efficiency in FNP. Surprisingly, the *pde2* primer set only worked efficiently in FNN23. The efficiency testing of *pde2* in FNN25 was performed twice, however none of the attempts showed that the primer annealing and amplification occurs efficiently. In order to compare the gene expression of interest in at least two subspecies, FNN23 and FNN25 were chosen for the subsequent analysis. Due to the time constraints of the project, *pde2* was excluded from the analysis, as the primers worked only in one subspecies and it would not be possible to design a new set of primers and generate a second set of data for comparison with FNN23.

Each set of primers was designed as two alternatives (*disA* 1 and 2, *relA/spoT psh* 1 and 2, *relA/spoT smh A* and B, see Table 3.5.), therefore based on the results of the efficiency testing, only one set of primers with the highest efficiency was chosen for each subspecies. The value that was closest to 2.0 was chosen as the highest efficiency for a particular set of primers. It was decided that gene expression in FNN23 would be tested using *rpoA*, *disA* 2, *relA/spoT smh B* and *relA/spoT psh* 2, while the expression profile in FNN25 would be analysed using *rpoA*, *disA* 1, *relA/spoT smh A* and *relA/spoT psh* 2 (values in red boxes, Table 3.5.).

#### 3.4.3. Optimisation of qRT-PCR – assay n. 1

Similarly to the RNA extraction, it was necessary to optimise the qRT-PCR analysis and the preparatory steps leading to it. The synthesis of cDNA used in the first qRT-PCR was performed using 12 µl RNA extracted from each subspecies in order to obtain high quality, concentrated cDNA. Subsequently, 1 µl cDNA was used for the gene expression analysis (see section 2.16.). When the assay results from FNN25 were analysed, it was noticed that the housekeeping gene

*rpoA* did not maintain a uniform expression and there were differences in the values of  $C_p$  (the point at which the fluorescence of the sample crosses the detection limit) between the time points with the values being 18.62, 17.88 and 23.26 for T4, T8 and T24, respectively (Fig. 3.29. B). When it comes to FNN23, the *rpoA* expression was uniform at T4 (17.35) and T8 (17.54), however the  $C_p$  value at T24 was equal to the  $C_p$  value of the negative control (34.74), suggesting that either the concentration of cDNA was very low or it was degraded and there was no amplification (Fig. 3.29. A).

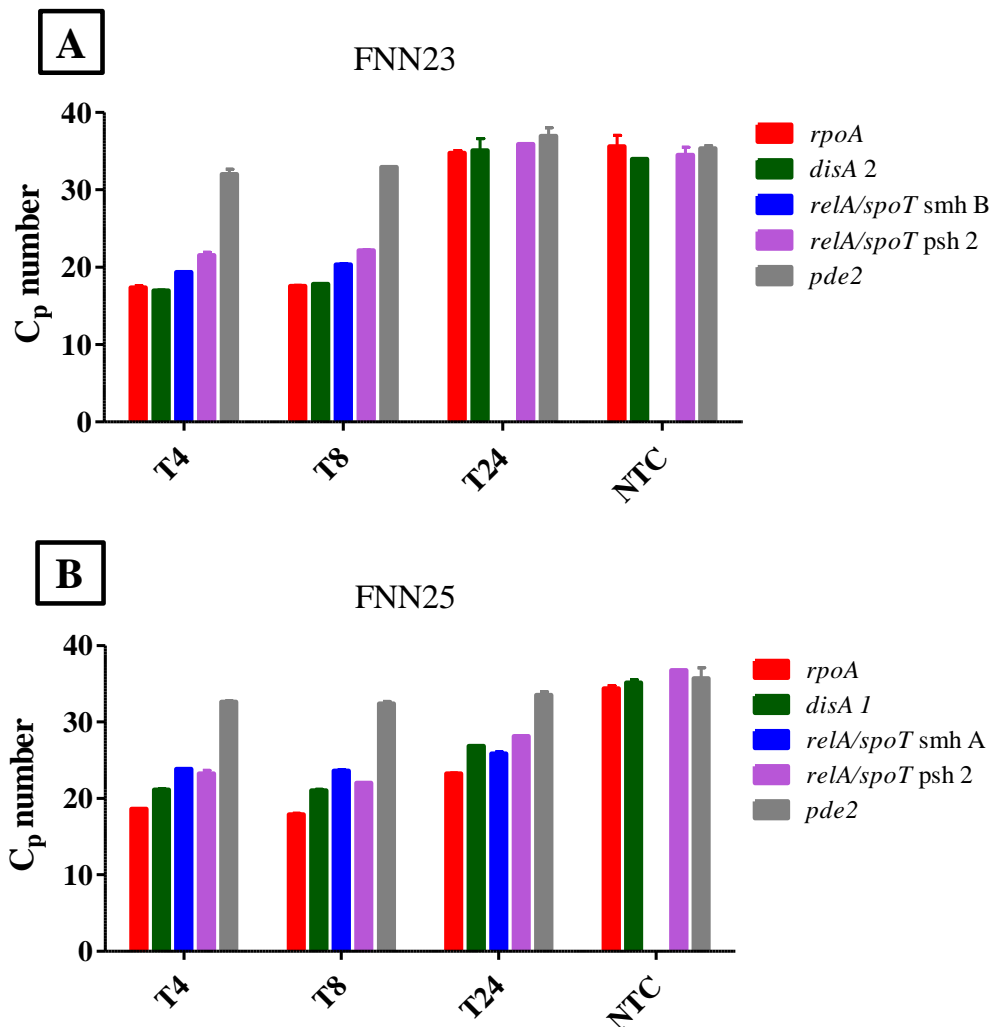


**Figure 3.29. Differential expression of target genes in FNN23 and FNN25 – assay n. 1.** The expression levels are presented as  $C_p$  values, which describe the point at which the fluorescence of the sample crosses the threshold. Nuclease-free water was used instead of the cDNA template in the negative, no template control (NTC). Each bar shows a mean of two technical replicates. Error bars show standard deviation.

Additionally, the *relA/spoT smh* gene product was not detected in FNN23 in the sample T24. This further indicates problems with T24 cDNA used in this analysis.

Even if *pde2* primers were shown not to anneal with sufficient efficiency, they were used one more time to completely rule out the use of this set of primers. As both graphs in Fig. 3.29. show, the  $C_p$  values of *pde2* gene in each sample were equal to the  $C_p$  values of the negative controls, which implies that the primers did not anneal at the site of the target gene and there was no specific amplification.

Due to the unstable expression of *rpoA* in both subspecies, it was not possible to standardise the expression of the target genes against the expression of the housekeeping gene, that is why the results are presented as  $C_p$  values rather than fold expression. In order to overcome this issue, it was decided to extract new sets of RNA samples from both subspecies and increase the number of bacteria used for the extraction from  $1 \times 10^9$  to  $5 \times 10^9$  to maximise the RNA concentration and thus maximise the accuracy of qRT-PCR gene expression detection.

#### 3.4.4. Optimisation of qRT-PCR – assay n. 2

In order to obtain more accurate gene expression results, RNA was extracted from a higher number of bacteria as stated above. The concentration of the extracted RNA was measured as stated in Table 3.6.

Sample	RNA concentration before DNase treatment ( $\mu\text{g/ml}$ )	RNA concentration after DNase treatment ( $\mu\text{g/ml}$ )
FNN23 T4	806.34	16.98
FNN23 T8	2597.3	176.00
FNN23 T24	791.37	114.9
FNN25 T4	1093.6	171.6
FNN25 T8	718.5	121.3
FNN25 T24	190.13	23.22

**Table 3.6. Concentration of RNA used in the qRT-PCR assay n. 2.** After the DNase I treatment, all samples were confirmed to be pure using conventional PCR.

Due to notable differences in the concentration of RNA samples, the volume of RNA template, and therefore the mass of each RNA sample to be reverse transcribed was standardised based on the sample with the lowest concentration ( T4 for FNN23 and T24 for FNN25). The volume of each FNN23 RNA aliquot was used as follows: 12  $\mu$ l T4, 1.15  $\mu$ l T8 and 1.8  $\mu$ l T24. The volume of each FNN25 RNA aliquot was used as follows: 1.6  $\mu$ l T4, 2.3  $\mu$ l T8 and 12  $\mu$ l T24. When the qRT-PCR analysis was performed with the new set of cDNA samples, *rpoA* again demonstrated unstable expression in both subspecies (Fig. 3.30), that is why the graphs present the results as  $C_p$  values.

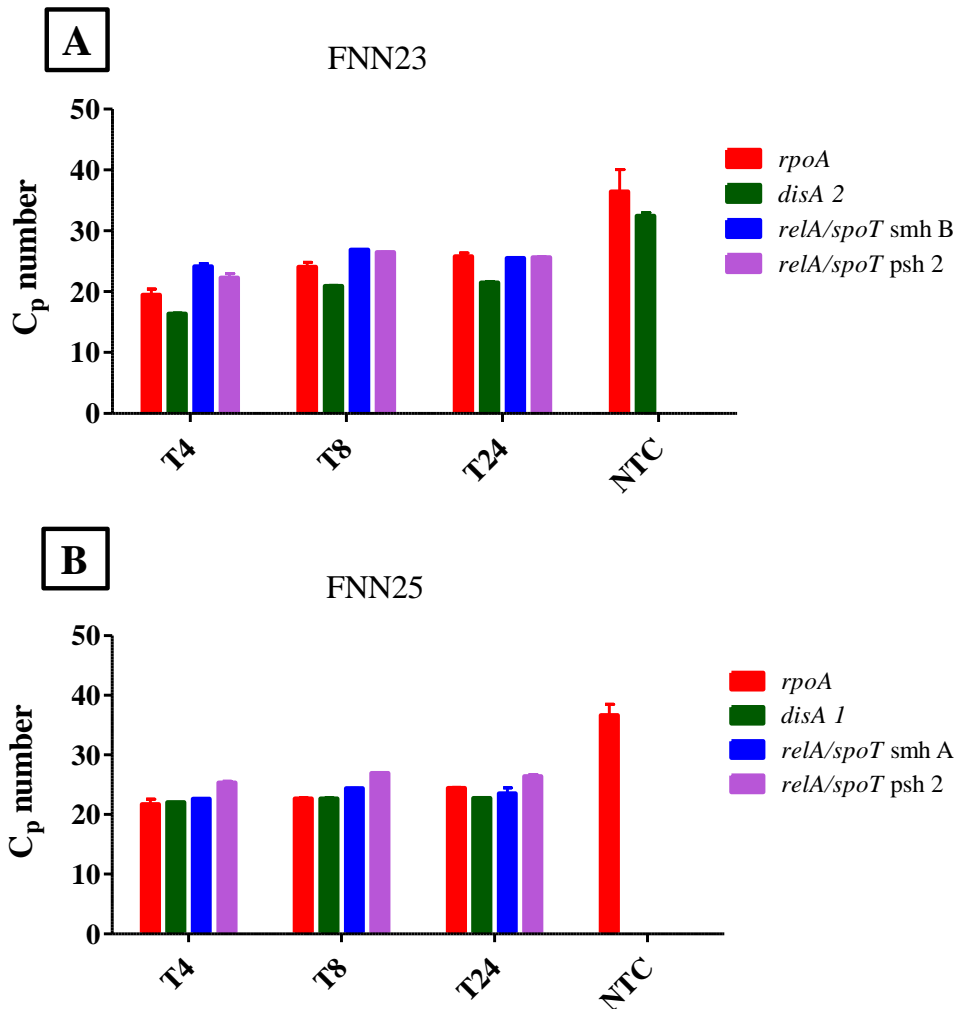


**Figure 3.30. Differential expression of target genes in FNN23 and FNN25 – assay n. 2.** The expression levels are presented as  $C_p$  values. Nuclease-free water was used instead of the cDNA template in the negative, no template control (NTC). Each bar shows a mean of two technical replicates. Error bars show standard deviation.

The results show that the issue with the FNN23 T24 sample was resolved as the  $C_p$  values were not equal to the  $C_p$  values of NTC. However, the problem with varying cDNA template concentration was not ruled out, as *rpoA* levels differed at each time point in each subspecies. This was the reason why it was not possible to draw any conclusions from the expression values of the target genes studied. In order to confirm whether the cDNA sample concentration differed, the sample concentrations were quantified using a nanodrop and variation was observed (Table 3.7.)

Sample	cDNA concentration ( $\mu\text{g/ml}$ )
FNN23 T4	180.25
FNN23 T8	167.11
FNN23 T24	157.92
FNN25 T4	186.50
FNN25 T8	191.92
FNN25 T24	215.11

**Table 3.7. Concentration of cDNA used in the qRT-PCR assay n. 2.** Notable differences can be observed between the cDNA samples.

Regarding the FNN23 sample set, the biggest difference was observed between T4 and T24 (22.33  $\mu\text{g/ml}$ ). The biggest difference in the sample set FNN25 was similarly found between T4 and T24 (28.61  $\mu\text{g/ml}$ ). Based on this observation it was decided that a new set of cDNA samples would be synthesised using a higher volume of RNA template and the final cDNA samples would be normalised to a desired concentration rather than using very small volumes of RNA.

#### 3.4.5. Optimisation of qRT-PCR – assay n. 3

New cDNA sample sets were reverse transcribed using 12  $\mu\text{l}$  of less concentrated T4 FNN23 and T24 FNN25 RNA template and 10  $\mu\text{l}$  of more concentrated T8 and T24 FNN23; T4 and T8

FNN25. The concentration of the newly synthesised cDNA was quantified using a nanodrop and the samples were subsequently diluted with nuclease-free water to equalise the concentration of FNN25 samples based on FNN T4 and concentration of FNN23 samples based on FNN23 T24 (Table 3.8.):

Sample	Initial cDNA concentration ( $\mu\text{g/ml}$ )	Standardised cDNA concentration ( $\mu\text{g/ml}$ )
FNN23 T4	352.48	341.20
FNN23 T8	406.16	337.56
FNN23 T24	377.38	338.10
FNN25 T4	408.82	373.74
FNN25 T8	396.36	372.23
FNN25 T24	365.21	363.20

**Table 3.8. Concentration of cDNA used in the qRT-PCR assay n. 3.** The concentration of the samples was adjusted to the sample with the lowest concentration in each sample set.

The concentration of the standardised cDNA samples remained considerably high even after dilution. In order to add one more layer of confirmation that the DNase I treated RNA as well as cDNA samples were pure and of high quality, a conventional PCR was performed using Uni 16S I primers, comparing untreated RNA extracts, DNase I treated RNA extracts and cDNA samples synthesised from the latter (Fig. 3.31.).

Interestingly, FNN23 RNA extracts untreated with DNase I do not seem to be contaminated with gDNA, as there are no bands visible in the corresponding wells. However, the purity of the RNA samples cannot be confirmed as smearing can be seen in each lane containing untreated RNA (Fig. 3.31. A). When the samples were treated with the DNase I enzyme, the smearing was eliminated, which shows that the DNase I digestion cannot be omitted during any RNA extraction. All treated FNN23 samples were successfully reverse transcribed into cDNA.

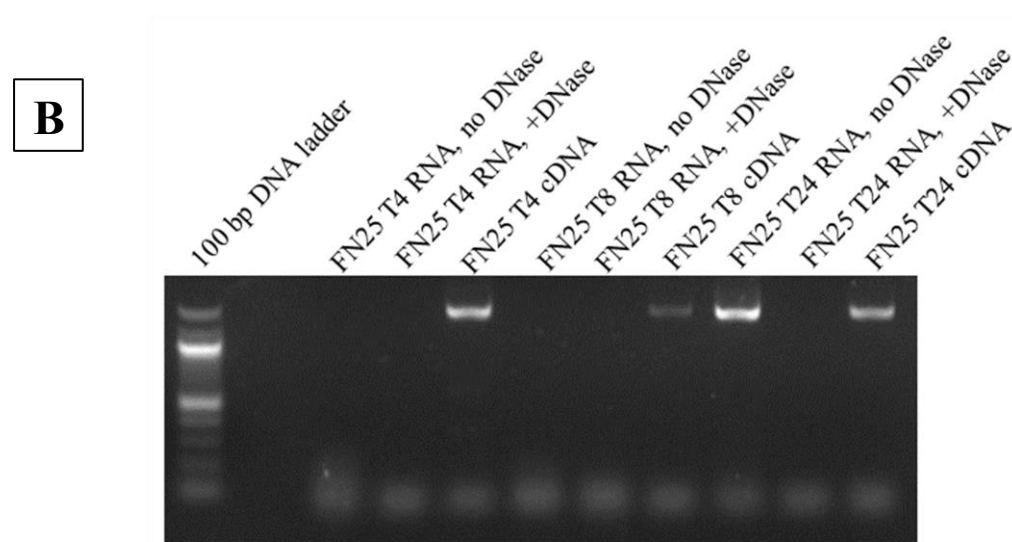
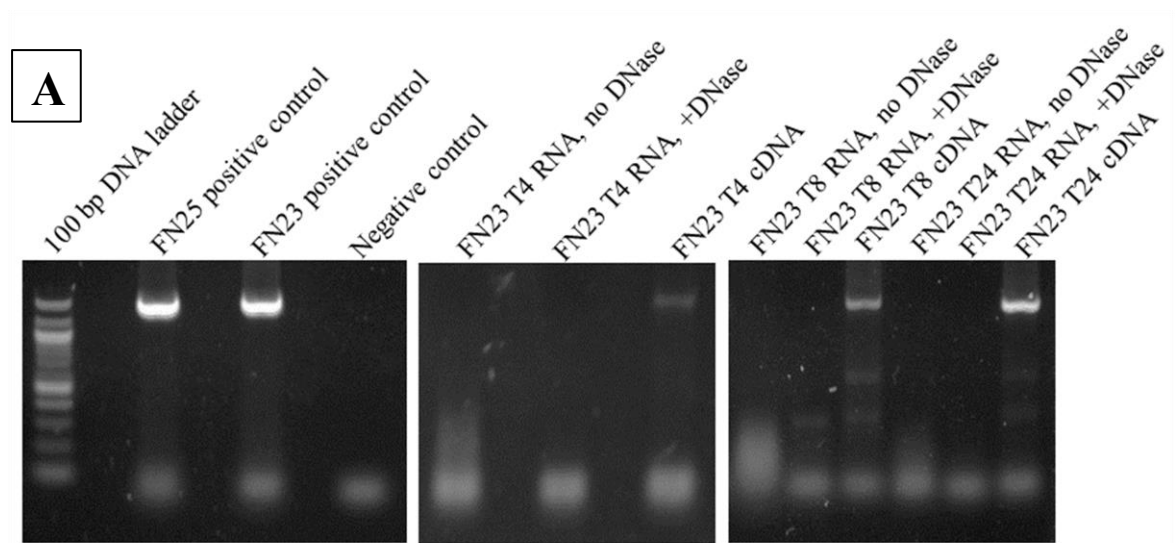


**Figure 3.31. Confirmation of sample purity and quality.** A) FNN23 sample set. B) FNN25 sample set. All RNA extracts treated with DNase I enzyme were confirmed to be pure and to produce cDNA of sufficient quality.

Concerning the FNN25 sample set, it can be seen that only untreated T24 RNA was heavily contaminated with gDNA, which was demonstrated by a bright, well-defined band. Gentle smearing is visible in untreated RNA T4 and T8. Purified RNA, which was confirmed not to be contaminated with gDNA provided a high quality template for cDNA synthesis (Fig. 3.31. B). This allowed the progression to the qRT-PCR assay.

The analysis of the data obtained from this qRT-PCR assay showed that even after a careful concentration equalisation of cDNA samples, the expression of *rpoA* was not stable in both subspecies and there were differences between the time points (Fig. 3.32.)

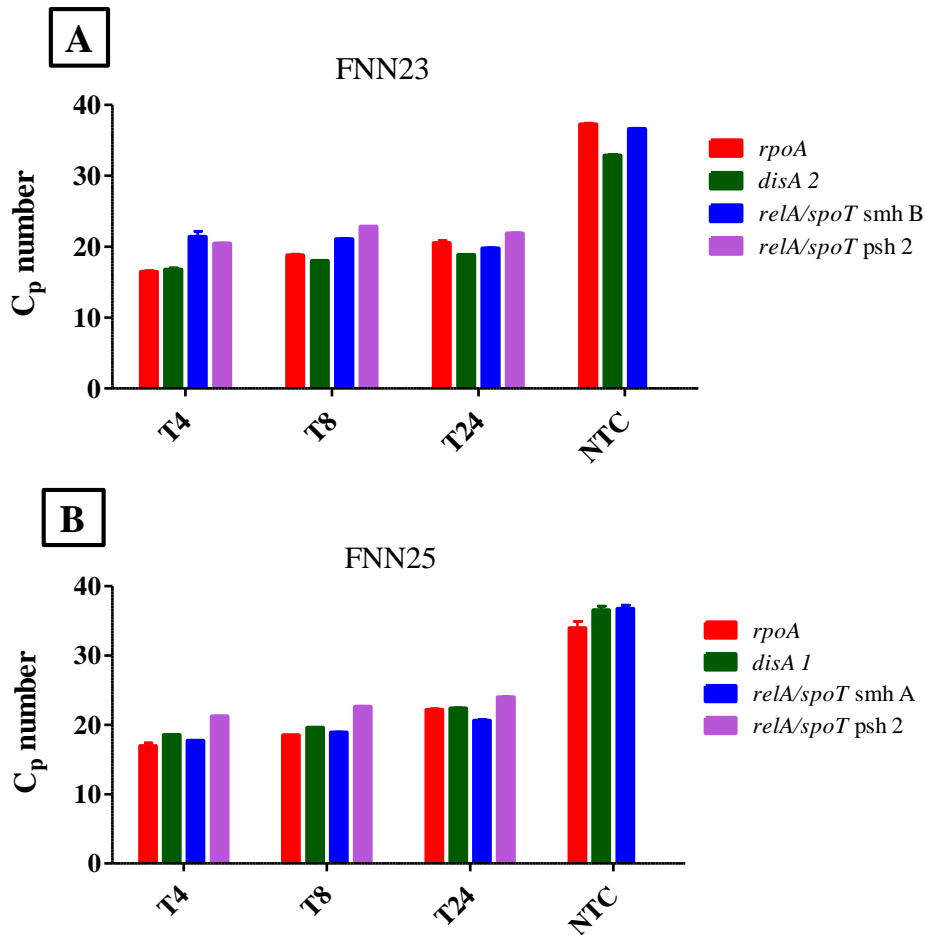


**Figure 3.32. Differential expression of target genes in FNN23 and FNN25 – assay n. 3.** The expression levels are presented as  $C_p$  values. Nuclease-free water was used instead of the cDNA template in the negative, no template control (NTC). Each bar shows a mean of two technical replicates. Error bars show standard deviation.

The  $C_p$  values of *rpoA* in FNN23 differed as follows: 16.45 (T4), 18.78 (T8) and 20.52 (T24). A difference in values for FNN25 was observed as well: 16.97 (T4), 18.52 (T8) and 22.19 (T24). Due to the time restrictions of the project it was not possible to continue optimising the qRT-PCR protocol. Due to the differences in *rpoA*  $C_p$  values, it was not possible to calculate

an accurate change in the expression of the target genes using the housekeeping gene. That is why it was decided to calculate the expression change in separate groups of target genes using the  $C_p$  value of each T4 sample as a reference for its corresponding group. The expression was calculated using the following formula:

$$\text{Relative expression} = 2^{(Ct(\text{reference T4}) - Ct(\text{test}))}$$

The T4 sample in each group of genes of interest was given an expression value of 1. The expression level analysis showed that all genes of interest in FNN25 were downregulated over time when compared to the expression of T4 sample. (Fig. 3.33. B). Surprisingly, the expression of *relA/spoT smh* in FNN23 was slightly upregulated at T8 (1.27-fold) and then considerably upregulated at T24 (3.14-fold). This was the only gene that was upregulated in this study. The housekeeping gene *rpoA* was confirmed to have varying levels of expression and is therefore not suitable for the use as a reference gene in this study.

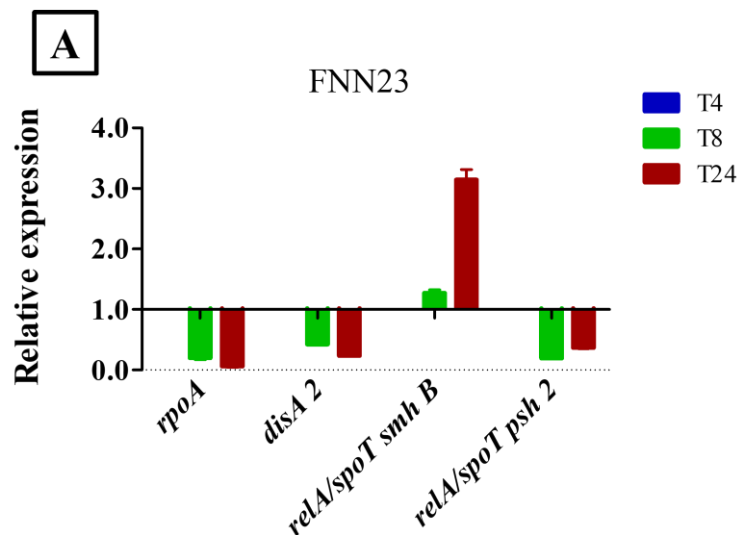


**Figure 3.33. Relative expression of target genes in FNN23 (A) and FNN25 (B).** Graph B and the figure legend can be found on the next page.

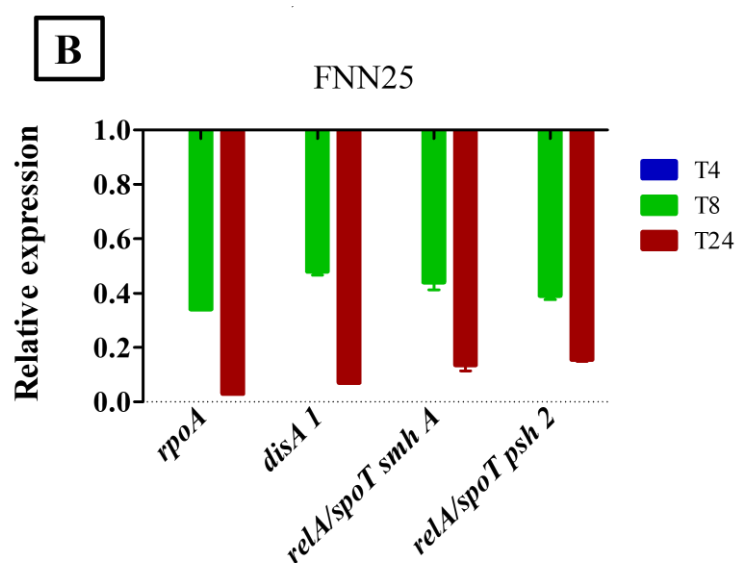


**Figure 3.33. Relative expression of target genes in FNN23 (A) and FNN25 (B).** Fold expression was calculated using T4 of each target gene as a reference. Each bar shows a mean of two technical replicates. Error bars show standard deviation.

In addition to the analysis of expression of the target genes modulating the level of CDNs and other nucleotide-containing signalling molecules, this study also focused on the quantification of metabolites, more specifically CDNs, extracted from *F. nucleatum* subspecies grown on agar plates as well as in biofilms.

#### 3.4.6. Quantification of CDNs

*F. nucleatum* subspecies were grown on agar plates and in mono-species biofilms and the metabolites c-di-AMP and c-di-GMP were extracted as described in section 2.10. and 2.11. All subspecies were included in the extraction of metabolites from the bacteria grown on the agar plates. Due to the failure to grow FNP in mono-species biofilms, this subspecies was excluded from the analysis.

The metabolites were previously extracted and quantified by Dr Sarah Kuehne using liquid *F. nucleatum* subspecies cultures. The analysis showed that all *F. nucleatum* subspecies produced c-di-AMP, but no c-di-GMP was detected (Fig. 3.34.)

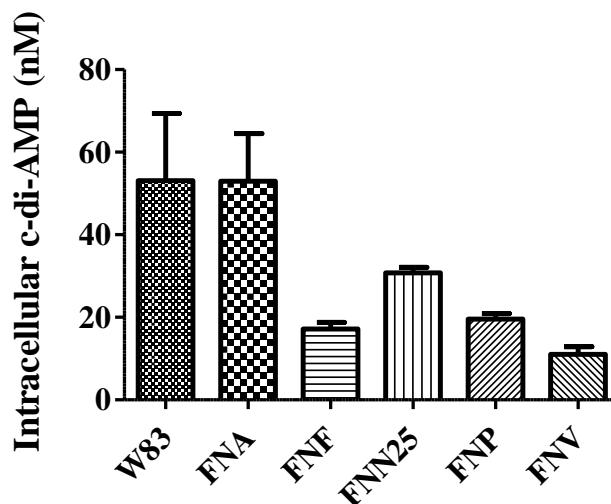


**Figure 3.34. Quantification of intracellular c-di-AMP from liquid *F. nucleatum* subspecies cultures.** *Porphyromonas gingivalis* W83 was used as a positive control. Metabolite concentration was quantified using LC-MS/MS. Error bars show standard deviation, n=3.

The amount of metabolite produced was quantified using Liquid Chromatography – Tandem Mass Spectrometry (LC-MS/MS). *Porphyromonas gingivalis* W83, a highly virulent and invasive strain (Mendez *et al.*, 2019) was used as a positive control, as it was expected to produce higher levels of CDNs. The concentration of the metabolite quantified from *F. nucleatum* subspecies ranged from 11.02 nM (FNV) to 52.95 nM (FNA). The concentration of *P. gingivalis* W83 was 53.1 nM.

In order to find out whether the *F. nucleatum* subspecies produce c-di-GMP and what the level of production is, one of the aims of this project was to extract the CDNs from a much more concentrated bacterial suspension, which would be obtained by growing the subspecies on agar plates and subsequently resuspending the content of each plate in medium. Surprisingly, no

c-di-GMP was detected. The amount of c-di-AMP detected was lower compared to the preliminary results obtained by Dr Kuehne (Fig. 3.35.) Based on the initial quantification values, FNN25 produced the highest amount of c-di-AMP, while FNN23 produced the lowest amount of c-di-AMP.

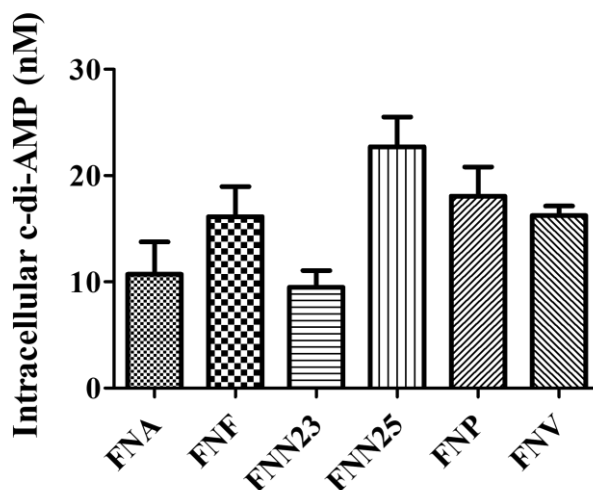


**Figure 3.35. Quantification of intracellular c-di-AMP from *F. nucleatum* subspecies grown on agar plates.** Metabolite concentration was quantified using LC-MS/MS. Error bars show standard deviation, n=3.

These values, however, do not take into account the amount of bacterial suspension from which the metabolites were extracted. That is why it was necessary to relate the metabolite concentration to the amount of protein in each sample representing the amount of starting material used for the extraction. The amount of protein was quantified using a Bicinchoninic acid (BCA) assay (section 2.12.) and the amount of c-di-AMP per microgram of protein was calculated. The results showed that FNF produced significantly the highest amount of c-di-AMP among all the subspecies (Fig. 3.36.). The lowest amount of detected c-di-AMP was produced by FNA, FNN23 and FNP. A significantly higher metabolite amount was produced by FNN25 and FNV. These results indicate that *F. nucleatum* subspecies produce different

amounts of CDNs, more specifically c-di-AMP, when grown on agar plates and do not seem to be producing c-di-GMP when grown on agar plates and in liquid cultures.

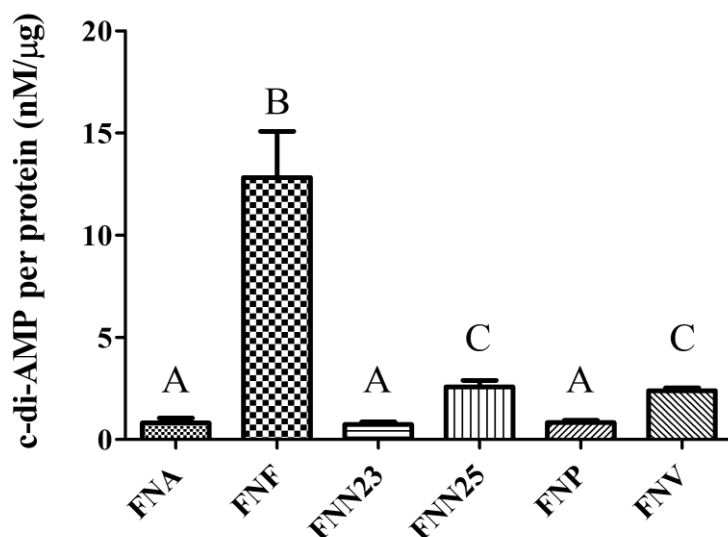


**Figure 3.36. The concentration of c-di-AMP from *F. nucleatum* subspecies grown on agar plates related to the amount of protein.** The highest amount of c-di-AMP was detected in FNF. Differences between the subspecies were analysed using Kruskal-Wallis test and Mann-Whitney test. Different letters indicate significant difference ( $p \leq 0.05$ ). If the subspecies share the same letter, the difference is non-significant. Error bars show standard deviation,  $n=3$ .

After the extraction and quantification of the bacteria grown on the agar plates, the metabolites were extracted from single-species biofilms. When the biofilms were detached from the multi-well plates in which they were grown for five and seven days, upon visual examination the amount of starting material was similar to the amount of bacteria obtained from the agar plates. However when the quantification results were returned from the facility performing the LC-MS/MS, it was found that c-di-AMP was detected only in FNA grown for five days and in FNF and FNV grown for seven days. C-di-GMP was not detected in any of the samples. The mean concentrations of the quantified c-di-AMP metabolite were 3.65 nM, 2.19 nM and 3.55 nM, respectively. These values were well below the Lower Limit of Quantification (LLOQ), which was 19.8 nM. The LLOQ is defined as the lowest concentration of the metabolite analysed

which can be quantified precisely and accurately (Vashist and Luong, 2018). It is advised that any values detected below the LLOQ should be reported as zero concentration. That is why the c-di-AMP concentrations detected in the biofilm samples do not provide any conclusive results, however the values are informative for a future metabolite extraction from single-species biofilms. Therefore, it was decided the quantified concentration would be related to the amount of protein in the sample used for the extraction, which can provide a starting point for further research.

Based on the results obtained, FNA grown in a single-species biofilm for five days produced the highest amount of c-di-AMP (444.37 pM/ $\mu$ g), while FNF biofilm grown for seven days produced the lowest amount of the metabolite (250.56 pM/ $\mu$ g) (Fig. 3.37.) The amount of the metabolite detected in FNV biofilm grown for seven days was 283.54 pM/ $\mu$ g.

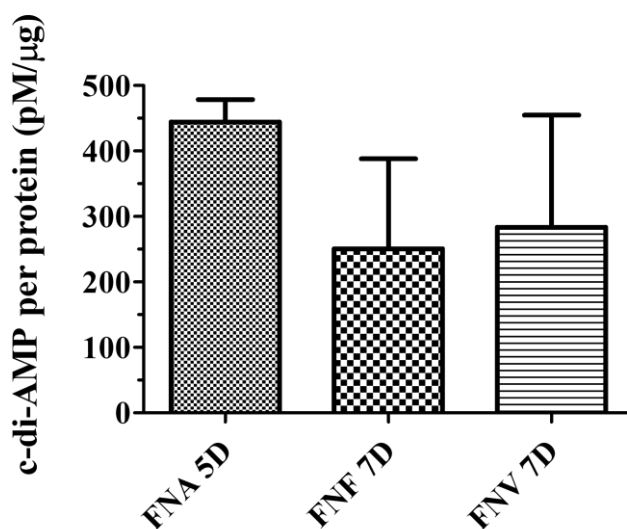


**Figure 3.37. The concentration of c-di-AMP in single-species biofilms related to the amount of protein.** The highest concentration of c-di-AMP was produced by FNA biofilm grown for five days. Error bars show standard deviation, n=3 (FNA 5D), n=2 (FNF 7D, FNV 7D).

### 3.4.7. Chapter conclusions

Primer validation test using conventional PCR showed that the primers designed for the genes of interest amplified specifically when FNN23 was used to provide the DNA template. Interestingly, the efficiency of annealing tested by qRT-PCR was ideal only in FNN23 and FNN25, with *rpoA*, *disA*, *relA/spoT* small hydrolase and *relA/spoT* (p)ppGpp synthetase/hydrolase primer sets having the desired efficiency values while *pde2* primer set did not fulfil this criterion and it was excluded from the analysis. During the qRT-PCR optimisation it was found out that the concentration of cDNA should be carefully controlled and equalised to add an extra layer of accuracy in the assay. Housekeeping gene *rpoA* was confirmed not to be suitable for the needs of this project as it repeatedly exhibited unstable expression. Due to the absence of an alternative reference gene, the T4 expression level from each group of target genes was used as a reference value. The results revealed that all genes of interest were downregulated over time in FNN25. Interestingly, *relA/spoT* encoding for the small (p)ppGpp hydrolase was the only gene upregulated over time in FNN23.

Additionally, the quantification of CDNs extracted from bacteria grown on agar plates showed that the production of c-di-AMP varies among subspecies, with FNF being the strongest c-di-AMP producer. When the CDNs were extracted from single-species biofilms, the concentration detected was much lower than the LLOQ, however based on the results obtained, FNA grown in a biofilm for five days produced the highest amount of c-di-AMP. C-di-GMP was not detected in any sample analysed.

## **CHAPTER 4: DISCUSSION**

In this work focusing on characterisation of *F. nucleatum* biofilms and CDN production, the communication system of *F. nucleatum* subspecies utilising CDNs was studied using multiple powerful techniques, such as qRT-PCR and LC/MS-MS.

#### **4.1. Characterisation of *Fusobacterium nucleatum* subspecies**

The growth of individual subspecies was characterised in detail and colony as well as cell morphology were found to be distinct for each subspecies. Scanning electron microscopy was invaluable in providing accurate measurements of the bacterial cells and showed that FNP was significantly longer than the rest of the subspecies ( $p < 0.0001$ ).

Next, the bacteria were grown in anaerobic conditions, their natural environment, in order to characterise their growth using the Miles and Misra (1938) method and the spectrophotometric method. The Miles and Misra method showed that all the subspecies with the exception of FNP were found to reach maximum growth at T24, however FNP reached the highest bacterial concentration at T8. This might have been caused by FNP consuming the nutrients from the medium at a much higher rate compared to the other subspecies. Alternatively, FNP might be producing a particular toxic metabolite, which is excreted into the medium and prevents further growth of bacteria, as it is in the case of *E. coli* secreting acetate during growth in liquid medium. Increased concentration of acetate limits further growth of *E. coli* (Pinhal *et al.*, 2019). The generated growth curves provided data to calculate the doubling time of each subspecies and notable differences were observed among the subspecies. However, it needs to be taken into consideration that the data collection for the growth curves occurs every 2 hours for the first 8 hours and then at 24 and 48 hours after the inoculation of the sub-culture and the long gap between T8 and T24 might introduce inaccuracy and an element of unknown to growth curve generation. Another factor affecting the calculation of the generation time might be

differences in the initial number of bacteria, which were not accounted for in the described experiments.

When the growth curve of FNN25 was generated using the automated spectrophotometer, a considerably long lag phase was observed. This could mean that FNN cultures need a longer time of incubation in order to reach an optical density above the detection limit of the instrument. An additional issue with the spectrophotometric method was the autoaggregation of the bacterial cells, which confirmed that this method is not suitable for *F. nucleatum*.

In addition to growth in anaerobic conditions, *F. nucleatum* subspecies were grown in conditions containing oxygen and viability of all subspecies was still detected after eight hours of exposure to oxygen. Surprisingly, FNN25, FNP and FNV were viable even after 24 hours. However, it needs to be taken into consideration that the bacteria were sub-cultured at T0 into a medium that was conditioned in an anaerobic chamber overnight in order to start with a viable culture. The sub-culture might have remained anaerobic for a longer time, with the oxygen from the surrounding air diffusing into the medium at a very low rate, thus allowing bacterial growth. If the time constraints of the project allowed more experiments, the overnight culture would be sub-cultured into a non-conditioned, fully oxygenated sterile medium and the growth of bacteria would be monitored. Additionally, a well-characterised obligate anaerobe, such as *P. gingivalis*, would be used as a control for this experiment.

The confirmation of subspecies identity using conventional PCR and 16S rRNA gene sequencing showed that the similarity values among subspecies ranged from 97.22% (FNA vs. FNP) to 99.34% (FNF vs. FNV). Varying levels of similarity might be caused by the fact that the subspecies do not usually inhabit the same niche together and therefore their genome evolution might have been subjected to different selective pressures. FNA has been mostly isolated from the intestinal and vaginal mucosa (Allen-Vercoe, Strauss and Chadee, 2011;

Gonzales-Marin, Spratt and Allaker, 2013). However, it was also reported in refractory periodontitis and necrotising ulcerative gingivitis (Gonzales-Marin, Spratt and Allaker, 2013). FNN has been mostly isolated from periodontal infections (Nie *et al.*, 2015). FNV, FNF and according to some authors FNP as well were isolated from healthy sites, but none of the authors specified what these healthy sites were (Gonzales-Marin, Spratt and Allaker, 2013; Nie *et al.*, 2015). What researchers know with a high degree of certainty is that *F. nucleatum* subspecies are associated with multiple diseases in varying locations of the human body. Additionally, their invasive potential allows them to translocate from one site to another, increasing their repertoire of colonised environments. These factors might affect the differences between the subspecies. In addition to the comparison of the 16S rRNA gene sequences, it would be interesting to compare whole genome sequences of individual *F. nucleatum* subspecies in order to understand possible adaptations to different niches as well as possible pathogenicity genes unique to specific subspecies.

## **4.2. Characterisation of mono-species *Fusobacterium nucleatum* biofilms and multi-species periodontitis-related biofilms**

### *4.2.1. Single-species biofilms*

Once the subspecies were characterised, they were subsequently grown individually in single-species biofilms and the biofilm-forming ability was found to differ among subspecies at different time points. This agrees with a study performed by Thurnheer and colleagues (2019), who focused on growing *F. nucleatum* subspecies in multi-species biofilms. They found out that there were significant differences in the total bacterial numbers among the biofilms containing different *F. nucleatum* subspecies, which shows that there are variations in the biofilm forming ability among the subspecies.

However, certain issues have to be considered when drawing conclusions from the data obtained in this study. Biofilms were found to be very fragile when incubated in all types of plates used, even when grown on Nunc™ Thermanox™ coverslips. When the plates were handled during the AS change and preparation for the subsequent analysis, it was noticed that the biofilm layers were easily disturbed and considerably large amounts of the biofilms were aspirated either when the AS was removed or when the biofilms were washed with PBS. This could have led to false results when biomass was quantified. The biofilm fragility could have been caused by multiple factors.

Firstly, the polystyrene surface of the multi-well plates is different from the tooth surface, which serves as a natural substrate for plaque formation. Secondly, the composition of the AS is unlike that of the GCF, which constantly washes the biofilm in the periodontal pocket, especially when it comes to nutrients. Thirdly, the pH of the environment differs between physiological and laboratory conditions. These three issues could be addressed in future experiments by growing the biofilms on different surfaces, such as hydroxyapatite discs, which serve as a tooth enamel equivalent (Blumhagen *et al.*, 2014). Biofilms could also be grown in different media, such as sterilised saliva (Periasamy *et al.*, 2009) or blood plasma (Subbarao *et al.*, 2019), both from healthy donors. The pH of the medium could be adjusted, as it was performed by Chew *et al.* (2012), who successfully grew stable FNP biofilms for a subsequent proteomic investigation. Additionally, and most importantly, *F. nucleatum* subspecies naturally live in multi-species communities and do not appear as mono-species biofilms. The importance of a presence of a binding partner was confirmed by Periasamy *et al.* (2009). They discovered that *F. nucleatum* ssp. *polymorphum* did not aggregate in mono-species biofilms and needed *Actinomyces naeslundii* in order to form stable biofilms when grown in saliva. This supports the findings of this project which showed that FNP formed very little biomass on its own when studied by

crystal violet staining and SEM. Moreover, no FNP biofilm was obtained for the extraction of CDNs (section 4.4.2.).

Micrographs produced using the SEM showed that in single-species *F. nucleatum* biofilms, bacteria do not cover the whole surface of the coverslip, but rather appear in patches. While this could have been caused by the abovementioned reasons, another reason could have been the detachment of the biofilms during the preparation. The dehydration protocol consists of multiple wash steps with ethanol and these washes might have removed the biofilm layer. In order to limit the detachment of the fragile biofilms and to strengthen the 3D structure, osmium vapour can be used prior to the fixation with glutaraldehyde. This protocol was successfully applied previously in order to preserve biofilms on microalgae with an additional aim to conserve the ECM (Barreto and Meyer, 2007). Future studies could also involve looking at possible preservation of ECM in *F. nucleatum* biofilms due to the fact that micrographs of biofilms obtained in this study seem to lack ECM. Moreover, the addition of osmium vapour might increase the structural strength of FNP. Cells observed in the biofilm grown for seven days had blunt, angular ends that seemed to be broken during the SEM preparation.

When individual SEM micrographs were analysed, an interesting phenomenon emerged. Individual bacteria with a different morphology from *F. nucleatum* were observed in the biofilms studied. These bacteria were shorter and had a bulky shape and round caps. It was confirmed not to be contamination, thus it was hypothesised that the observed cells were old *F. nucleatum* bacteria. These different morphotypes were observed mostly in biofilms incubated for seven days, which could indicate a higher age of the cells. This was previously shown in *F. necrophorum*, which exhibits different morphologies depending on culture medium and the age of the culture (Atlas of Oral Microbiology, 2015, p. 81).

#### 4.2.2. Multi-species biofilms

Two subspecies of *F. nucleatum* were selected for incubation in multi-species periodontitis-related biofilms, FNP and FNN23. It was shown that when FNN23 was introduced into a multi-species biofilm, the total biomass was significantly higher than when FNP was incorporated, both when quantified by crystal violet staining and evaluated visually by SEM. The study of Thurnheer *et al.* (2019), mentioned earlier, showed very similar results, when biofilms containing FNP produced significantly less total biomass than biofilms containing FNN (OMZ 598 – personal collection). Brennan and Garrett (2019) stated in their review that the strain FNN23 was originally isolated from the urogenital tract. If this site was considered the site of origin, FNN23 could possibly gain either more adhesive or additional aggregation/adhesion proteins due to the evolutionary pressures that FNP has not been subjected to. However, individual subspecies have not been studied in depth using a proteomic approach, which could reveal the total protein composition. Thus, more research has to be done in order to confirm this hypothesis.

Future work could involve growing all the *F. nucleatum* subspecies in multi-species biofilms. A biofilm model with up to 11 subspecies could be used in order to study specific interactions of individual subspecies in the context of periodontitis-related biofilm. Additionally, mutated subspecies, namely FNN23, being the only genetically tractable subspecies, could be introduced into these multi-species models. Mutants that could be studied would be deficient for the synthases and hydrolases regulating the level of c-di-AMP and c-di-GMP and the biofilm biomass and architecture would be analysed.

### **4.3. Optimisation of RNA extraction from *Fusobacterium nucleatum* subspecies**

During the optimisation process, it was demonstrated that *F. nucleatum* is a sturdy bacterium and the commercially available kits are not able to disrupt the bacterial cells and extract pure RNA from the cultures. A multi-step disruption protocol proved to be efficient in breaking the bacterial cells open and allowed the extraction of the nucleic acid. A subsequent digestion of contaminating gDNA in liquid rather than on-column successfully purified the RNA isolated. Multiple factors have to be considered when aiming to extract pure RNA. The samples can easily be contaminated, either by working on a surface that has not been cleaned thoroughly or by unaware face or hair touching, that is why a very high level of cleanliness and personal control have to be applied. These factors could have caused both primer and sample contamination during the first stages of the optimisation process. Next, when the RNA is isolated and quantified using a nanodrop, the total concentration of the nucleic acid is measured rather than RNA only, even if specific settings for RNA quantification are selected. This was shown by the RNA quantification of total extracts, which were confirmed to be contaminated using conventional PCR. A high concentration of the sample does not necessarily mean a high RNA concentration. In future RNA extractions, an additional purity check can be added by measuring 260/280 or 260/230 ratios, which can indicate the quality of the sample (Desjardins and Conklin, 2010).

The optimised protocol will allow a multitude of molecular analyses using RNA as the molecule of interest, not only in the context of CDNs, but also in the wider context of *F. nucleatum* virulence and immune modulation and evasion.

#### **4.4. Analysis of differential expression of genes involved in synthesis and hydrolysis of cyclic di-nucleotides (CDNs) and quantification of CDNs**

##### *4.4.1. Differential expression of genes analysed by qRT-PCR*

Expression of the genes associated with production and degradation of c-di-AMP and alarmones was analysed at three time points of the exponential phase – T4, T8 and T24 in FNN23 and FNN25. Interestingly, all the genes studied were shown to be downregulated over time, apart from *relA/spoT* encoding for the small (p)ppGpp hydrolase, which was found to be significantly upregulated over time with respect to T4.

The pattern of expression observed may be connected to the growth conditions of the culture studied. Bacteria were grown in highly nutritious liquid medium and only planktonic bacteria were harvested to be analysed by qRT-PCR. To the best of our knowledge, CDNs and alarmones were mostly studied in biofilms and therefore our results can only be reversely related to the published data.

The fundamental premise is that a high level of either c-di-AMP (Peng *et al.*, 2016) or c-di-GMP (Gürsoy *et al.*, 2017) causes biofilm formation. Kim and Davey (2020) found out that mutants of *P. gingivalis* defective for genes encoding enzymes regulating the concentration of (p)ppGpp produced higher amounts of biofilm biomass. Based on their results, the assumption would be that the absence of alarmones increases the biofilm formation while an increased concentration of alarmones might either prevent biofilm formation or cause the biofilm dispersal.

Downregulation of the genes studied in this project might mean that the bacteria growing in liquid medium in the exponential phase did not have to face the lack of nutrients or any dramatic change of the environment. Therefore, they did not need to initiate the aggregation into a biofilm, which would not be beneficial at this point. In order to limit the non-beneficial energy

expenditure, the bacteria might have downregulated the production of the enzymes needed for the synthesis and hydrolysis of CDNs as well as alarmones. Also, (p)ppGpp is produced at basal levels during the exponential phase and regulates the growth rate (Hauryliuk *et al.*, 2015). As the bacteria were approaching the end of the exponential phase, the need for production of synthetases was decreasing, that is why the genes might have been downregulated. The upregulation of the only gene in FNN23, *relA/spoT* (small (p)ppGpp hydrolase), might have indicated that the bacterial culture experienced a stress stimulus during the incubation which caused the upregulation of the bifunctional gene. Repeating the analysis at least two more times in the future could confirm or reject the pattern observed.

A very important part of the differential gene expression analysis is the presence of the endogenous control, also known as a housekeeping gene, which is required for the expression normalization. The housekeeping gene used in this study was *rpoA* (DNA-directed RNA polymerase subunit alpha), however the experiments showed that it should not have been used as it did not exhibit stable expression over time. In order to confirm the data obtained in this study and to further support the hypothesis described above, it is important to thoroughly test and choose more than one suitable housekeeping gene, which could be used for more accurate calculation of the gene expression levels. The FNN23-specific 16S rRNA gene, which was not used in this study due to the time constraints, could be used in future experiments as an endogenous control. Other routinely used bacterial housekeeping genes are *gyrA* (DNA gyrase A), *recA* (Recombinase A) or *ftsZ* (Cell division protein FtsZ), just to name a few (Rocha, Santos and Pacheco, 2015).

Surprisingly, it was found that the primers used in this study worked with a high efficiency only in FNN23 and FNN25. The primer set targeting *pde2* gene even only worked in FNN23. This might mean that the sequences of the genes of interest in FNA, FNP and FNV (and FNN25 in

the case of *pde2*) differ substantially from the genes found in FNN23, which were used to design the primers. It would be interesting to find the differences between these genes using a multiple sequence alignment and to design new sets of primers specific for each subspecies and analyse the gene expression.

Future work could also involve growing a complete set of *F. nucleatum* subspecies in single-species biofilms and analyse the gene expression in biofilm-embedded bacteria as well as the planktonic bacteria. This might provide more information on how bacteria adapt their gene expression when switching to a sessile lifestyle and shed more light on the activity of genes involved in the synthesis and hydrolysis of CDNs and alarmones.

#### 4.4.2. Quantification of CDNs

During this project, CDNs were quantified from bacteria grown on agar plates and from biofilm-embedded bacteria. Interestingly, only c-di-AMP was detected in all the samples analysed. Significant differences in the amount of c-di-AMP per protein were observed among subspecies, with FNF being the strongest c-di-AMP producer. FNA, FNN23 and FNP were found to produce the lowest amount of c-di-AMP. However, these results have to be reported with caution. In order to relate the quantified CDNs to the amount of bacterial mass they were extracted from, the BCA assay was used to quantify the amount of protein in the sample used for the extraction. This assay uses the protein pellet which is left after the extraction. It was noticed that during the final extraction steps the pelleted proteins were gradually lost due to the removal of the supernatant which contained the CDNs. That is why the amount of protein quantified using this assay might not be accurate and this might lead to inaccuracy when reporting the amount of c-di-AMP per protein in the sample. To try to correct this issue, a higher number of RPM/g could be used during the centrifugation to obtain a more compact pellet.

Alternatively, the amount of c-di-AMP could be reported in relation to the mass of the initial bacterial pellet. Interestingly, Chaudhuri *et al.* (2014) studying diguanylate cyclase in *P. gingivalis* and its production of c-di-GMP did not report the quantified c-di-GMP with respect to the protein content or the mass of the bacterial pellet used for the extraction, they simply report the “parent ion intensity”.

Quantification of CDNs extracted from biofilms was successful only in three samples – FNA grown for five days, FNF grown for seven days and FNV grown for seven days. All the other samples tested were reported to contain less than zero nM of c-di-AMP (data not shown). Even in the three samples that were quantified, the amount of c-di-AMP was well below the LLOQ, which indicated that the amount of starting material used for the extraction was probably too low. As described in the Results section, the amount of starting material examined visually suggested the amount was sufficient for the extraction. However, only about 15-20% of the total biofilm mass encompasses bacterial cells. The remaining 80% is the ECM encasing the bacteria (Plančak, Musić and Puhar, 2015). This might be the reason why the concentration of quantified c-di-AMP was so low and no c-di-GMP was detected. In order to overcome this obstacle, the biofilms will need to be grown in much higher amounts, so that the quantified CDNs can be reported with confidence.

#### **4.5. Concluding remarks**

Many research groups admit that the involvement of *F. nucleatum* subspecies in diseases affecting patients’ lives, from periodontitis to colorectal cancer, is undeniable. Yet, the precise molecular mechanisms of *F. nucleatum* virulence are largely unknown. The importance of signalling molecules, especially CDNs in the virulence and biofilm formation was studied in

periodontal pathogens such as *P. gingivalis*. It is surprising that even if *F. nucleatum* is a key bridging microbe in the formation of periodontitis-related biofilms, very little is known about how CDNs affect the aggregation of *F. nucleatum* subspecies into the biofilms. This work provided the data which can serve as a starting platform for further research, not only in the context of periodontal disease. CDNs do not only regulate biofilm formation in bacteria, but also bind specific receptors on eukaryotic cells and elicit an immune response in the host tissues. Due to this potent reaction of the immune system, the CDNs could be used as adjuvants in immune therapies (Wang *et al.*, 2017). Understanding the CDNs primarily in the biofilm formation and virulence of *F. nucleatum* subspecies might provide more information on the prevention and treatment of periodontal diseases as well as systemic diseases caused by these microbes, revealing new therapeutic targets. Additionally, CDNs could serve as biomarkers used for diagnostic purposes. In a broader view, this could lead to understanding the virulence of other periodontal pathogens and possibly discovery of novel immune therapies.

## References

- Abranches, J., Martinez, A. R., Kajfasz, J. K., Chavez, V., Garsin, D. A. and Lemos, J. A. (2009) 'The Molecular Alarmone (p)ppGpp Mediates Stress Responses, Vancomycin Tolerance, and Virulence in *Enterococcus faecalis*', *Journal of Bacteriology*, 191(7), pp. 2248–2256. doi: 10.1128/JB.01726-08.
- Allen-Vercoe, E., Strauss, J. and Chadee, K. (2011) '*Fusobacterium nucleatum*', *Gut Microbes*, 2(5), pp. 294–298. doi: 10.4161/gmic.2.5.18603.
- De Andrade, K. Q., Almeida-Da-Silva, C. L. C. and Coutinho-Silva, R. (2019) 'Immunological pathways triggered by *Porphyromonas gingivalis* and *Fusobacterium nucleatum*: Therapeutic possibilities?', *Mediators of Inflammation*, 2019. doi: 10.1155/2019/7241312.
- Aylikci, B. and Çolak, H. (2013) 'Halitosis: From diagnosis to management', *Journal of Natural Science, Biology and Medicine*, 4(1), pp. 14–23. doi: 10.4103/0976-9668.107255.
- Barreto, M. and Meyer, J. J. M. (2007) 'The preservation of biofilms on macroalgae by osmium vapour', *South African Journal of Botany*, 73(1), pp. 64–69. doi: 10.1016/j.sajb.2006.08.004.
- Bian, J., Liu, X., Cheng, Y. Q. and Li, C. (2013) 'Inactivation of cyclic di-GMP binding protein TDE0214 affects the motility, biofilm formation, and virulence of *Treponema denticola*', *Journal of Bacteriology*, 195(17), pp. 3897–3905. doi: 10.1128/JB.00610-13.
- Blumhagen, A., Singh, P., Mustapha, A., Chen, M., Wang, Y. and Yu, Q. (2014) 'Plasma deactivation of oral bacteria seeded on hydroxyapatite disks as tooth enamel analogue', *American Journal of Dentistry*, 27(2), pp. 84–90.
- Bowen, W. H., Burne, R. A., Wu, H. and Koo, H. (2018) 'Oral Biofilms: Pathogens, Matrix, and Polymicrobial Interactions in Microenvironments', *Trends in Microbiology*, 26(3), pp. 229-242. doi: 10.1016/j.tim.2017.09.008.
- Brennan, C. A. and Garrett, W. S. (2019) '*Fusobacterium nucleatum* — symbiont, opportunist and oncobacterium', *Nature Reviews Microbiology*, 17, pp.156-166. doi: 10.1038/s41579-018-0129-6.
- Burhenne, H. and Kaefer, V. (2013) 'Quantification of Cyclic Dinucleotides by Reversed-Phase LC-MS/MS', in Gehring, C. (ed.) *Cyclic Nucleotide Signaling in Plants: Methods and Protocols*. Totowa, NJ: Humana Press, pp. 27–37. doi: 10.1007/978-1-62703-441-8\_3.
- ten Cate, J. M. (2006) 'Biofilms, a new approach to the microbiology of dental plaque', *Odontology*, 94(1), pp. 1–9. doi: 10.1007/s10266-006-0063-3.
- Chaudhuri, S., Pratap, S., Paromov, V., Li, Z., Mantri, C. K. and Xie, H. (2014) 'Identification of a diguanylate cyclase and its role in *Porphyromonas gingivalis* virulence', *Infection and Immunity*, 82(7), pp. 2728–2735. doi: 10.1128/IAI.00084-14.

Chew, J., Zilm, P. S., Fuss, J. M. and Gully, N. J. (2012) 'A proteomic investigation of *Fusobacterium nucleatum* alkaline-induced biofilms', *BMC Microbiology*, 12, p. 189. doi: 10.1186/1471-2180-12-189.

Chukkapalli, S. S., Rivera-Kweh, M. F., Velsko, I. M., Chen, H., Zheng, D., Bhattacharyya, I., Gangula, P. R., Lucas, A. R. and Kesavalu, L. (2015) 'Chronic oral infection with major periodontal bacteria *Tannerella forsythia* modulates systemic atherosclerosis risk factors and inflammatory markers', *Pathogens and Disease*, 73(3). doi: 10.1093/FEMSPD/FTV009.

Desjardins, P. and Conklin, D. (2010) 'NanoDrop microvolume quantitation of nucleic acids', *Journal of Visualized Experiments*, (45). doi: 10.3791/2565.

Dias da Purificação, A., de Azevedo, N. M., Guarany de Araujo, G., Franciso de Souza, R. and Rodrigues Guzzo, C. (2020) 'The World of Cyclic Dinucleotides in Bacterial Behavior', *Preprints*, (January), pp. 1–40. doi: 10.20944/preprints202001.0120.v1.

Dominy, S. S., Lynch, C., Ermini, F., Benedyk, M., Marczyk, A., Konradi, A., Nguyen, M., Haditsch, U., Raha, D., Griffin, C., Holsinger, L. J., Arastu-Kapur, S., Kaba, S., Lee, A., Ryder, M. I., Potempa, B., Mydel, P., Hellvard, A., Adamowicz, K., Hasturk, H., Walker, G. D., Reynolds, E. C., Faull, R. L. M., Curtis, M. A., Dragunow, M. and Potempa, J. (2019) '*Porphyromonas gingivalis* in Alzheimer's disease brains: Evidence for disease causation and treatment with small-molecule inhibitors', *Science Advances*, 5(1), pp. 1–22. doi: 10.1126/sciadv.aau3333.

Erchick, D. J., Rai, B., Agrawal, N. K., Khatry, S. K., Katz, J., LeClerq, S. C., Reynolds, M. A. and Mullany, L. C. (2019) 'Oral hygiene, prevalence of gingivitis, and associated risk factors among pregnant women in Sarlahi District, Nepal', *BMC Oral Health*, 19(1), p. 2. doi: 10.1186/s12903-018-0681-5.

Eroshenko, G. A., Vidyaeva, N. A. and Kutylev, V. V. (2010) 'Comparative analysis of biofilm formation by main and nonmain subspecies *Yersinia pestis* strains', *FEMS Immunology and Medical Microbiology*, 59(3), pp. 513–520. doi: 10.1111/j.1574-695X.2010.00719.x.

Fahmi, T., Faozia, S., Port, G. C. and Cho, K. H. (2019) 'The second messenger C-di-AMP regulates diverse cellular pathways involved in stress response, biofilm formation, cell wall homeostasis, SpeB expression, and virulence in *Streptococcus pyogenes*', *Infection and Immunity*, 87(6), e00147-19. doi: 10.1128/IAI.00147-19.

Germain, E., Guiraud, P., Byrne, D., Douzi, B., Djendli, M. and Maisonneuve, E. (2019) 'YtfK activates the stringent response by triggering the alarmone synthetase SpoT in *Escherichia coli*', *Nature Communications*, 10(1), pp. 1–12. doi: 10.1038/s41467-019-13764-4.

Gonzales-Marin, C., Spratt, D. A. and Allaker, R. P. (2013) 'Maternal oral origin of *Fusobacterium nucleatum* in adverse pregnancy outcomes as determined using the 16S-23S rRNA gene intergenic transcribed spacer region', *Journal of Medical Microbiology*, 62(PART1), pp. 133–144. doi: 10.1099/jmm.0.049452-0.

Gürsoy, U. K., Gürsoy, M., Könönen, E. and Sintim, H. O. (2017) 'Cyclic dinucleotides in oral bacteria and in oral biofilms', *Frontiers in Cellular and Infection Microbiology*, 7(JUN), pp. 1–5. doi: 10.3389/fcimb.2017.00273.

Vander Haar, E. L., So, J., Gyamfi-Bannerman, C. and Han, Y. W. (2018) ‘*Fusobacterium nucleatum* and adverse pregnancy outcomes: Epidemiological and mechanistic evidence’, *Anaerobe*, 50, pp. 55–59. doi: 10.1016/j.anaerobe.2018.01.008.

Han, Y. W. (2015) ‘*Fusobacterium nucleatum*: A commensal-turned pathogen’, *Current Opinion in Microbiology*, 0, pp. 141–147. doi: 10.1016/j.mib.2014.11.013.

Hauryliuk, V., Atkinson, G. C., Murakami, K. S., Tenson, T. and Gerdes, K. (2015) ‘Recent functional insights into the role of (p)ppGpp in bacterial physiology’, *Nature Reviews Microbiology*, 13, pp. 298–309. doi: 10.1038/nrmicro3448.

He, J., Yin, W., Galperin, M. Y. and Chou, S.-H. (2020) ‘SURVEY AND SUMMARY Cyclic di-AMP, a second messenger of primary importance: tertiary structures and binding mechanisms’, *Nucleic Acids Research*, 48(6), pp. 2807–2829. doi: 10.1093/nar/gkaa112.

Holmes, A., Birse, L., Jackson, R. W. and Holden, N. J. (2014) ‘An optimized method for the extraction of bacterial mRNA from plant roots infected with *Escherichia coli* O157:H7’, *Frontiers in Microbiology*, 5(JUN), p. 286. doi: 10.3389/fmicb.2014.00286.

Huang, R., Li, M. and Gregory, R. L. (2011) ‘Bacterial interactions in dental biofilm’, *Virulence*, 2(5), pp. 435–444. doi: 10.4161/viru.2.5.16140.

Ishihara, K. (2010) ‘Virulence factors of *Treponema denticola*’, *Periodontology 2000*, 54(1), pp. 117–135. doi: 10.1111/j.1600-0757.2009.00345.x.

Janda, J. M. and Abbott, S. L. (2007) ‘16S rRNA gene sequencing for bacterial identification in the diagnostic laboratory: Pluses, perils, and pitfalls’, *Journal of Clinical Microbiology*, 45(9), pp. 2761–2764. doi: 10.1128/JCM.01228-07.

Jang, Y. J., Choi, Y. J., Lee, S. H., Jun, H. K. and Choi, B. K. (2013) ‘Autoinducer 2 of *Fusobacterium nucleatum* as a target molecule to inhibit biofilm formation of periodontopathogens’, *Archives of Oral Biology*, 58(1), pp. 17–27. doi: 10.1016/j.archoralbio.2012.04.016.

Jati, A. S., Furquim, L. Z. and Consolaro, A. (2016) ‘Gingival recession: Its causes and types, and the importance of orthodontic treatment’, *Dental Press Journal of Orthodontics*, 21(3), pp. 18–29. doi: 10.1590/2177-6709.21.3.018-029.oin.

Kabwe, M., Brown, T. L., Dashper, S., Speirs, L., Ku, H., Petrovski, S., Chan, H. T., Lock, P. and Tucci, J. (2019) ‘Genomic, morphological and functional characterisation of novel bacteriophage FNU1 capable of disrupting *Fusobacterium nucleatum* biofilms’, *Scientific Reports*, 9(1), pp. 1–12. doi: 10.1038/s41598-019-45549-6.

Karunakaran, E., Mukherjee, J., Ramalingam, B. and Biggs, C. A. (2011) “‘Biofilmology’: A multidisciplinary review of the study of microbial biofilms”, *Applied Microbiology and Biotechnology*, 90(6), pp. 1869–1881. doi: 10.1007/s00253-011-3293-4.

Kim, H. M. and Davey, M. E. (2020) ‘Synthesis of ppGpp impacts type IX secretion and biofilm matrix formation in *Porphyromonas gingivalis*’, *npj Biofilms and Microbiomes*, 6(1). doi: 10.1038/s41522-020-0115-4.

Kook, J. K., Park, S. N., Lim, Y. K., Choi, M. H., Cho, E., Kong, S. W., Shin, Y., Paek, J. and Chang, Y. H. (2013) ‘*Fusobacterium nucleatum* subsp. *fusiforme* Gharbia and Shah 1992 is a later synonym of *Fusobacterium nucleatum* subsp. *vincentii* Dzinik et al. 1990’, *Current Microbiology*, 66(4), pp. 414–417. doi: 10.1007/s00284-012-0289-y.

Kriebel, K., Hieke, C., Müller-Hilke, B., Nakata, M. and Kreikemeyer, B. (2018) ‘Oral biofilms from symbiotic to pathogenic interactions and associated disease - Connection of periodontitis and rheumatic arthritis by peptidylarginine deiminase’, *Frontiers in Microbiology*, 9, p. 53. doi: 10.3389/fmicb.2018.00053.

Krzyżek, P. (2019) ‘Challenges and limitations of anti-quorum sensing therapies’, *Frontiers in Microbiology*, 10(OCT). doi: 10.3389/fmicb.2019.02473.

Külekcı, G., Çiftçi, S., Keskin, F., Kiliç, A. O., Türkoğlu, S., Badur, S., Develioğlu, Ö. N., Leblebicioğlu, B. and Külekcı, M. (2001) ‘PCR analysis of *Actinobacillus actinomycetemcomitans*, *Porphyromonas gingivalis*, *Treponema denticola* and *Fusobacterium nucleatum* in middle ear effusion’, *Anaerobe*, 7(5), pp. 241-246. doi: 10.1006/anae.2001.0400.

Lane, D. J. (1991) ‘16S/23S rRNA sequencing’, in E. Stackebrandt and M. Goodfellow (ed.) *Nucleic acid techniques in bacterial systematics*. New York: John Wiley & Sons, pp. 115-175.

Larsen, T. and Fiehn, N.-E. (2017) ‘Dental biofilm infections - an update’, *APMIS*, 125(4), pp. 376–384. doi: 10.1111/apm.12688.

Lima, B. P., Shi, W. and Lux, R. (2017) ‘Identification and characterization of a novel *Fusobacterium nucleatum* adhesin involved in physical interaction and biofilm formation with *Streptococcus gordonii*’, *MicrobiologyOpen*, 6(3). doi: 10.1002/mbo3.444.

Liu, L., Liang, L., Liang, H., Wang, M., Lu, B., Xue, M., Deng, J. and Chen, Y. (2019) ‘*Fusobacterium nucleatum* Aggravates the Progression of Colitis by Regulating M1 Macrophage Polarization via AKT2 Pathway’, *Frontiers in Immunology*, 10(JUN), p. 1324. doi: 10.3389/fimmu.2019.01324.

Liu, P.-F., Huang, I.-F., Shu, C.-W. and Huang, C.-M. (2013) ‘Halitosis Vaccines Targeting FomA, a Biofilm-bridging Protein of *Fusobacteria nucleatum*’, *Current Molecular Medicine*, 13(8), pp. 1358–1367. doi: 10.2174/15665240113139990063.

McGuire, A. M., Cochrane, K., Griggs, A. D., Haas, B. J., Abeel, T., Zeng, Q., Nice, J. B., Macdonald, H., Birren, B. W., Berger, B. W., Allen-Vercoe, E. and Earl, A. M. (2014) ‘Evolution of invasion in a diverse set of *Fusobacterium species*’, *mBio*, 5(6). doi: 10.1128/mBio.01864-14.

Mendez, K. N., Hoare, A., Soto, C., Bugueño, I., Olivera, M., Meneses, C., Pérez-Donoso, J. M., Castro-Nallar, E. and Bravo, D. (2019) ‘Variability in Genomic and Virulent Properties of *Porphyromonas gingivalis* Strains Isolated From Healthy and Severe Chronic Periodontitis Individuals’, *Frontiers in cellular and infection microbiology*, 9, p. 246. doi: 10.3389/fcimb.2019.00246.

Merritt, J., Niu, G., Okinaga, T. and Qi, F. (2009) 'Autoaggregation response of *Fusobacterium nucleatum*', *Applied and Environmental Microbiology*, 75(24), pp. 7725–7733. doi: 10.1128/AEM.00916-09.

Miles, A. A., Misra, S. S. and Irwin, J. O. (1938) 'The estimation of the bactericidal power of the blood', *Journal of Hygiene*, 38(6), pp. 732–749. doi: 10.1017/S002217240001158X.

Millhouse, E., Jose, A., Sherry, L., Lappin, D. F., Patel, N., Middleton, A. M., Pratten, J., Culshaw, S. and Ramage, G. (2014) 'Development of an in vitro periodontal biofilm model for assessing antimicrobial and host modulatory effects of bioactive molecules', *BMC Oral Health*, 14(1), pp. 1–11. doi: 10.1186/1472-6831-14-80.

Nayak, A., Bhat, K., Shivanaikar, S., Pushpa, P., Kugaji, M. and Kumbar, V. (2018) 'Detection of red complex organisms in chronic periodontitis by multiplex polymerase chain reaction', *Journal of Advanced Clinical & Research Insights*, 5(5), pp. 139–144. doi: 10.15713/ins.jcri.231.

Nie, S., Tian, B., Wang, X., Pincus, D. H., Welker, M., Gilhuley, K., Lu, X., Han, Y. W. and Tang, Y. W. (2015) '*Fusobacterium nucleatum* subspecies identification by matrix-assisted laser desorption ionization - Time of flight mass spectrometry', *Journal of Clinical Microbiolog*, 53(4), pp. 1399–1402. doi: 10.1128/JCM.00239-15.

Orme, R., Douglas, C. W. I., Rimmer, S. and Webb, M. (2006) 'Proteomic analysis of *Escherichia coli* biofilms reveals the overexpression of the outer membrane protein OmpA', *Proteomics*, 6(15), pp. 4269–4277. doi: 10.1002/pmic.200600193.

Park, J., Shokeen, B., Haake, S. K. and Lux, R. (2016) 'Characterization of *Fusobacterium nucleatum* ATCC 23726 adhesins involved in strain-specific attachment to *Porphyromonas gingivalis*', *International Journal of Oral Science*, 8(3), pp. 138–144. doi: 10.1038/ijos.2016.27.

Peng, X., Zhang, Y., Bai, G., Zhou, X. and Wu, H. (2016) 'Cyclic di-AMP mediates biofilm formation', *Molecular Microbiology*, 99(5), pp. 945–959. doi: 10.1111/mmi.13277.

Periasamy, S., Chalmers, N. I., Du-Thumm, L. and Kolenbrander, P. E. (2009) '*Fusobacterium nucleatum* ATCC 10953 requires *Actinomyces naeslundii* ATCC 43146 for growth on saliva in a three-species community that includes *Streptococcus oralis* 34', *Applied and Environmental Microbiology*, 75(10), pp. 3250–3257. doi: 10.1128/AEM.02901-08.

Petri, J., Nakatani, Y., Montgomery, M. G., Ferguson, S. A., Aragão, D., Leslie, A. G. W., Heikal, A., Walker, J. E. and Cook, G. M. (2019) 'Structure of F1-ATPase from the obligate anaerobe *Fusobacterium nucleatum*', *Open Biology*, 9(6). doi: 10.1098/rsob.190066.

Pinhal, S., Ropers, D., Geiselmann, J. and De Jong, H. (2019) 'Acetate metabolism and the inhibition of bacterial growth by acetate', *Journal of Bacteriology*, 201(13). doi: 10.1128/JB.00147-19.

Plančak, D., Musić, L. and Puhar, I. (2015) 'Quorum Sensing of Periodontal Pathogens', *Acta Stomatologica Croatica*, 49(3), p. 234. doi: 10.15644/ASC49/3/6.

- Ramage, G., Lappin, D. F., Millhouse, E., Malcolm, J., Jose, A., Yang, J., Bradshaw, D. J., Pratten, J. R. and Culshaw, S. (2017) 'The epithelial cell response to health and disease associated oral biofilm models', *Journal of Periodontal Research*, 52(3), pp. 325–333. doi: 10.1111/jre.12395.
- Rio, D. C., Ares, M., Hannon, G. J. and Nilsen, T. W. (2010) 'Purification of RNA Using TRIzol (TRI Reagent)', *Cold Spring Harbor Protocols*, 2010(6), p. pdb.prot5439. doi: 10.1101/pdb.prot5439.
- Rocha, D. J. P., Santos, C. S. and Pacheco, L. G. C. (2015) 'Bacterial reference genes for gene expression studies by RT-qPCR: survey and analysis', *Antonie van Leeuwenhoek, International Journal of General and Molecular Microbiology*, 108(3), pp. 685–693. doi: 10.1007/s10482-015-0524-1.
- Ronneau, S. and Hallez, R. (2019) 'Make and break the alarmone: Regulation of (p)ppGpp synthetase/hydrolase enzymes in bacteria', *FEMS Microbiology Reviews*, 43(4), pp. 389–400. doi: 10.1093/femsre/fuz009.
- Sahni, J., Talegaonkar, S., Tariq, M., Ahmad, Z., Ali, J., Baboota, S. and Iqbal, Z. (2012) 'Treatment modalities and evaluation models for periodontitis', *International Journal of Pharmaceutical Investigation*, 2(3), p. 106. doi: 10.4103/2230-973x.104394.
- Sanders, B.E., Umana, A., Lemkul, J.A., Slade, D.J. (2018) 'FusoPortal: an Interactive Repository of Hybrid MinION-Sequenced Fusobacterium Genomes Improves Gene Identification and Characterization', *mSphere*, 3 (4), e00228–18. doi: 10.1128/mSphere.00228-18
- Sherry, L., Lappin, G., O'Donnell, L. E., Millhouse, E., Millington, O. R., Bradshaw, D. J., Axe, A. S., Williams, C., Nile, C. J. and Ramage, G. (2016) 'Viable compositional analysis of an eleven species oral polymicrobial biofilm', *Frontiers in Microbiology*, 7(JUN), pp. 1–13. doi: 10.3389/fmicb.2016.00912.
- Signat, B., Roques, C., Poulet, P. and Duffaut, D. (2011) 'Role of *Fusobacterium nucleatum* in periodontal health and disease', *Current Issues in Molecular Biology*, 13(2), pp. 25–36. doi: 10.21775/cimb.013.025.
- Stead, M. B., Agrawal, A., Bowden, K. E., Nasir, R., Mohanty, B. K., Meagher, R. B. and Kushner, S. R. (2012) 'RNA snap™: a rapid, quantitative and inexpensive, method for isolating total RNA from bacteria', *Nucleic Acids Research*, 40(20), pp. e156–e156. doi: 10.1093/nar/gks680.
- Stewart, P. S. (2003) 'Diffusion in biofilms', *Journal of Bacteriology*, 185(5), pp. 1485–1491. doi: 10.1128/JB.185.5.1485-1491.2003.
- Stiefel, P., Mauerhofer, S., Schneider, J., Maniura-Weber, K., Rosenberg, U. and Ren, Q. (2016) 'Enzymes enhance biofilm removal efficiency of cleaners', *Antimicrobial Agents and Chemotherapy*, 60(6), pp. 3647–3652. doi: 10.1128/AAC.00400-16.
- Subbarao, K., Nattuthurai, G., Sundararajan, S., Sujith, I., Joseph, J. and Syedshah, Y. (2019) 'Gingival crevicular fluid: An overview', *Journal of Pharmacy and Bioallied Sciences*, 11(Suppl 2), pp. S135–S139. doi: 10.4103/JPBS.JPBS\_56\_19.

'Subgingival Microbes' (2015) in *Atlas of Oral Microbiology*. Elsevier, pp. 67–93. doi: 10.1016/b978-0-12-802234-4.00004-5.

Sun, J., Daniel, R., Wagner-Döbler, I. and Zeng, A. P. (2004) 'Is autoinducer-2 a universal signal for interspecies communication: A comparative genomic and phylogenetic analysis of the synthesis and signal transduction pathways', *BMC Evolutionary Biology*, 4, p. 36. doi: 10.1186/1471-2148-4-36.

Tan, S. C. and Yiap, B. C. (2009) 'DNA, RNA, and protein extraction: The past and the present', *Journal of Biomedicine and Biotechnology*, 2009. doi: 10.1155/2009/574398.

Thairu, Y., Usman, Y. and Nasir, I. (2014) 'Laboratory perspective of gram staining and its significance in investigations of infectious diseases', *Sub-Saharan African Journal of Medicine*, 1(4), p. 168. doi: 10.4103/2384-5147.144725.

Thurnheer, T., Karygianni, L., Flury, M. and Belibasakis, G. N. (2019) '*Fusobacterium* Species and Subspecies Differentially Affect the Composition and Architecture of Supra- and Subgingival Biofilms Models', *Frontiers in Microbiology*, 10(July). doi: 10.3389/fmicb.2019.01716.

Todd, S. M., Settlege, R. E., Lahmers, K. K. and Slade, D. J. (2018) '*Fusobacterium* Genomics Using MinION and Illumina Sequencing Enables Genome Completion and Correction', *mSphere*, 3(4), pp. 1–9. doi: 10.1128/msphere.00269-18.

Umana, A., Sanders, B. E., Yoo, C. C., Casasanta, M. A., Udayasuryan, B., Verbridge, S. S. and Slade, D. J. (2019) 'Reevaluating the *Fusobacterium* Virulence Factor Landscape', *bioRxiv*, p. 534297. doi: 10.1101/534297.

Vashist, S. K. and Luong, J. H. T. (2018) 'Bioanalytical Requirements and Regulatory Guidelines for Immunoassays', in *Handbook of Immunoassay Technologies*. Elsevier, pp. 81–95. doi: 10.1016/b978-0-12-811762-0.00004-9.

Verbeke, F., De Craemer, S., Debunne, N., Janssens, Y., Wynendaele, E., Van de Wiele, C. and De Spiegeleer, B. (2017) 'Peptides as quorum sensing molecules: Measurement techniques and obtained levels in vitro and in vivo', *Frontiers in Neuroscience*, 11, p. 183. doi: 10.3389/fnins.2017.00183.

De Vos, W. M. (2015) 'Microbial biofilms and the human intestinal microbiome', *npj Biofilms and Microbiomes*, 1, p. 15005. doi: 10.1038/npjbiofilms.2015.5.

Wang, C., Sinn, M., Stifel, J., Heiler, A. C., Sommershof, A. and Hartig, J. S. (2017) 'Synthesis of All Possible Canonical (3'-5'-Linked) Cyclic Dinucleotides and Evaluation of Riboswitch Interactions and Immune-Stimulatory Effects', *Journal of the American Chemical Society*, 139(45), pp. 16154–16160. doi: 10.1021/jacs.7b06141.

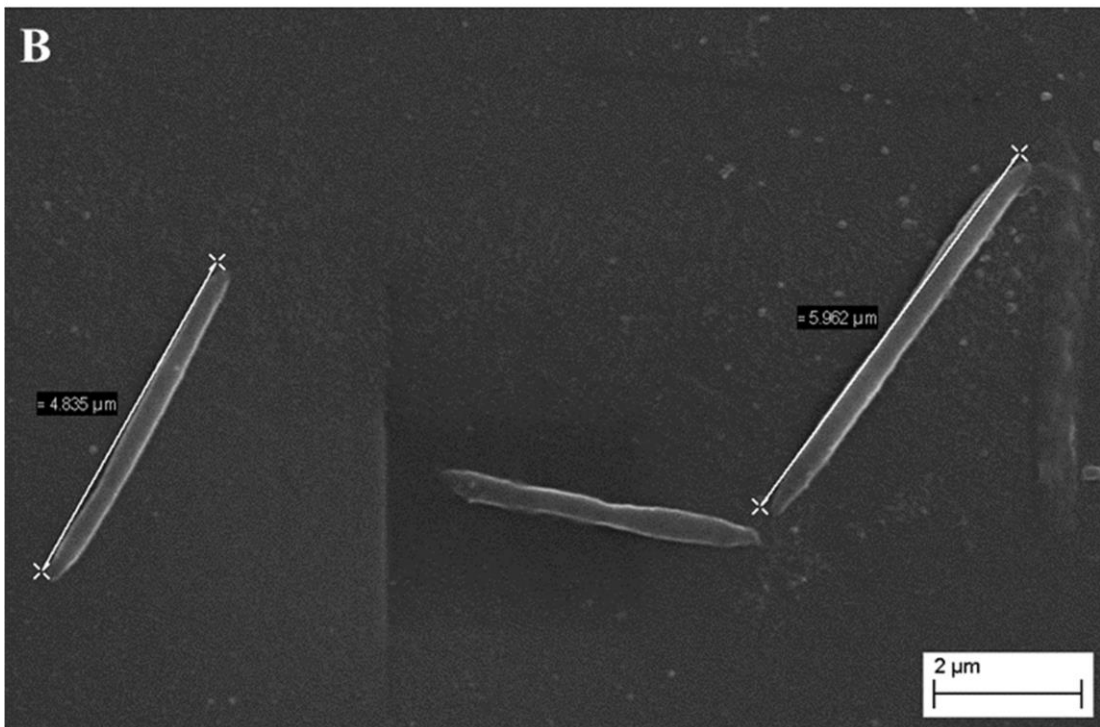
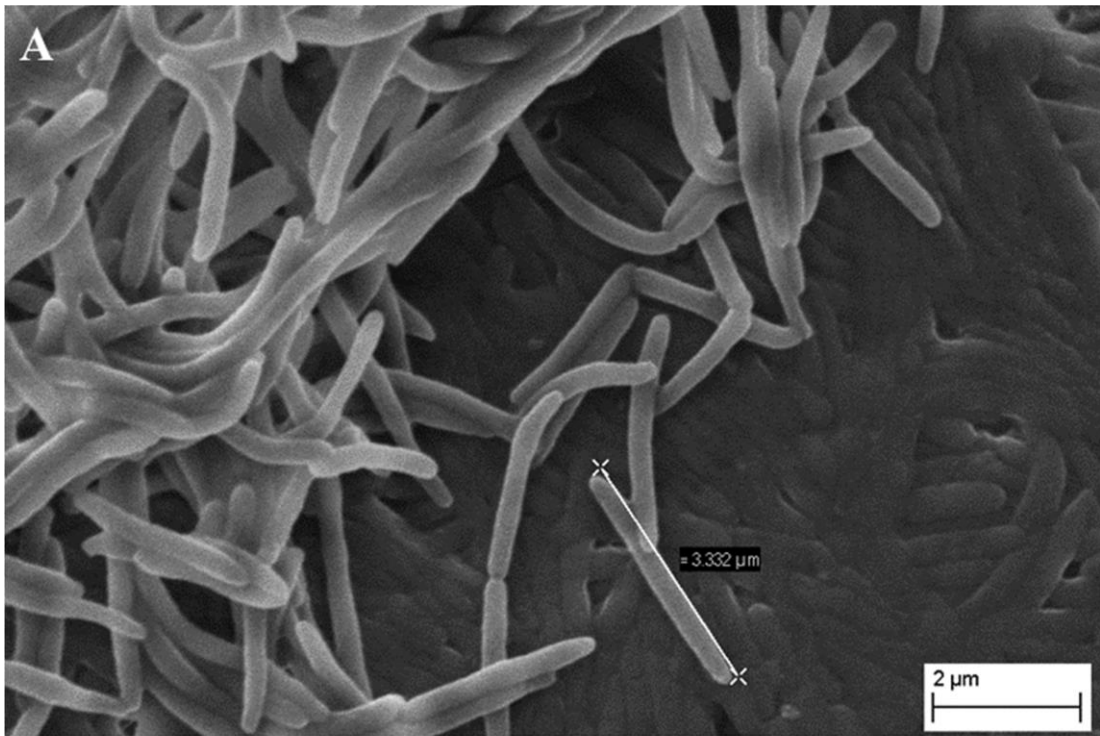
Wu, C., Amar Mohamed Al Mamun, A., Thanh Luong, T., Hu, B., Gu, J., Huck Lee, J., Das, A., Ton-That, H., Wu, C. C. and Mamun AAM, A. (2018) 'Forward Genetic Dissection of Biofilm Development by *Fusobacterium nucleatum*: Novel Functions of Cell Division Proteins FtsX and EnvC', *mBio*, 9(2). doi: 10.1128/mBio.00360-18.

Zhou, Youlian, He, H., Xu, H., Li, Y., Li, Z., Du, Y., He, J., Zhou, Yongjian, Wang, H. and Nie, Y. (2016) 'Association of oncogenic bacteria with colorectal cancer in South China', *Oncotarget*, 7(49), pp. 80794–80802. doi: 10.18632/oncotarget.13094.

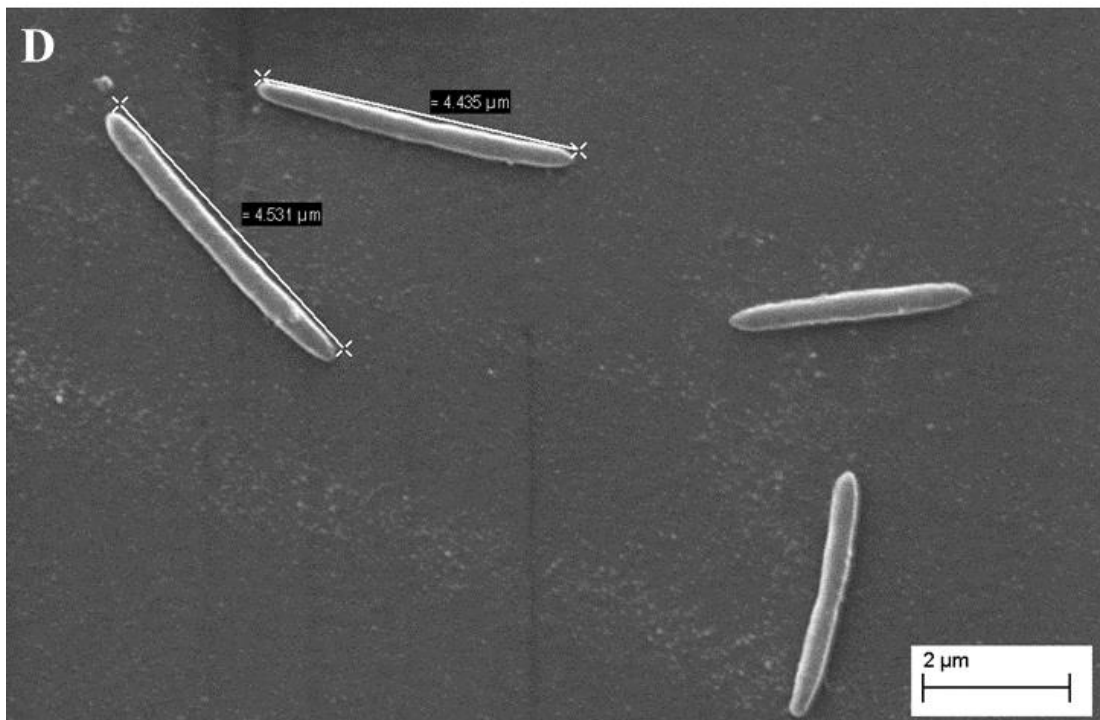
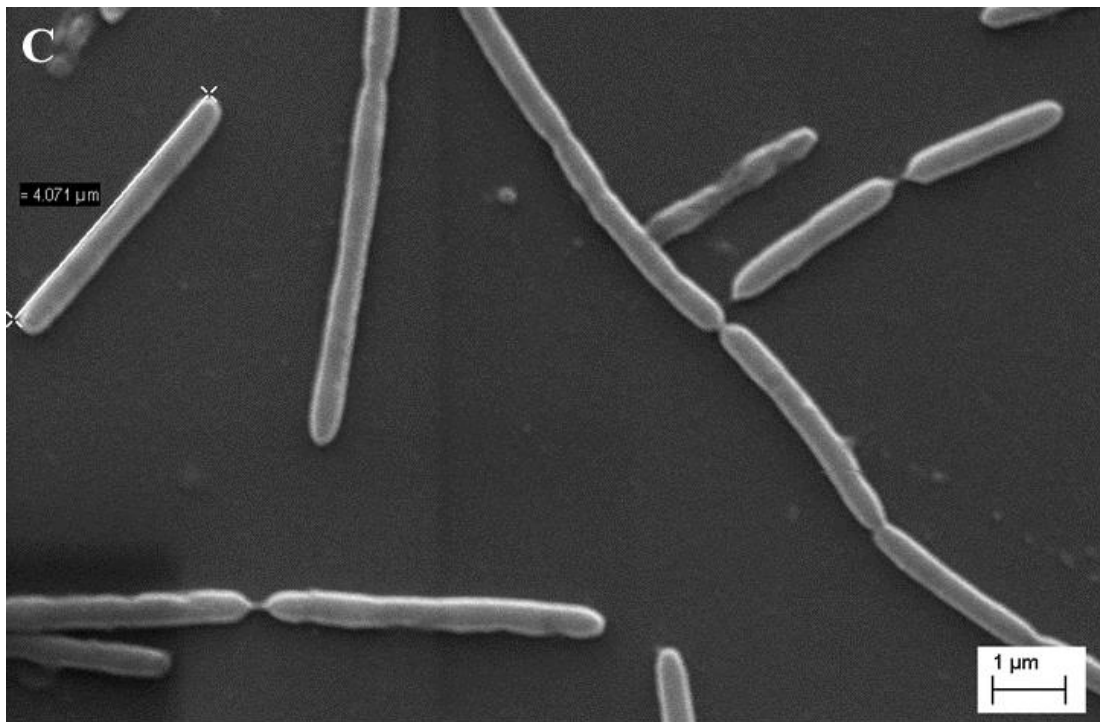
## **APPENDICES**

## **Appendix 1**

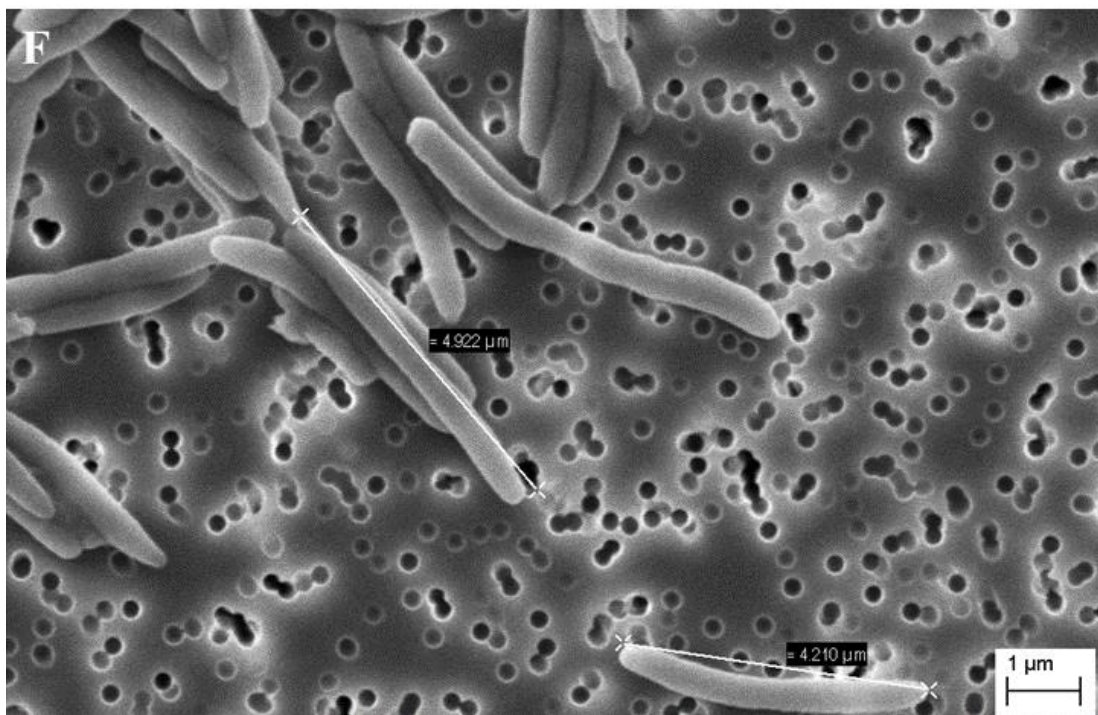
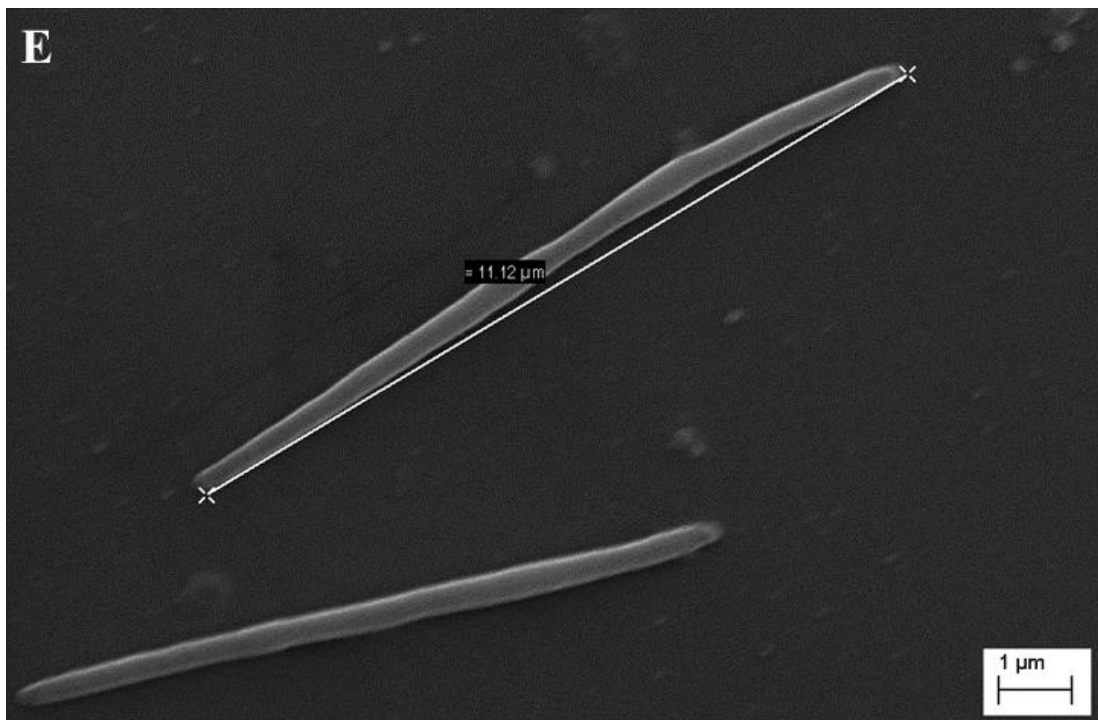
As a part of a detailed *F. nucleatum* subspecies characterisation, individual cells of each subspecies were visualised using SEM and Zeiss EVO MA 10 software was used to measure the length of individual cells. The micrographs attached below contain the lines which were drawn manually and the software calculated the resulting cell length. The measurement was performed at 20 000x magnification. For each measurement, ten cells were randomly selected from each subspecies.



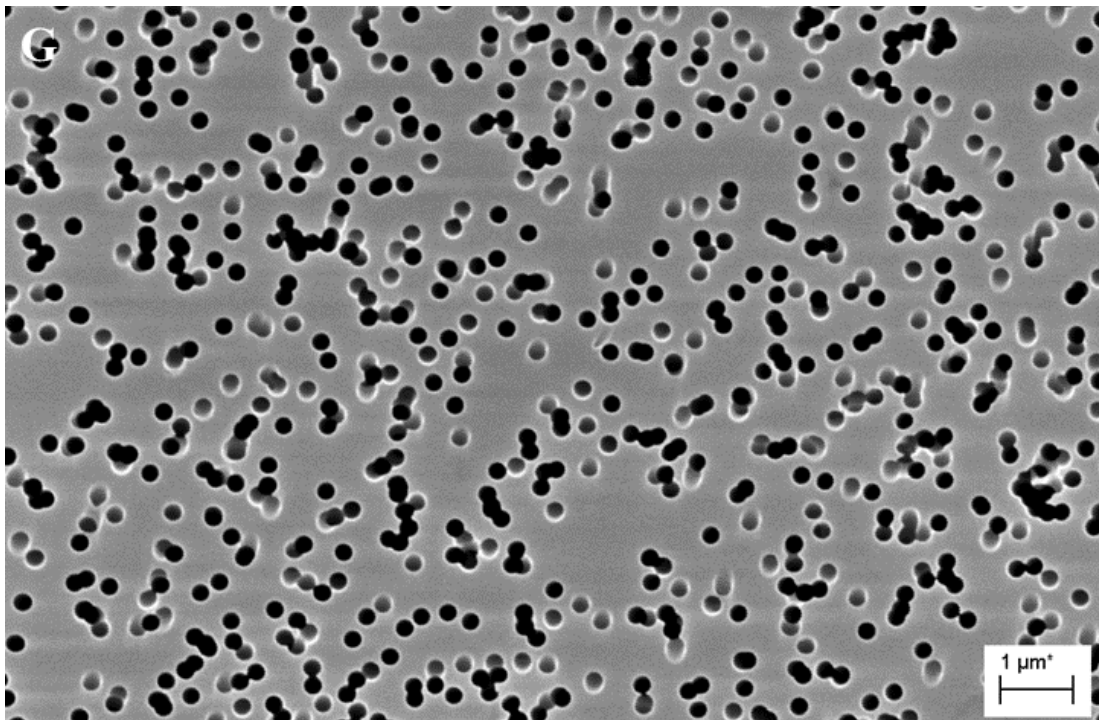
**Appendix 1. Scanning electron micrographs of all *F. nucleatum* subspecies.** Micrographs showing individual bacterial cells with the corresponding lines drawn when measuring the size of the cells. A – FNA, B – FNF. Magnification 20 000x.



**Appendix 1. Scanning electron micrographs of all *F. nucleatum* subspecies (continued).** Micrographs showing individual bacterial cells with the corresponding lines drawn when measuring the size of the cells. C – FNN 23726, D – FNN 25586. Magnification 20 000x.



**Appendix 1. Scanning electron micrographs of *F. nucleatum* subspecies (continued).** Micrographs showing individual bacterial cells with the corresponding lines drawn when measuring the size of the cells. E – FNP, F – FNV. Magnification 20 000x.



**Appendix 1. Scanning electron micrographs of *F. nucleatum* subspecies (continued).** Micrographs showing individual bacterial cells with the corresponding lines drawn when measuring the size of the cells. G – Isopore™ membrane only. Magnification 20 000x.

## **Appendix 2**

*F. nucleatum* subspecies were grown in oxic conditions in order to find out whether this bacterium is an obligate or a facultative anaerobe. Individual sub-cultures were incubated with a loose lid in a shaking incubator and the viable cell count showed that all the subspecies were viable for at least eight hours. The subspecies were statistically analysed at each time point to find the statistical significance among them. A detailed table of the statistical results can be found on the next page.

<b>Kruskal-Wallis test T0</b>
0.012

<b>Mann-Whitney test T0</b>	FNA	FNF	FNN23	FNN25	FNP	FNV
FNA	x	0.050	0.050	0.127	0.275	0.083
FNF		x	0.050	0.050	0.050	0.083
FNN23			x	0.050	0.050	0.083
FNN25				x	0.050	1.000
FNP					x	0.083
FNV						x

Legend for colour-coding	non-significant
	significant

<b>Kruskal-Wallis test T2</b>
0.072

<b>Mann-Whitney test T2</b>	FNA	FNF	FNN23	FNN25	FNP	FNV
FNA	x	0.050	0.275	0.513	0.513	0.248
FNF		x	0.050	0.050	0.050	0.083
FNN23			x	0.184	0.513	0.083
FNN25				x	0.275	0.564
FNP					x	0.248
FNV						x

<b>Kruskal-Wallis test T4</b>
0.085

<b>Mann-Whitney test T4</b>	FNA	FNF	FNN23	FNN25	FNP	FNV
FNA	x	0.050	0.513	0.127	0.275	0.564
FNF		x	0.050	0.050	0.050	1.000
FNN23			x	0.127	0.275	0.564
FNN25				x	0.513	0.083
FNP					x	0.374
FNV						x

<b>Kruskal-Wallis test T6</b>
0.036

<b>Mann-Whitney test T6</b>	FNA	FNF	FNN23	FNN25	FNP	FNV
FNA	x	0.046	0.827	0.050	0.127	0.248
FNF		x	0.046	0.046	0.046	0.076
FNN23			x	0.050	0.127	0.248
FNN25				x	0.513	0.564
FNP					x	1.000
FNV						x

<b>Kruskal-Wallis test T8</b>
0.037

<b>Mann-Whitney test T8</b>	FNA	FNF	FNN23	FNN25	FNP	FNV
FNA	x	0.050	0.513	0.050	0.127	0.248
FNF		x	0.050	0.050	0.050	0.083
FNN23			x	0.050	0.184	0.248
FNN25				x	0.513	0.248
FNP					x	0.564
FNV						x

**Appendix 2. Statistical analysis of growth profiles of *F. nucleatum* subspecies grown in oxidic conditions.** The remaining time points and the legend continued on the next page.

<b>Kruskal-Wallis test T24</b>
0.015

<b>Mann-Whitney test T24</b>	FNA	FNF	FNN23	FNN25	FNP	FNV
FNA	x	1.000	1.000	0.037	0.317	0.053
FNF		x	1.000	0.037	0.317	0.053
FNN23			x	0.037	0.317	0.053
FNN25				x	0.046	0.083
FNP					x	0.236
FNV						x

<b>Kruskal-Wallis test T48</b>
1.000

<b>Mann-Whitney test T48</b>	FNA	FNF	FNN23	FNN25	FNP	FNV
FNA	x	1.000	1.000	1.000	1.000	1.000
FNF		x	1.000	1.000	1.000	1.000
FNN23			x	1.000	1.000	1.000
FNN25				x	1.000	1.000
FNP					x	1.000
FNV						x

**Appendix 2. Statistical analysis of growth profiles of *F. nucleatum* subspecies grown in oxic conditions (continued).** The data did not conform to a normal distribution, that is why the bacterial numbers in CFU/ml were analysed among groups (individual time points) using Kruskal-Wallis test. Mann-Whitney test was subsequently used to find the statistical significance between specific pairs of subspecies. The results were considered to be statistically significant if  $p \leq 0.050$ . Orange colour highlights non-significant results, blue colour highlights significance.

### **Appendix 3**

Differences between bacterial species and their subsequent classification have been studied using multiple approaches, from the oldest method of discerning bacterial species based on their morphology, to much more accurate proteomic and genomic approaches. One of the most recent genomic techniques for classification of bacteria is analysis of a highly conserved 16S rRNA gene sequence of bacteria (Kook *et al.*, 2017). In order to find the degree of similarity between *F. nucleatum* subspecies, complete sequences of the 16S rRNA gene from each subspecies were obtained from NCBI repository and were then analysed using the multiple sequence alignment tool Clustal Omega and the identity percentage was calculated (Table 3.1.). The complete sequence alignment can be found starting on the next page.

FNP	AAAGATTNAACGAAGAGTTTGATCCTGGCTCAGGATGAACGCTGACAGAATGCTTAACAC	60
FNF	AAAGATTGAACGAAGAGTTTGATCCTGGCTCAGGATGAACGCTGACAGAATGCTTAACAC	60
FNN	-----TTGATCTTGGCTCATGATGAACGCTGACAGAATGCTTAACAC	42
FNA	-----AGAGTTTGATCCTGGCTCAGGATGAACGCTGACAGAATGCTTAACAC	47
FNV	-----GAACGCTGACAGAATGCTTAACAC	24
	*****	
FNP	ATGCAAGTCAACTTGAA-----CTTCGGTTTGGGTGGCGGACGGGTGAGTA	106
FNF	ATGCAAGTCAACTTGAATTTGGGTT-TTTAACTTAGGTTTGGGTGGCGGACGGGTGAGTA	119
FNN	ATGCAAGTCAACTTGAATTTGGGTTTTTTAACTTCGATTTGGGTGGCGGACGGGTGAGTA	102
FNA	ATGCAAGTCAACTTGAATTTGGGTT-TTTAACTTAGATTTGGGTGGCGGACGGGTGAGTA	106
FNV	ATGCAAGTCAACTTGAATTTGGGTT-TTTAACTTAGGTTTGGGTGGCGGACGGGTGAGTA	83
	***** * *****	
FNP	ACGCGTAAAGAACTTGCCTCACAGATAGGGACAACATTTGGAAACGAATGCTAATACCTG	166
FNF	ACGCGTAAAGAACTTGCCTCACAGGTAGGGACAACATTTGGAAACGAATGCTAATACCTA	179
FNN	ACGCGTAAAGAACTTGCCTCACAGCTAGGGACAACATTTGGAAACGAATGCTAATACCTN	162
FNA	ACGCGTAAAGAACTTGCCTCACAGTTAGGGACAACATTTGAAATGAATGCTAATACCTG	166
FNV	ACGCGTAAAGAACTTGCCTCACAGTTAGGGACAACATTTGGAAACGAATGCTAATACCTA	143
	***** ***** * *****	
FNP	ATATTATGATTTTAGGGCATCTAGGATTATGAAAGCTATAATGCGCTGTGAGAGAGCTTT	226
FNF	ATATTATGATAATAGGGCATCTATAAATTATGAAAGCTATAAGCGCTGTGAGAGAGCTTT	239
FNN	ATATTATGATTTAGGGCATCTAGAATTATGAAAGCTATAATGCGCTGTGAGAGAGCTTT	222
FNA	ATATTATGATTTAAAGGCATCTTAGAATTATGAAAGCTATAAGCACTGTGAGAGAGCTTT	226
FNV	ATATTATGATAATAGGGCATCTATNATTATGAAAGCTATAAGCGCTGTGAGAGAGCTTT	203
	***** ** ***** ** ***** * *****	
FNP	GCGTCCCATTAGCTAGTTGGAGAGGTAACGGCTCACCAAGGCATGATGGGTAGCCGGCC	286
FNF	GCGTCCCATTAGCTAGTTGGAGAGGTAACGGCTCACCAAGGCATGATGGGTAGCCGGCC	299
FNN	GCGTCCCATTAGCTAGTTGGAGAGGTAACGGCTCACCAAGGCATGATGGGTAGCCGGCC	282
FNA	GCGTCCCATTAGCTAGTTGGAGAGGTAACGCTCACCAAGGCATGATGGGTAGCCGGCC	286
FNV	GCGTCCCATTAGCTAGTTGGAGAGGTAACGGCTCACCAAGGCATGATGGGTAGCCGGCC	263
	***** *****	
FNP	TGAGAGGGTGATCGGCCACAAGGGGACTGAGACACGGCCCTTACTCCTACGGGAGGCAGC	346
FNF	TGAGAGGGTGATCGGCCACAAGGGGACTGAGACACGGCCCTTACTCCTACGGGAGGCAGC	359
FNN	TGAGAGGGTGACCGGCCACAAGGGGACTGAGACACGGCCCTTACTCCTACGGGAGGCAGC	342
FNA	TGAGAGGGTGAAACCGGCCACAAGGGGACTGAGACACGGCCCTTACTCCTACGGGAGGCAGC	346
FNV	TGAGAGGGTGATCGGCCACAAGGGGACTGAGACACGGCCCTTACTCCTACGGGAGGCAGC	323
	***** *****	
FNP	AGTGGGGAATATTGGACAATGGACCAAGAGTCTGATCCAGCAATTCTGTGTGCACGATGA	406
FNF	AGTGGGGAATATTGGACAATGGACCGAGAGTCTGATCCAGCAATTCTGTGTGCACGATGA	419
FNN	AGTGGGGAATATTGGACAATGGACCGAGAGTCTGATCCAGCAATTCTGTGTGCACGATGA	402
FNA	AGTGGGGAATATTGGACAATGGACCGAGAGTCTGATCCAGCAATTCTGTGTGCACGATGA	406
FNV	AGTGGGGAATATTGGACAATGGACCAAGAGTCTGATCCAGCAATTCTGTGTGCACGATGA	383
	***** *****	
FNP	AGTTTTTCGGAATGTAAAGTGCTTTCAGTTGGGAAGAAAATAATGACGGTACCAACAGAA	466
FNF	AGTTTTTCGGAATGTAAAGTGCTTTCAGTTGGGAAGAAAATAATGACGGTACCAACAGAA	479
FNN	CGTTTTTCGGAATGTAAAGTGCTTTCAGTTGGGAAGAAAATAATGACGGTACCAACAGAA	462
FNA	AGTTTTTCGGAATGTAAAGTGCTTTCAGTTGGGAAGAAAATAATGACGGTACCAACAGAA	466
FNV	AGTTTTTCGGAATGTAAAGTGCTTTCAGTTGGGAAGAAAATAATGACGGTACCAACAGAA	443
	***** *****	
FNP	GAAGTGACGGCTAAATACGTGCCAGCAGCCGCGGTAATACGTATGTCACCAATGCGTTATC	526
FNF	GAAGTGACGGCTAAATACGTGCCAGCAGCCGCGGTAATACGTATGTCACCA-GCGTTATC	538
FNN	GAAGTGACGGCTAAATACGTGCCAGCAGCCGCGGTAATACGTATGTCACCA-GCGTTATC	521
FNA	GAAGTGACGGCTAAATACGTGCCAGCAGCCGCGGTAATACGTATGTCACCA-GCGTTATC	525
FNV	GAAGTGACGGCTAAATACGTGCCAGCAGCCGCGGTAATACGTATGTCACCA-GCGTTATC	502
	***** * *****	

**Appendix 3. Multiple sequence alignment of all 5 *F. nucleatum* subspecies.** The alignment continued on the next page.

FNP	CGGATTTATTGGGCGTAAAGCGCGTCTAGGTGGTTATNTAAGTCTGATGTGAAAAATGCAG	586
FNF	CGGATTTATTGGGCGTAAAGCGCGTCTAGGTGGTTATGTAAGTCTGATGTGAAAAATGCAG	598
FNN	CGGATTTATTGGGCGTAAAGCGCGTCTAGGTGGTTATGTAAGTCTGATGTGAAAAATGCAG	581
FNA	CGGATTTATTGGGCGTAAAGCGCGTCTAGGTGGTTATGTAAGTCTGATGTGAAAAATGCAG	585
FNV	CGGATTTATTGGGCGTAAAGCGCGTCTAGGTGGTTATGTAAGTCTGATGTGAAAAATGCAG *****	562
FNP	GGCTCAACTCTGTATTGCGTTGAAAACCTGTGTAAGTCTGATGTGAAAAATGCAG	646
FNF	GGCTCAACTCTGTATTGCGTTGAAAACCTGTGTAAGTCTGATGTGAAAAATGCAG	658
FNN	GGCTCAACTCTGTATTGCGTTGAAAACCTGTGTAAGTCTGATGTGAAAAATGCAG	641
FNA	GGCTCAACTCTGTATTGCGTTGAAAACCTGTGTAAGTCTGATGTGAAAAATGCAG	645
FNV	GGCTCAACTCTGTATTGCGTTGAAAACCTGTGTAAGTCTGATGTGAAAAATGCAG *****	622
FNP	CTACAAGTGTAGAGGTGAAATTCGTAGATATTTGTAGGAATGCCGATGGGGAAGCCAGCT	706
FNF	CTACAAGTGTAGAGGTGAAATTCGTAGATATTTGTAGGAATGCCGATGGGGAAGCCAGCT	718
FNN	CTACAAGTGTAGAGGTGAAATTCGTAGATATTTGTAGGAATGCCGATGGGGAAGCCAGCT	701
FNA	CTACAAGTGTAGAGGTGAAATTCGTAGATATTTGTAGGAATGCCGATGGGGAAGCCAGCT	705
FNV	CTACAAGTGTAGAGGTGAAATTCGTAGATATTTGTAGGAATGCCGATGGGGAAGCCAGCT *****	682
FNP	TACTGGACAGATACTGACGCTGAAGCGCGAAAGCGTGGGTAGCAAACAGGATTAGATAACC	766
FNF	TACTGGACAGATACTGACGCTGAAGCGCGAAAGCGTGGGTAGCAAACAGGATTAGATAACC	778
FNN	TACTGGACAGATACTGACGCTGAAGCGCGAAAGCGTGGGTAGCAAACAGGATTAGATAACC	761
FNA	TACTGGACAGATACTGACGCTGAAGCGCGAAAGCGTGGGTAGCAAACAGGATTAGATAACC	765
FNV	TACTGGACAGATACTGACGCTGAAGCGCGAAAGCGTGGGTAGCAAACAGGATTAGATAACC *****	742
FNP	CTGGTAGTCCACGCCGTAACGATGATTACTAGGTGTTGGGGTTCGAACCTCAGCGCCCA	826
FNF	CTGGTAGTCCACGCCGTAACGATGATTACTAGGTGTTGGGGTTCGAACCTCAGCGCCCA	838
FNN	CTGGTAGTCCACGCCGTAACGATGATTACTAGGTGTTGGGGTTCGAACCTCAGCGCCCA	821
FNA	CTGGTAGTCCACGCCGTAACGATGATTACTAGGTGTTGGGGTTCGAACCTCAGCGCCCA	825
FNV	CTGGTAGTCCACGCCGTAACGATGATTACTAGGTGTTGGGGTTCGAACCTCAGCGCCCA *****	802
FNP	AGCAAACCGGATAAGTAATCCGCCTGGGGAGTACGTACGCAAGTATGAAACTCAAAGGAA	886
FNF	AGCAAACCGGATAAGTAATCCGCCTGGGGAGTACGTACGCAAGTATGAAACTCAAAGGAA	898
FNN	AGCAAACCGGATAAGTAATCCGCCTGGGGAGTACGTACGCAAGTATGAAACTCAAAGGAA	881
FNA	AGCAAACCGGATAAGTAATCCGCCTGGGGAGTACGTACGCAAGTATGAAACTCAAAGGAA	885
FNV	AGCAAACCGGATAAGTAATCCGCCTGGGGAGTACGTACGCAAGTATGAAACTCAAAGGAA *****	862
FNP	TTGACGGGGACCCGCACAAGCGGTGGAGCATGTGGTTTAATTCGACGCAACGCGAGGAAC	946
FNF	TTGACGGGGACCCGCACAAGCGGTGGAGCATGTGGTTTAATTCGACGCAACGCGAGGAAC	958
FNN	TTGACGGGGACCCGCACAAGCGGTGGAGCATGTGGTTTAATTCGACGCAACGCGAGGAAC	941
FNA	TTGACGGGGACCCGCACAAGCGGTGGAGCATGTGGTTTAATTCGACGCAACGCGAGGAAC	945
FNV	TTGACGGGGACCCGCACAAGCGGTGGAGCATGTGGTTTAATTCGACGCAACGCGAGGAAC *****	922
FNP	CTTACCAGCGTTTGACATCTTAGGAATGAGACAGAGATGTTTCAGTGTCCCTTCGGGGAA	1006
FNF	CTTACCAGCGTTTGACATCTTAGGAATGAGACAGAGATGTTTCAGTGTCCCTTCGGGGAA	1018
FNN	CTTACCAGCGTTTGACATCTTAGGAATGAGACAGAGATGTTTCAGTGTCCCTTCGGGGAA	1001
FNA	CTTACCAGCGTTTGACATCTTAGGAATGAGACAGAGATGTTTCAGTGTCCCTTCGGGGAA	1005
FNV	CTTACCAGCGTTTGACATCTTAGGAATGAGACAGAGATGTTTCAGTGTCCCTTCGGGGAA *****	982
FNP	ACCTAAAGACAGGTGGTGCATGGCTGTCGTGAGATGTTGGGTTAAGT	1066
FNF	ACCTAAAGACAGGTGGTGCATGGCTGTCGTGAGATGTTGGGTTAAGT	1078
FNN	ACCTAAAGACAGGTGGTGCATGGCTGTCGTGAGATGTTGGGTTAAGT	1061
FNA	ACCTAAAGACAGGTGGTGCATGGCTGTCGTGAGATGTTGGGTTAAGT	1065
FNV	ACCTAAAGACAGGTGGTGCATGGCTGTCGTGAGATGTTGGGTTAAGT *****	1042

**Appendix 3. Multiple sequence alignment of all 5 *F. nucleatum* subspecies (continued).**  
The alignment continued on the next page.

FNP	CCCGCAACGAGCGCAACCCCTTTCGTATGTTACCATCATTAAGTTGGGGACTCATGCGAT	1126
FNF	CCCGCAACGAGCGCAACCCCTTTCGTATGTTACCATCATTAAGTTGGGGACTCATGCGAT	1138
FNN	CCCGCAACGAGCGCAACCCCTTTCGTATGTTACCATCATTAAGTTGGGGACTCATGCGAT	1121
FNA	CCCGCAACGAGCGCAACCCCTTTCGTATGTTACCATCATTAAGTTGGGGACTCATGCGAT	1125
FNV	CCCGCAACGAGCGCAACCCCTTTCGTATGTTACCATCATTAAGTTGGGGACTCATGCGAT	1102
	*****	
FNP	ACTGCCTCGATGAGCAGGAGGAAGGTGGGGATGACGTCAAGTCATCATGCCCTTATAC	1186
FNF	ACTGCCTACGATGAGTAGGAGGAAGGTGGGGATGACGTCAAGTCATCATGCCCTTATAC	1198
FNN	ACTGCCTACGATGAGTAGGAGGAAGGTGGGGATGACGTCAAGTCATCATGCCCTTATAC	1181
FNA	ACTGCCTACGATGAGTAGGAGGAAGGTGGGGATGACGTCAAGTCATCATGCCCTTATAC	1185
FNV	ACTGCCTACGATGAGTAGGAGGAAGGTGGGGATGACGTCAAGTCATCATGCCCTTATAC	1162
	*****	
FNP	GCTGGGCTACACACGTGCTACAATGGGTAGTACAGAGAGTGCCAAAGCCGTGAGGTGGAG	1246
FNF	GCTGGGCTACACACGTGCTACAATGGGTAGAACAGAGAGTGCCAAAGCTGTGAAGTGGAG	1258
FNN	GCTGGGCTACACACGTGCTACAATGGGTAGAACAGAGAGTGCCAAAGCCGTGAGGTGGAG	1241
FNA	GCTGGGCTACACACGTGCTACAATGGGTAGAACAGAGAGTGCCAAAGCCGTGAGGTGAAG	1245
FNV	GCTGGGCTACACACGTGCTACAATGGGTAGAACAGAGAGTGCCAAAGCTGTGAAGTGGAG	1222
	*****	
FNP	CTAATCTCAGAAAACCTATTCTTAGTTCGGATTGTACTCTGCAACTCGAGTACATGA-AGT	1305
FNF	CTAATCTCAGAAAACCTATTCTTAGTTCGGATTGTACTCTGCAACTCGAGTAACATGAAGT	1318
FNN	CTAATCTCAGAAAACCTATTCTTAGTTCGGATTGTACTCTGCAACTCGAGTA-CATGAAGT	1300
FNA	CTAATCTCAGAAAACCTATTCTTAGTTCGGATTGTACTCTGCAACTCGAGTA-CATGAAGT	1304
FNV	CTAATCTCAGAAAACCTATTCTTAGTTCGGATTGTACTCTGCAACTCGAGTA-CATGAAGT	1281
	*****	
FNP	TGGAATCGCTA-----GTAATGTCGCGGTGAATACGTTCTCGGGTCTTGTA	1351
FNF	TGGAATCGCTAGTAATCGCGAATCAGCAATGTCGCGGTGAATACGTTCTCGGGTCTTGTA	1378
FNN	TGGAATCGCTAGTAATCGCGAATCAGCAATGTCGCGGTGAATACGTTCTCGGGTCTTGTA	1360
FNA	TGGAATCGCTAGTAATCGCGAATCAGCAATGTCGCGGTGAATACGTTCTCGGGTCTTGTA	1364
FNV	TGGAATCGCTAGTAATCGCGAATCAGCAATGTCGCGGTGAATACGTTCTCGGGTCTTGTA	1341
	*****	
FNP	CACACCGCCCGTCACACCACANNANTAT-----	1380
FNF	CACACCGCCCGTCACACCACAA-----	1400
FNN	CACACCGCCCGTCACACCACGAGAGTTGGTTGCACCTGAAG-TAGCAGGCCTAACCGTAA	1419
FNA	CACACCGCCCGTCACACCACGAGAGTTGGTTGCACCTGAAG-TAGCAGGCCTAACCGTAA	1423
FNV	CACACCGCCCGTCACACCACGAGAGTTGGTTGCACCNTGAAGTAGCAGGCCTAACCGTAA	1401
	*****	
FNP	-----	1380
FNF	-----	1400
FNN	GGAGGGATGTTCCGAGGGTGTGATTAGCGATTGGGGTGAAGTCGTAACAAGGTAGCCGTA	1479
FNA	GGAGGGATGTTCCGAGGGTGTGATTAGCGATTGGGGTGAAGTCGTAACAAGGTAAACC---	1480
FNV	GGAGG-----	1406

### Appendix 3. Multiple sequence alignment of all 5 *F. nucleatum* subspecies (continued).

The order of the subspecies follows the order created by Clustal Omega, online tool generating sequence alignments. The alignment shows a very high level of sequence similarity. The sites with differing nucleotide bases are highlighted in yellow, identity of bases is shown by asterisks (\*) and the columns in which the only differing base is N (undetermined) are highlighted in blue. Gaps in the sequences are shown by a dash (-).

## **Appendix 4**

Mono-species biofilms were grown for three, five and seven days and the biomass formed was subsequently quantified with Crystal violet stain. Statistical analysis was performed in order to find the differences in the biofilm formation of the subspecies at these three time points. A detailed table of results can be found on the next page.

Legend for colour-coding	non-significant
	significant

<b>Kruskal-Wallis test</b>
0.002

<b>Mann-Whitney test</b>	<b>SS 3 days</b>	<b>SS 5 days</b>	<b>SS 7 days</b>
SS 3 days	x	0.009	0.009
SS 5 days		x	0.016
SS 7 days			x

<b>Kruskal-Wallis test</b>
0.014

<b>Mann-Whitney test</b>	<b>FNA 3 days</b>	<b>FNA 5 days</b>	<b>FNA 7 days</b>
FNA 3 days	x	0.009	0.175
FNA 5 days		x	0.047
FNA 7 days			x

<b>Kruskal-Wallis test</b>
0.004

<b>Mann-Whitney test</b>	<b>FNF 3 days</b>	<b>FNF 5 days</b>	<b>FNF 7 days</b>
FNF 3 days	x	0.009	0.076
FNF 5 days		x	0.009
FNF 7 days			x

<b>Kruskal-Wallis test</b>
0.009

<b>Mann-Whitney test</b>	<b>FNN23 3 days</b>	<b>FNN23 5 days</b>	<b>FNN23 7 days</b>
FNN23 3 days	x	0.009	0.009
FNN23 5 days		x	0.754
FNN23 7 days			x

<b>Kruskal-Wallis test</b>
0.006

<b>Mann-Whitney test</b>	<b>FNN25 3</b>	<b>FNN25 5 days</b>	<b>FNN25 7 days</b>
FNN25 3	x	0.175	0.009
FNN25 5 days		x	0.009
FNN25 7 days			x

<b>Kruskal-Wallis test</b>
0.004

<b>Mann-Whitney test</b>	<b>FNP 3 days</b>	<b>FNP 5 days</b>	<b>FNP 7 days</b>
FNP 3 days	x	0.009	0.009
FNP 5 days		x	0.076
FNP 7 days			x

<b>Kruskal-Wallis test</b>
0.009

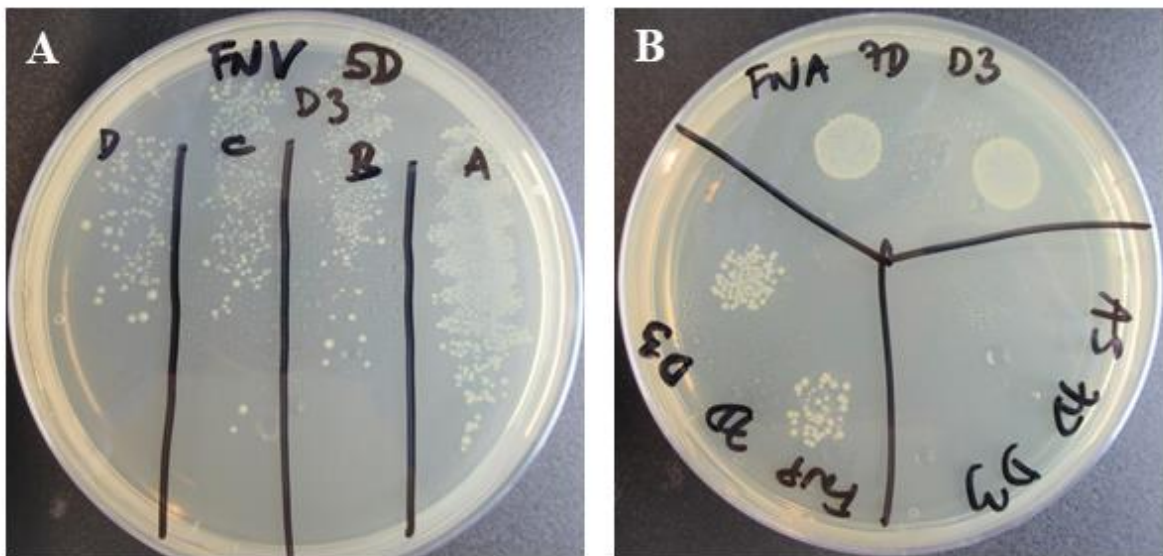
<b>Mann-Whitney test</b>	<b>FNV 3 days</b>	<b>FNV 5 days</b>	<b>FNV 7 days</b>
FNV 3 days	x	0.009	0.009
FNV 5 days		x	0.602
FNV 7 days			x

#### Appendix 4. Statistical analysis of the amount of biofilm formed by individual subspecies.

The data did not conform to a normal distribution. Individual groups were analysed using Kruskal-Wallis test first to find the overall significance within each species. When the significance was confirmed, the Mann-Whitney test was performed comparing specific pairs of time points as shown in the tables. The results were considered to be statistically significant if  $p \leq 0.050$ . Orange colour highlights non-significant results, blue colour highlights significance.

## Appendix 5

Mono-species biofilms grown for Crystal violet biomass quantification and the SEM were regularly checked for contaminants. Because the plates were handled every day in order to change the AS, there was a possibility of introducing contamination. In order to make sure that the biofilms were free of contaminants, each well with the biofilms incubated for the SEM was tested by streaking the supernatant on SAA (Appendix 5A). To confirm that the biofilms incubated for the Crystal violet biomass quantification were not contaminated, 20  $\mu$ l of the supernatant from two wells was spotted on SAA and incubated (Appendix 5B). The growth on the plates was then Gram-stained and confirmed to contain only *F. nucleatum* cells. The plates below are an example of the contamination check.



**Appendix 5. Contamination check of mono-species biofilms.** A) SAA plate with a contamination check of mono-species biofilms grown for the SEM. A loopful of supernatant was streaked on the agar and incubated. B) SAA plate with a contamination check of mono-species biofilms grown for the Crystal violet biomass quantification. 20  $\mu$ l of the supernatant was spotted on the agar. “FNA” and “FNP” show the contamination check of the biofilms, “AS” is the contamination check of the AS from the bacteria-free wells. The colony morphology and the Gram-stains of bacteria were analysed to confirm the absence of contaminants.

## **Appendix 6**

The amount of biofilm formed in the mono-species biofilms that were grown for three, five and seven days was not only analysed over time, as it was shown in Appendix 4. The biomass was also statistically analysed at individual time points and the biofilm formation of all subspecies was taken into consideration. A detailed table of the statistical results can be found overleaf.

<b>Kruskal-Wallis test - 3 days</b>
0.000053

Legend for colour-coding	non-significant
	significant

Mann-Whitney test - 3 days	SS	FNA	FNF	FNN23	FNN25	FNP	FNV
SS	x	0.076	0.251	0.754	0.009	0.009	0.009
FNA		x	0.251	0.016	0.009	0.009	0.009
FNF			x	0.117	0.009	0.009	0.009
FNN23				x	0.009	0.009	0.009
FNN25					x	0.009	0.175
FNP						x	0.009
FNV							x

<b>Kruskal-Wallis test - 5 days</b>
0.000066

Mann-Whitney test - 5 days	SS	FNA	FNF	FNN23	FNN25	FNP	FNV
SS	x	0.009	0.076	0.047	0.009	0.009	0.047
FNA		x	0.009	0.009	0.009	0.009	0.016
FNF			x	1.000	0.009	0.009	0.347
FNN23				x	0.009	0.009	0.465
FNN25					x	0.347	0.009
FNP						x	0.009
FNV							x

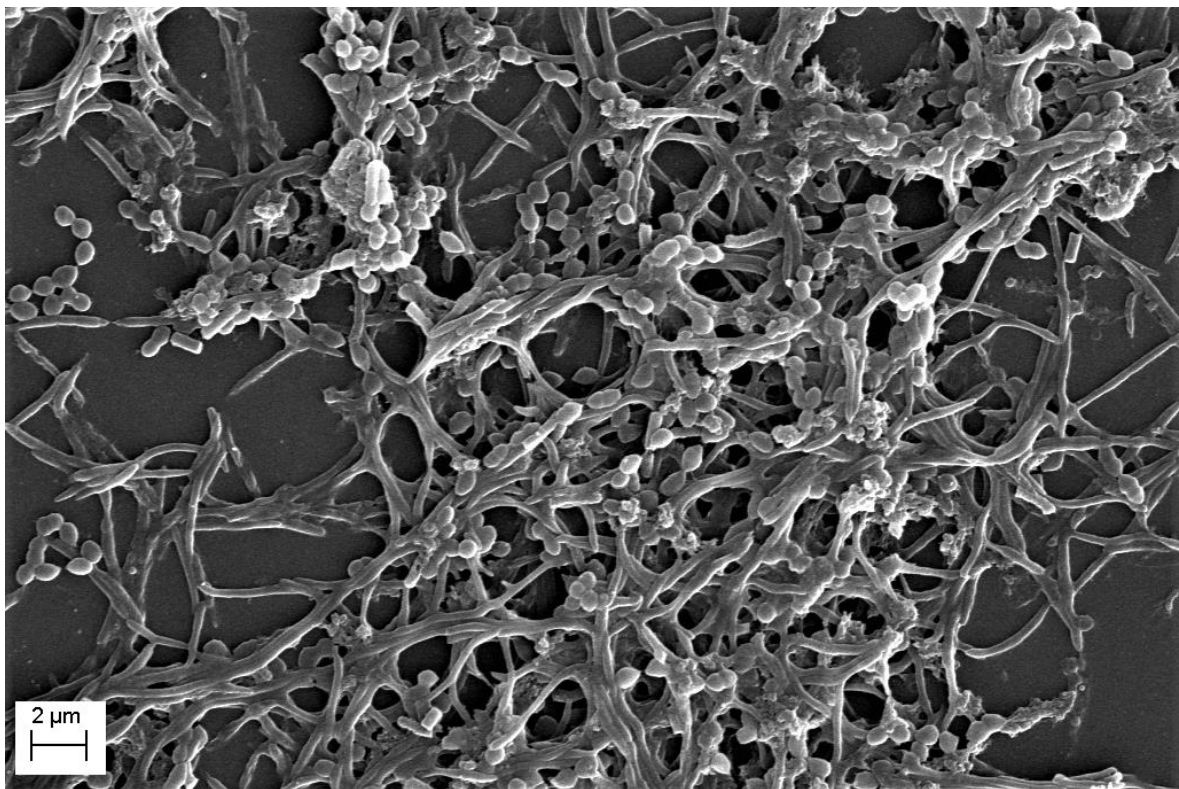
<b>Kruskal-Wallis test - 7 days</b>
0.00006

Mann-Whitney test - 7 days	SS	FNA	FNF	FNN23	FNN25	FNP	FNV
SS	x	0.009	0.009	0.009	0.009	0.009	0.028
FNA		x	0.028	0.009	0.009	0.465	0.009
FNF			x	0.009	0.075	0.076	0.016
FNN23				x	0.075	0.009	0.602
FNN25					x	0.009	0.346
FNP						x	0.009
FNV							x

**Appendix 6. Statistical analysis of the amount of biofilm formed by all subspecies at specific time points.** The data did not conform to a normal distribution therefore the individual groups were analysed using Kruskal-Wallis test and Mann-Whitney test. Data was considered statistically significant if  $p \leq 0.05$ . Orange colour highlights non-significant results, blue colour highlights significance.

## Appendix 7

All mono-species biofilms were monitored for contamination. In addition to plating the supernatant and the AS, contaminants could be detected when visualising the biofilms during the SEM. *F. nucleatum* has a specific morphology, which was confirmed during the early stages of the project. This made it easier to recognise the presence of the contaminants in biofilms. The micrograph below is an example of a contaminated experiment, clearly showing the presence of coccal contamination.

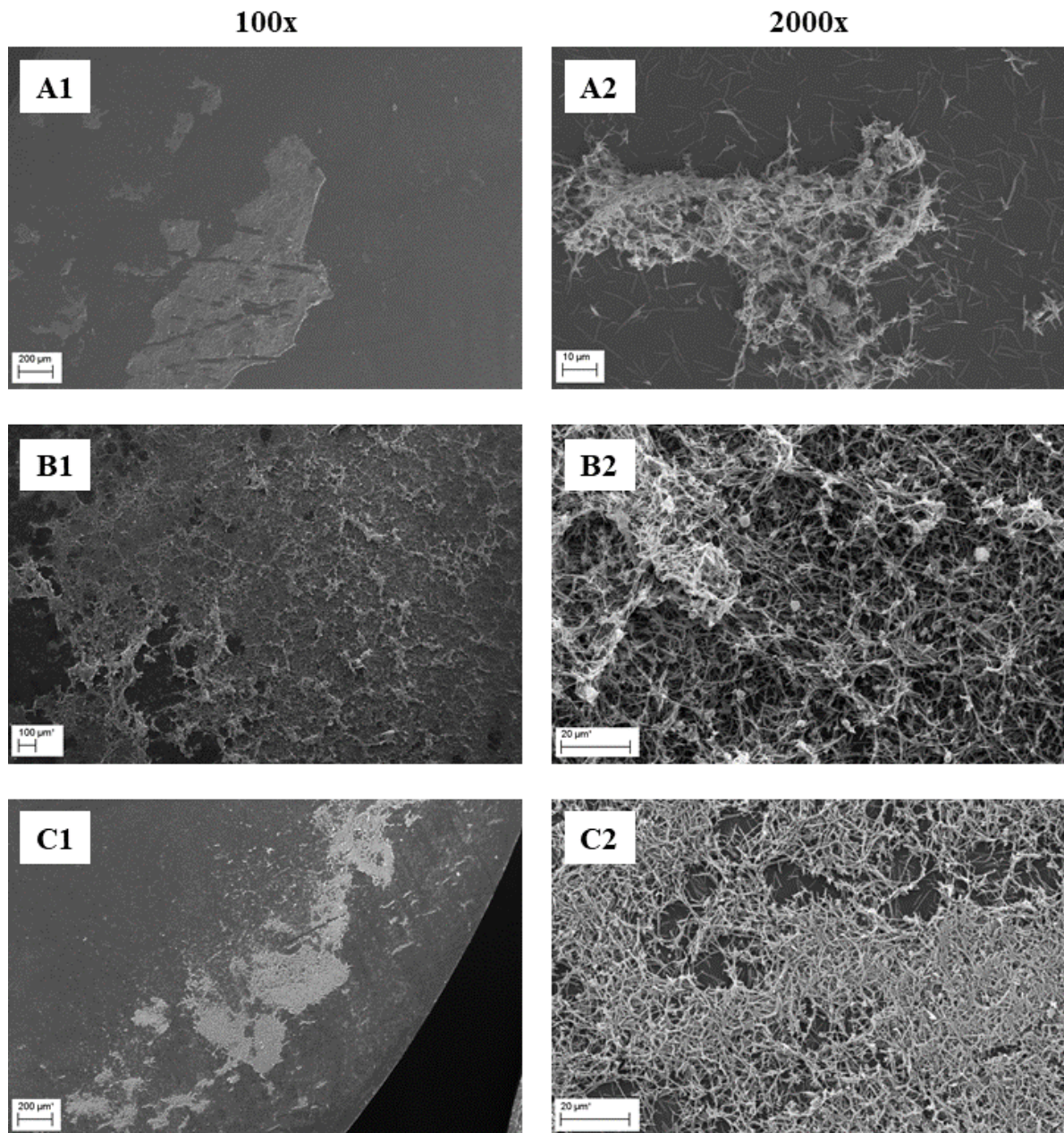


**Appendix 7. Micrograph of the mono-species biofilm obtained using SEM.** *F. nucleatum* ssp. *animalis* mono-species biofilm was grown for three days and was contaminated during the incubation. Coccal contamination is interspersed among FNA cells and can be clearly distinguished from FNA cells. Magnification 8000x.

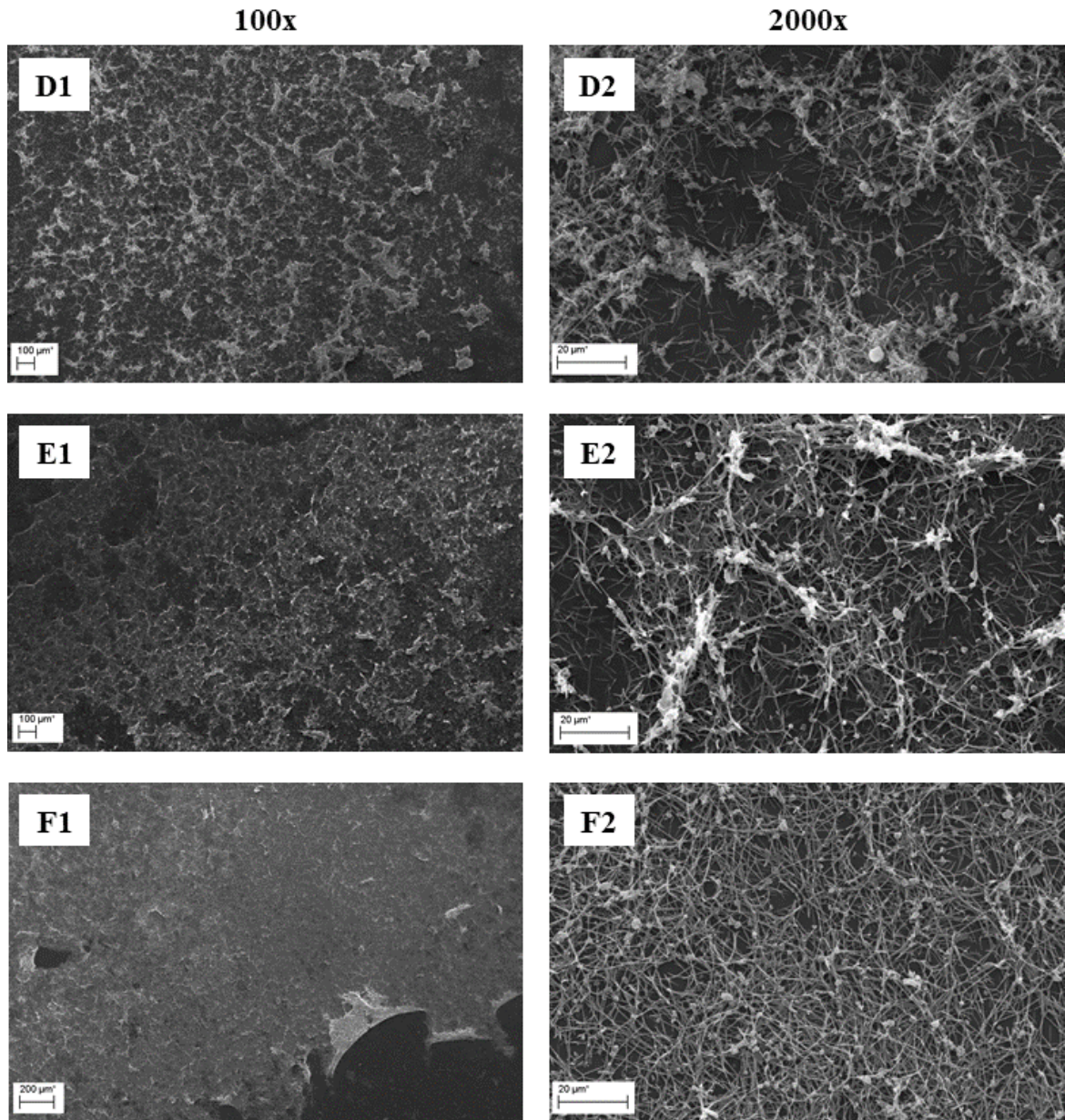
## **Appendix 8**

Mono-species biofilms were visualised using the SEM in order to study their 3D structure and observe possible differences in the biofilm formation between the subspecies. The main analysis of the biofilms was performed at 8000x magnification in order to obtain the highest possible detail of the biofilm architecture. Additionally, the biofilms were studied under a low magnification (100x) and a medium magnification (2000x) in order to analyse the overall biofilm layer and how this layer covers the Nunc™ Thermanox™ coverslip. All the subspecies were found not to form a homogeneous layer of biofilm, but they formed patches of micro-colonies.

Due to a technical issue during the SEM, some of the micrographs captured under a low magnification are missing (FNN23, FNN25 and FNP), however it was possible to observe the biofilm layer and it showed an identical pattern of biofilm formation to the rest of the subspecies.



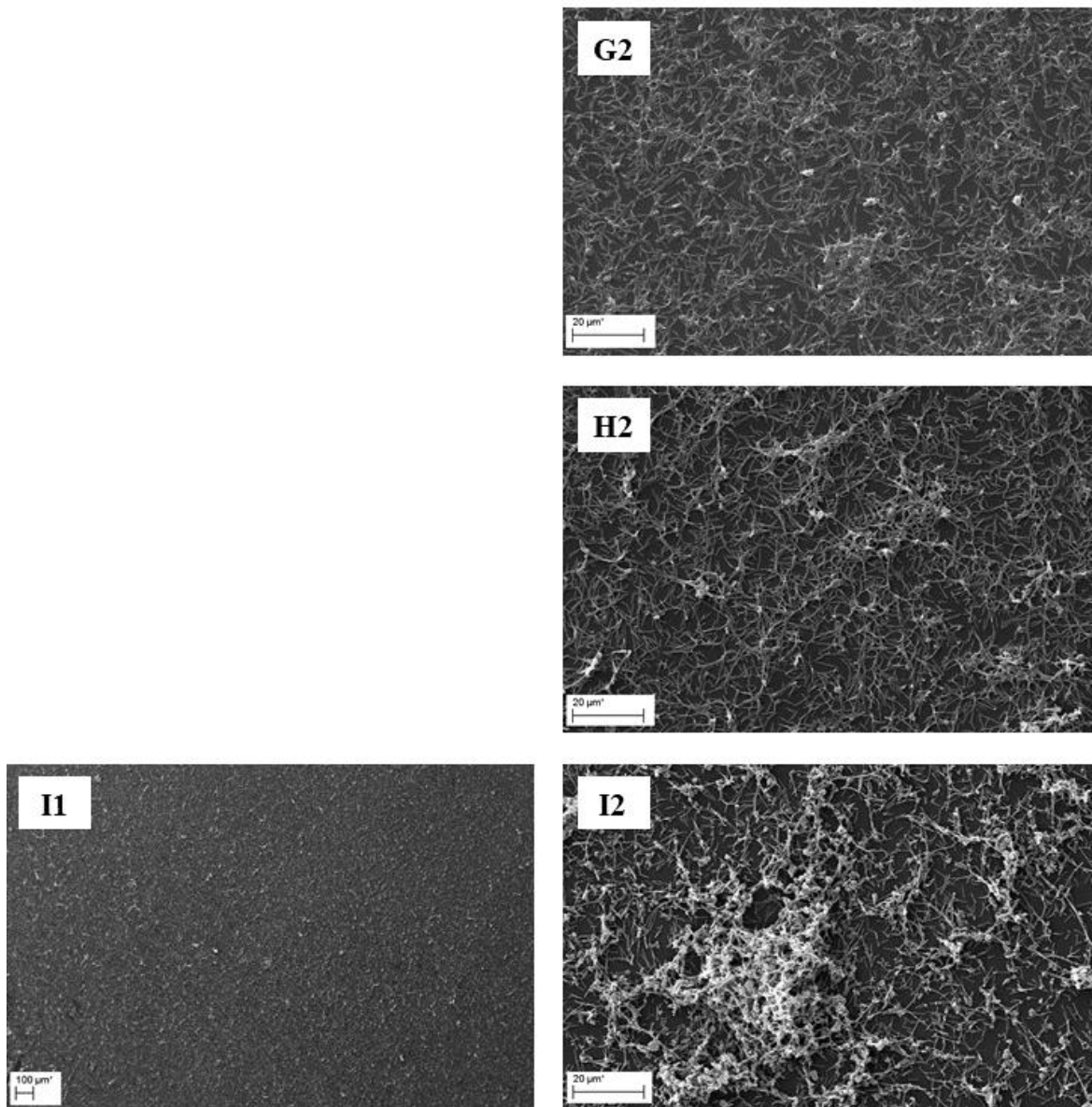
**Appendix 8. Mono-species FNA biofilms.** All micrographs show that the biofilm layer does not cover the surface of the coverslip completely. Patches of biofilm layer are observed. A – FNA 3 days; B – FNA 5 days; C – FNA 7 days. 1 – 100x magnification; 2 – 2000x magnification.



**Appendix 8. Mono-species FNF biofilms.** Micrographs show that the biofilm layer does not cover the surface of the coverslip completely. Patches of biofilm layer are observed. The fragility of the biofilms can be seen in F1, where the portion of the biofilm layer detached and folded over and covered the neighbouring area. D – FNF 3 days; E – FNF 5 days; F – FNF 7 days. 1 – 100x magnification; 2 – 2000x magnification.

100x

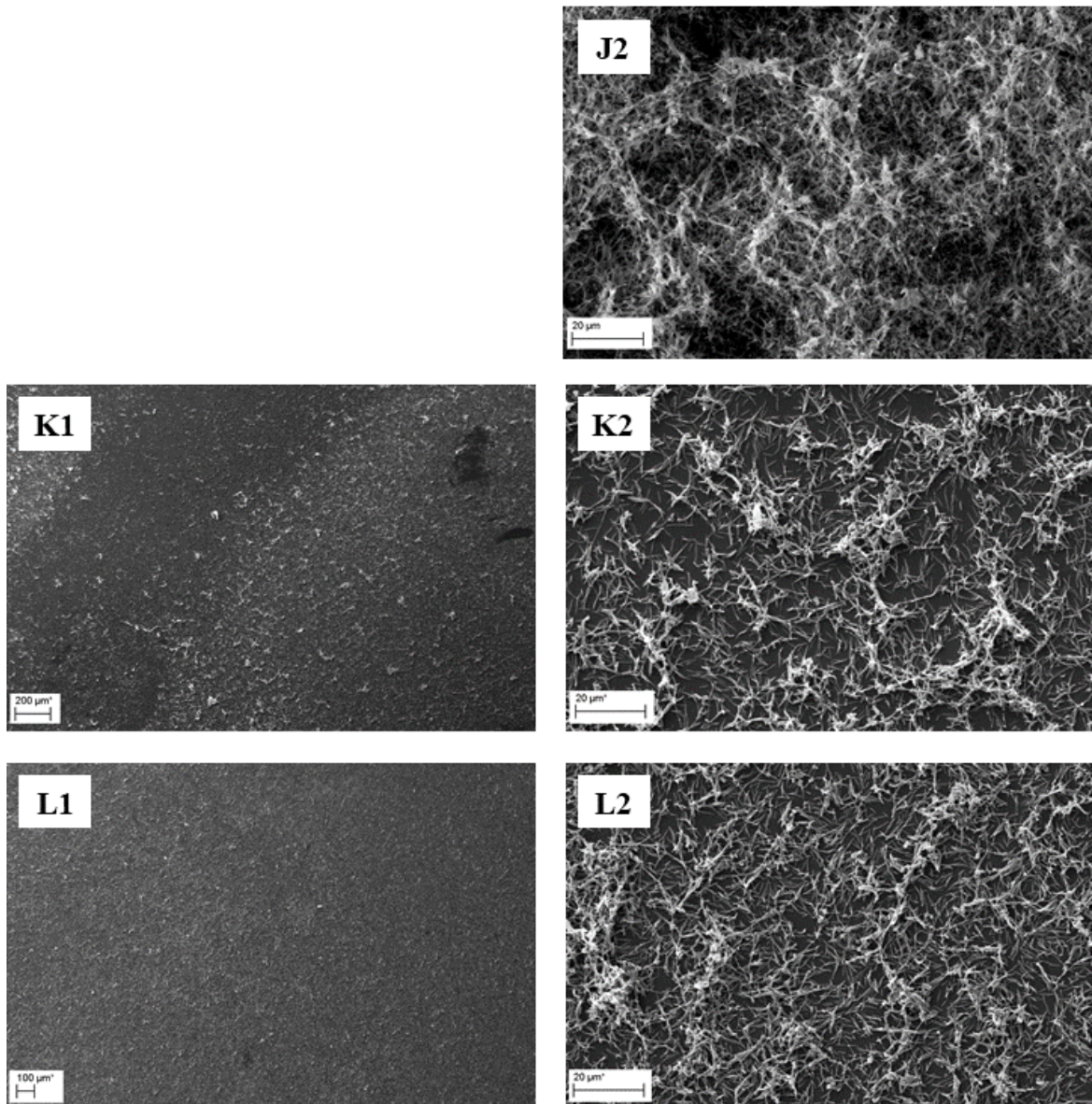
2000x



**Appendix 8. Mono-species FNN23 biofilms.** G1 and H1 are missing due to a technical issue during the SEM. It was observed that biofilms did not form a continuous layer. I1 seemed to form a continuous layer at 100x magnification, however increasing the magnification showed that also this layer was not homogeneous, but it grew in patches. G – FNN23 3 days; H – FNN23 5 days; I – FNN23 7 days. 1 – 100x magnification; 2 – 2000x magnification.

100x

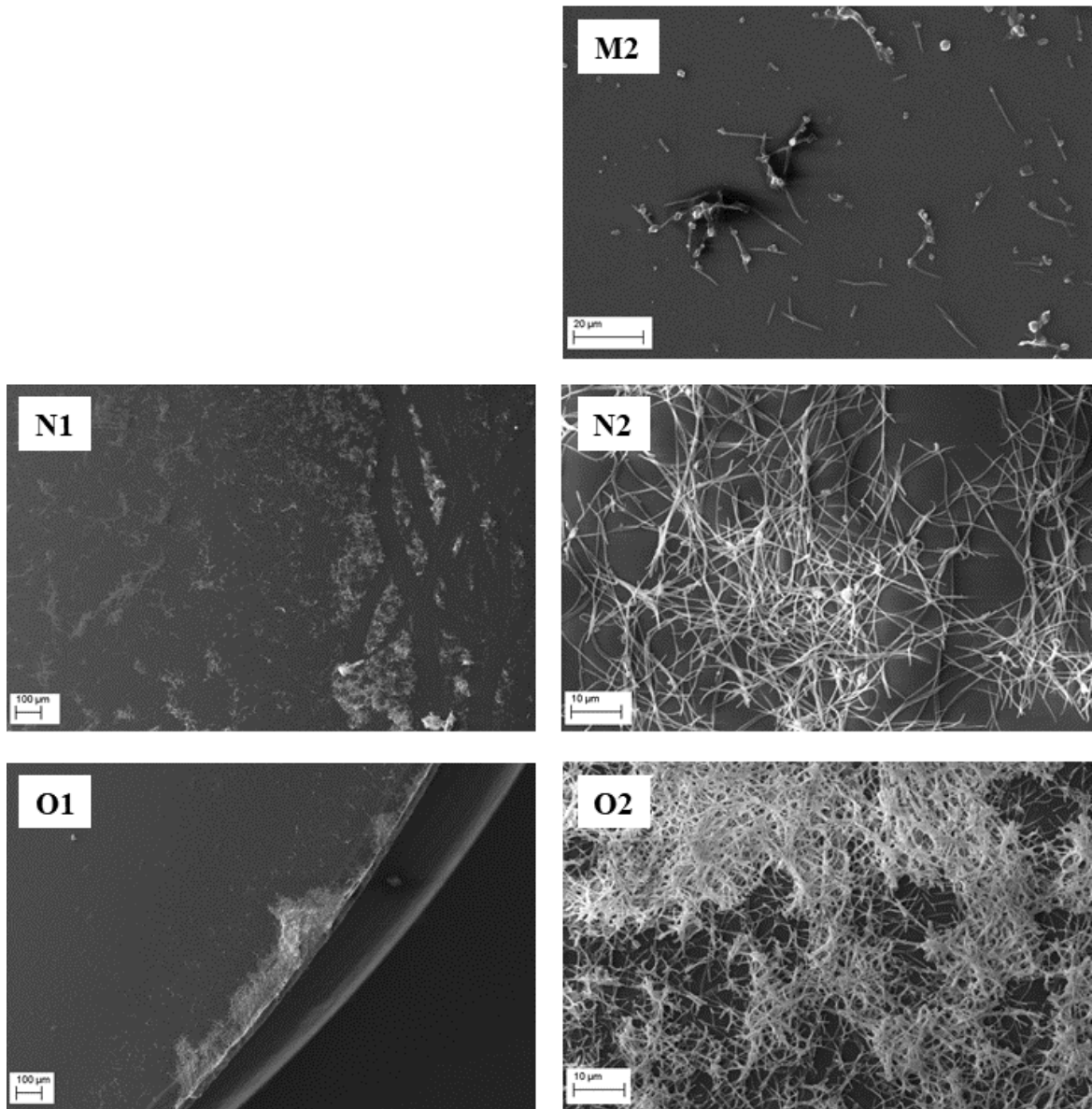
2000x



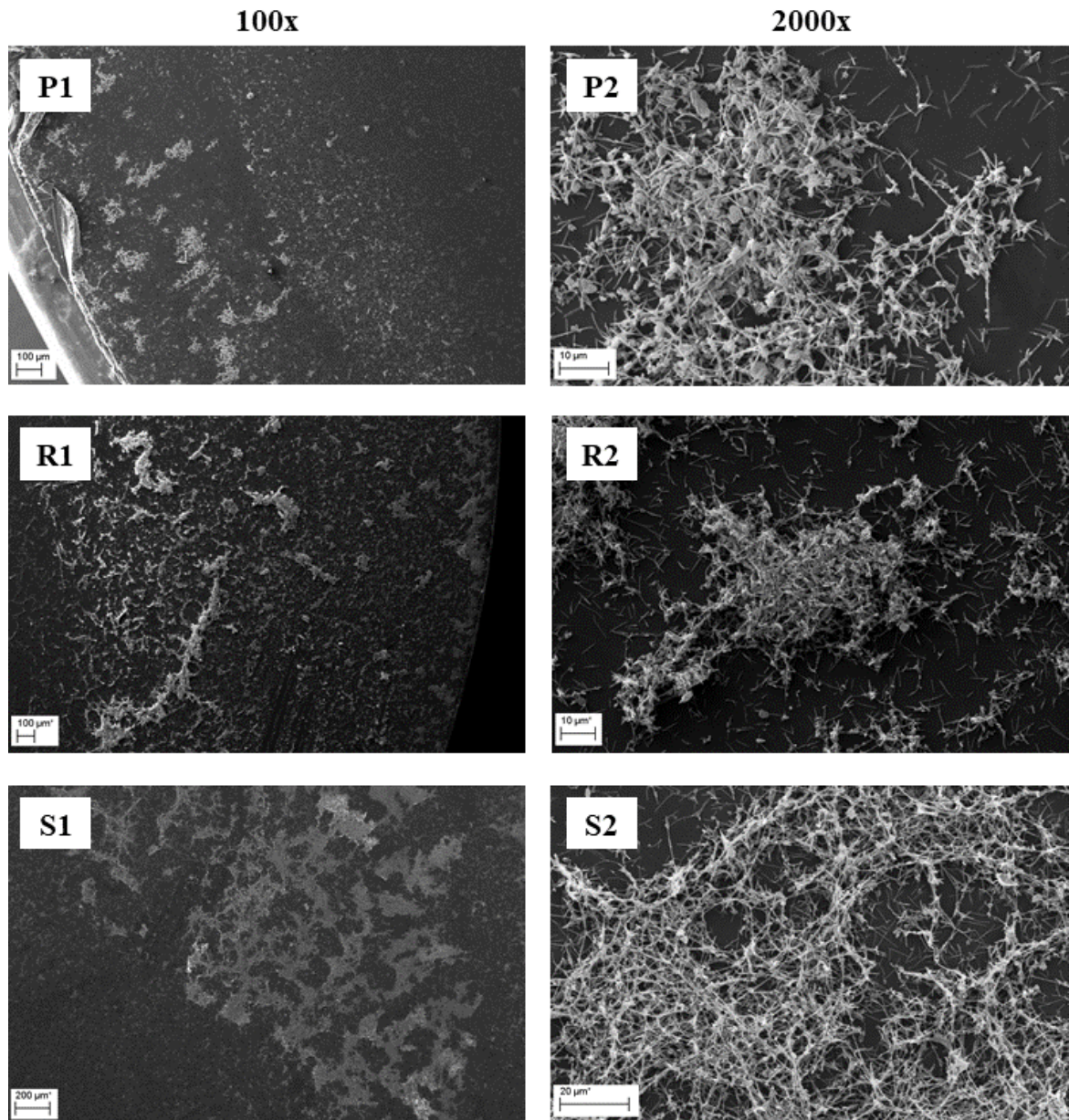
**Appendix 8. Mono-species FNN25 biofilms.** J1 is missing due to a technical issue during the SEM. Bacteria did not form a continuous layer of biofilm in K and L, as individual bacterial cells can be observed attached to the coverslip. Only J2 seems to form a thicker, more homogeneous layer of biofilm. J – FNN25 3 days; K – FNN25 5 days; L – FNN25 7 days. 1 – 100x magnification; 2 – 2000x magnification.

100x

2000x



**Appendix 8. Mono-species FNP biofilm.** M1 is missing due to a technical issue during the SEM. FNP was the weakest biofilm former, which can be seen in all the micrographs. When grown for three days, only a few individual bacterial cell were observed (M2). Even after the incubation for seven days, a very small area on the edge of the coverslip was covered with the biofilm (O1). M – FNP 3 days; N – FNP 5 days; O – FNP 7 days. 1 – 100x magnification; 2 – 2000x magnification.



**Appendix 8. Mono-species FNV biofilm.** All micrographs showed that the biofilm layer formed was not homogeneous, but bacteria were growing in patches in all three time points. P – FNV 3 days; R – FNV 5 days; S – FNV 7 days. 1 – 100x magnification; 2 – 2000x magnification.